2007

Elementary reactions involved in pollutant-forming mechanisms

Cheri Ann McFerrin
Louisiana State University and Agricultural and Mechanical College

ELEMENTARY REACTIONS INVOLVED IN POLLUTANT-FORMING MECHANISMS

A Dissertation

Submitted to the Graduate Faculty of the
Louisiana State University and
Agricultural and Mechanical College
in partial fulfillment of the
requirements for the degree of
Doctor of Philosophy

in

The Department of Chemistry

by
Cheri Ann McFerrin
B.S., Louisiana State University, 1988
August, 2007

For Thomas Wingate McFerrin Jr.

TABLE OF CONTENTS

ABSTRACT

The reactions of the hydroxyl radical (OH) with molecular chlorine (Reaction 1), methane (Reaction 2), and propane (Reaction 3) have been studied experimentally using a pulsed laser photolysis/pulsed-laser-induced fluorescence technique over wide ranges of temperatures (297-826, 298-1009, and 296-908 K, respectively) and at pressures between 6.68 and 24.15 kPascals. The rate coefficients for these reactions exhibit no dependence on pressure and exhibit positive temperature dependences that can be represented with modified three-parameter Arrhenius expressions within their corresponding temperature ranges: $k_1 = 3.59 \times 10^{-16} T^{1.35} \exp(-745K/T) cm^3 molecule^{-1} sec^{-1}$, $k_2 = 3.82 \times 10^{-19} T^{2.38} \exp(-1136K/T) cm^3 molecule^{-1} sec^{-1}$, and $k_3 = 6.64 \times 10^{-16} T^{1.46} \exp(-271K/T) cm^3 molecule^{-1} sec^{-1}$. For the OH + Cl_2 reaction, the potential energy surface has been studied using quantum chemical methods which suggests OH + Cl_2 → HOCl + Cl as the main channel of this reaction.

Density Functional Theory (DFT) along with Quadratic Configuration Interaction (QCISD(T)//DFT) calculations, with single, double, and triple electronic excitations, for the energetics of formation, stability, and reactivity of *ortho*-semiquinone, *para*-semiquinone, and the chloro-phenoxyl radicals have been performed using the 6-31G(d,p) basis set. Formation of these radicals from potential molecular precursors catechol, hydroquinone, and the chloro-phenols is readily achieved under combustion conditions through unimolecular scission of the phenoxyl-hydrogen bond or abstraction of the phenoxyl hydrogen by a hydrogen atom or hydroxyl radical. The resulting radicals are resonance stabilized and resist decomposition and oxidation. The calculations strongly suggest that combustion-generated semiquinone and chloro-phenoxyl radicals are sufficiently stable and resistant to oxidation to be considered persistent in the atmospheric environment.

Semiquinone radicals (*ortho*- and *para*-hydroxy substituted phenoxyl radicals and various derivatives) are suspected to be biologically active and may lead to DNA damage, pulmonary disease, cardiovascular disease, and liver dysfunction. These radicals thought to be highly stable with low reactivity due to resonance stabilization including both carbon-centered and oxygen-centered radical resonance structures and been reported in cigarette tar. Chloro-phenoxyl radicals, on the other hand, are implicated in polychlorinated-dibenzodioxin and -dibenzofuran formation mechanisms, EPA pollutants, in the low temperature sections of hazardous waste combustion.

CHAPTER 1. INTRODUCTION

The large variety of physical and chemical properties in hazardous waste makes finding a universal hazardous waste remediation method difficult. Incineration approaches a universal method when it takes advantage of the fact that all molecules may absorb infrared (thermal energy) radiation and decompose. EPA, under the guidance of RCRA (Resource Conservation and Recovery Act), began to regulate incinerator operations in 1981 such that each component of hazardous waste was destroyed/removed with an efficiency of 99.99%, that particulate emissions do not exceed 180 ng/dry standard m^3, and gaseous hydrochloride acid does not exceed 1.8 kg/hour, or that it is removed with an efficiency of not less than 99%.[1]

Presently, incinerators are initially success-tested by comparing results from a trial burn with RCRA standards. Trial burns measure the destruction efficiency of only a limited number of POHCs (principal organic hazardous constituents) under optimum incinerator operating conditions and are treated as representative of the minimum performance of the incinerator for other hazardous compounds. Observation of organic emissions from incinerators suggests that excursions from the optimum conditions are occurring, and the assumption trial burns are representative of daily operating conditions is not valid. Small excursions, such as atomization, poor mixing, or gas quenching can drop destruction efficiencies from greater than 99.99% to 99% or even less than 90% and are the controlling phenomena for incinerator efficiency.[2]

Unfortunately, incineration is producing hazardous waste which is more lethal than its feedstock.[3] Highly chlorinated organic pollutants such as polychlorinated-dibenzodioxins (PCDDs) and polychlorinated-dibenzofurans (PCDFs).are amongst the most lethal incineration products of combustion[4], and as a result, these congeners reside on the EPA list of hazardous pollutants.[5] These compounds cause or may cause cancer or other serious health effects, such as

reproductive effects or birth defects, or adverse environmental and ecological effects. While the EPA is required to control emissions of these compounds, increasing public concern over the benefits of incinerating waste versus the health risks from pollutants drives research to identify a quantitative model which can accurately predict pollutant formation. A clearer picture of the mechanisms responsible for producing environmental pollutants can only emerge as knowledge of the elementary reaction steps become more detailed.

The goal of this research is to apply and extend kinetics and dynamics theories to elementary reactions of interest in different combustion environments, with attention given to gas-phase reactions. Selected reactions containing reactive gas-phase species such as the hydroxyl radical, molecular oxygen, hydrogen atoms, and substituted and non-substituted aromatic radicals and precursors were chosen as these species are known to be present in combustion environment.[6-10] Free radical-molecule and unimolecular decomposition reactions are implicated in the production of pollutants during high temperature incineration; hence this work focuses on elementary reactions of this form.

The hydroxyl radical (OH•) and molecular chlorine (Cl_2) each play a key role in the chemistry of combustion and atmospheric processes. Numerical simulations of complicated pollutant-forming mechanisms require each step contain accurately determined rate coefficients in a wide range of temperature and pressure. Despite the importance of Reaction 1, it has not been studied at high temperature. As a result, Chapter 3 is devoted to the experimental and theoretical temperature and pressure-dependent kinetic investigation of the gas-phase reaction of the hydroxyl radical with molecular chlorine over a wider temperature range.

$$OH\bullet + Cl_2 \rightarrow \text{products} \qquad \text{(Reaction 1)}$$

Reaction 1 has been previously studied at low temperatures (231-354 K)[11-15] and the results of these studies are in agreement with each other within reported experimental errors. The importance of this reaction for atmospheric chemistry is described in the work of Gilles et al.[11] The current work represents the first experimental study of Reaction 1 carried out at high temperature in the range from 297 K (to compare with the earlier studies) to 826 K, which is relevant to combustion and thermal processes.

Reaction 1 plays a significant role in the formation of the hazardous emissions from combustion of chlorine-containing compounds[16-18] as, for example, it may be important in the control of the HCl to Cl_2 ratio. While molecular chlorine is an effective chlorinating agent and a powerful oxidant, the larger bond dissociation energy in HCl can result in significant sequestration of chlorine. In addition, Cl_2 is difficult to scrub from flue gas due to its relatively low water solubility. Therefore, emissions of Cl_2 should be controlled and minimized during the combustion process.[17]

The hydroxyl radical (OH•) is an important reactant in combustion chemistry. Using diode-laser absorption spectroscopy, Tamaru et al.[19] report hydroxyl radicals are present in a post-flame region (T=800-1400 K) lying between 2 premixed propane/air flames (fuel-in-air ratio = 0.65-1.0). The measured OH• concentrations in the post-flame did not vary significantly which suggests the post-flame region contents are close to chemical equilibrium for OH•.

In the late stages of chloro-hydrocarbon (CHC) combustion as well as post-combustion zones molecular chlorine (T < 900K) and the hydroxyl radical (T=800-1400 K) are favored at low temperatures. Cl_2 has also been linked to the homogeneous and catalytic formation of chlorinated dibenzo-p-dioxins (PCDD) and dibenzofurans (PCDF) in the low temperature section of combusters and incinerators.[20, 21]

A conservative estimate suggests 45 million tons of molecular chlorine (Cl_2) are produced globally each year making chlorine the most important industrial chemical.[22] PVC (polyvinyl chloride) plastic represents approximately 33% of the Cl_2 product array and is projected to rise to 50-55% due to the influence of construction. While there is a decline in demand for chlorine in some applications, such as the pulp and paper industry, global demand for molecular chlorine is expected to increase 2.8% per year.[23]

Given both the hydroxyl radical and molecular chlorine are present in post-flame regions of incinerators, one of the objectives of this work is to more accurately determine the experimental rate constant for Reaction 1.

To accurately determine the rate coefficients of hydroxyl radical reactions, experiments must be performed with sufficiently low initial concentrations of hydroxyl radicals, thus ensuring the absence of any complications due to possible fast secondary reactions. For this purpose, we have constructed a pulsed laser photolysis/pulsed-laser-induced fluorescence (PLP-PLIF) apparatus combined with a heatable, slow-flow reactor. This technique has excellent sensitivity to hydroxyl radicals, which allows one to perform OH• reaction rate measurements with the necessary low initial OH• concentrations.[24] Two reactions whose rate coefficients are relatively well-established, Reactions 2 and 3, were also studied in order to validate the experimental apparatus used here for the first time after its construction. (Numbers in parentheses indicate the experimental temperature ranges of the current study).

$OH• + CH_4 \rightarrow$ products	(298-1009 K)	(Reaction 2)
$OH• + C_3H_8 \rightarrow$ products	(296-908 K)	(Reaction 3)

In addition, the potential energy surface of Reaction 1 has been studied using two quantum chemical approaches, namely hybrid density functional theory (DFT) (B3LYP/6-31G(d,p) and BHandHLYP/6-31G(d,p)) and quadratic configuration interaction theory (QCISD(T)/6-31G(d,p)). Hybrid DFT is a common computational procedure which involves mixing of various amounts of the Hartree-Fock nonlocal exchange operator with DFT exchange-correlation functionals. Despite known deficiencies with DFT[25, 26], the BHandHLYP level of theory has risen in popularity due to its cost efficiency and its ability to order experimental values well.[27-29] The QCISD(T) method[30] involves a wavefunction expansion such that single, double, and triple electronic orbital excitations are included in its variational energy minimization treatment. QCISD(T) will be discussed in greater detail in Chapter 2.

In Chapter 4, DFT and QCISD(T) calculations of the energetics of formation, stability, and reactivity of *o*-semiquinone, *p*-semiquinone, and phenoxyl radicals have been performed. There is increasing experimental evidence that these radicals are environmentally persistent, present in airborne fine particulate matter (PM2.5), and whose principal source is combustion-generated particles.[31-33] These radicals are biologically active and may lead to DNA damage, pulmonary disease, cardiovascular disease, and liver dysfunction.[31,34] It is suspected that they are semiquinone-type radicals (*ortho*- and *para*-hydroxy substituted phenoxyl radicals and various derivatives) that have been reported in cigarette tar.[35-37] These radicals are strong enough reducing agents in aqueous solution at physiological pH's to reduce dissolved oxygen to form superoxide and other biologically-active, reactive oxygen species (ROS).[31, 38] However, the nature of the radicals in PM2.5 and combustion-generated particulate matter has not been conclusively demonstrated. Furthermore, recent experimental studies suggest that simple

phenoxyl-type radicals may be as persistent as semiquinone radicals and be more ubiquitous in the environment.[39]

For radicals to have environmentally significant concentrations, they require:

1. A molecular precursor and favorable route of formation;
2. Stability, i.e. being resistant to decomposition; and
3. Non-reactivity, i.e. being resistant to reaction with other molecular or radical species.

Formation of these radicals from potential molecular precursors catechol (1,2-dihydroxyl benzene), hydroquinone (1,4-dihydroxyl benzene), and phenol is readily achieved under combustion conditions through unimolecular scission of the phenoxyl-hydrogen bond[40] or abstraction of the phenoxyl hydrogen by a hydrogen atom or hydroxyl radical.[41-44] The resulting radicals are resonance stabilized and resist decomposition and oxidation. These calculations strongly suggest that combustion-generated semiquinone and phenoxyl radicals are sufficiently stable and resistant to oxidation to be persistent in the atmospheric environment.

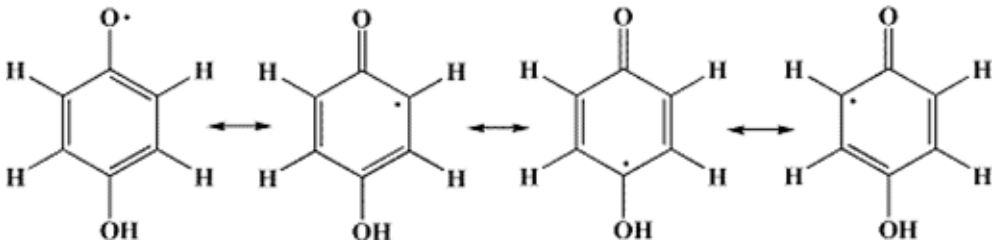

Figure 1: Resonance structures of *p*-semiquinone radical existing as both carbon-centered and oxygen-centered radicals. Similar schemes can be drawn for *o*-semiquinone and phenoxyl radicals.

Semiquinone radicals are thought to be highly stable with low reactivity due to resonance stabilization including both carbon-centered and oxygen-centered radical resonance structures (Figure 1). Consequently, they have been considered the most likely candidates for the observed

free radicals in combustion and atmospheric PM2.5.[35] Moreover, phenoxyl radicals may have similar chemical properties and exist in higher concentrations. Despite these radicals' resonance stabilization and the implication they are formed through the thermal degradation of precursors such as hydroquinone, catechol and phenol, there is no reported characterization of these radicals' formation from thermal degradation of these precursors in the gas phase.[39]

The thermal decomposition of the phenoxyl radical along with its and mono-hydroxylated substituted derivatives are representative of the types of steps thought to be of importance in pollutant formation. Using a mechanism proposed by Liu et al.[45] for the thermal decomposition of the phenoxyl radical, an *ab initio* study of the thermal decomposition of phenoxyl (for calibration), mono-hydroxylated phenoxyl radicals (Chapter 4), and poly-chlorinated phenoxyl radicals (Chapter 5) was undertaken. Transition state energies along with reaction energies have been calculated for each of these decomposition reactions where carbon monoxide and a substituted cyclopentadienyl radical are produced.

Bimolecular reaction radical-molecular oxygen reactions were included as it is the highest concentration reactive species in the atmosphere and the known principal route of consumption of most organic radicals under oxidative conditions.[46-55] Activation energies for the addition of molecular oxygen to the most reactive carbon atom (in all cases, the *para* position) range from 19.6 to 21.3 kcal mol^{-1} (BHandHLYP/6-31G(d,p)). Free energies for oxidation of semiquinone and phenoxyl radicals at 298K are positive and therefore thermodynamically unfeasible at this temperature.

In Chapter 4, calculations concerning the formation, stability, and reactivity of phenoxyl, *o*-semiquinone, and *p*-semiquinone radicals under combustion and atmospheric conditions are presented.

With regard to Chapter 5, chlorinated phenols (CPs) and various derivatives have been manufactured for various purposes including disinfection and vegetation control. Several highly CPs are considered hazardous waste[5], thus their disposal is subject to regulation by the EPA, controlled high-temperature incineration being the most common method. Unfortunately, CPs are precursors to the formation of polychlorinated dibenzo-p-dioxins and dibenzofurans (PCDD/F) upon heating or burning. Both gas-phase condensation reactions and transition metal surface-mediated reactions can convert some congeners of CPs to PCDD/F under the appropriate conditions.[56-63] Furthermore, CPs and PCDD/F can be formed as "products of incomplete combustion (PICS)" from combustion/thermal reaction in basically any process that contains a source of carbon, chlorine, and a catalytic transition metal. Because most combustion devices contain trace levels of transition metals and chlorine, CPs are nearly ubiquitous in the environment.

While a previous computational gas-phase study of phenol and *para*-substituted phenols states B3LYP underestimates the change in OH bond dissociation energies (after making comparisons with experimental values only performed in solution)[64], other DFT studies have reproduced experimental changes in OH bond dissociation energies satisfactorily when compared to experiment[65-71] using larger basis sets. These studies have undertaken only mono- or dichloro-substituent effects on the OH bond dissociation energy of phenol. In addition, while another study has undertaken the stabilities and geometries of the 19 congeners of chlorophenol using B3LYP/6-311+G(d,p)[72], this is the first study to undertake all the 19 congeners of chlorophenols' reactivities with DFT in terms of (i) unimolecular decomposition producing a hydrogen atom and a chlorinated phenoxyl radical, (ii) reaction with a hydrogen atom which abstracts hydrogen forming a chlorinated phenoxyl radical, (iii) reaction with a hydrogen atom

which displaces the hydroxyl radical forming a chlorinated benzene, and (iv) reaction with a hydroxyl radical which abstracts hydrogen producing water and a chlorinated phenoxyl radical. In some cases, QCISD(T)/6-31G(d,p)// BHandHLYP/6-31G(d,p) model chemistries are employed to validate the BHandHLYP/6-31G(d,p) ordering of results.

Amongst the mono-chlorinated phenols, it has been established OH bond dissociation energies are lowered by an electron-donating *para*-chloro substituent and increase in the presence of *ortho*- and *meta*-chloro substituents[65-67, 69-71] as these structures are stabilized by the presence of an internal hydrogen bond . As it happens with mono-chloro phenols, *ortho*-chloro phenol is the most stable.[72] The OH bond dissociation energies calculated herein with BHandHLYP/6-31G(d,p) are consistent with these previous findings. Augmenting this model chemistry with the 6-311++G(d,p) basis set did not change the relative ordering of bond dissociation energies and exaggerated the differences. As a result, the 6-31G(d,p) basis set was used most often as we are concerned with the relative bond dissociation energies.

Han et al.[72] *also* report the OH bond in phenol is lengthened (or destabilized) with an increasing degree of chlorine substitutions, and stabilized (amongst each homologue pattern) in cases where an internal hydrogen bond may be established. The DFT results in this work are congruent with these findings in terms of stabilities and geometries.

Earlier ab initio calculations have confirmed the phenoxyl radical[45] thermally decomposes after proceeding through a rate-determining bicyclic intermediate followed by alpha-CC bond cleavage to produce CO and a cyclopentadienyl radical. We report amongst the 19 congeners of chloro-phenoxyl radicals the activation energies inside each homologue pattern for concerted elimination of CO and a chlorinated cyclopentadienyl radical is lowered (relative to phenoxyl, Eact=62.9 kcal mol^{-1} (BHandHLYP/6-31G(d,p))) provided one *ortho*-hydrogen atom moiety is

adjacent to the carbon-carbon bond rupture. Furthermore, the results here show bond rupture is thermodynamically favored in the C-C bond adjacent to the hydrogen atom, as opposed to an adjacent chlorine atom, regardless of the congener. The results in Chapter 5 suggest the higher chlorinated congeners of the phenoxyl radical are more likely to decompose into CO and a chlorinated cyclopentadienyl radical, relative to the analogous reaction for phenoxyl, provided one *ortho*-hydrogen atom moiety is adjacent to the carbon-carbon bond rupture. The remaining chlorinated radicals then become more important in PCDD/F formation reactions which have been proposed to take place via radical-radical or radical-molecule addition pathways[59, 61, 73-78] due to their relative resistance to decomposition.

After one observes the modeled mechanistic work by Ryu et al.[77], which begins with unimolecular decomposition, for the 19 congeners of chlorophenol and the experimental system used to represent the 19 congeners of chlorophenol (an equimolar mixture phenol, 4-chlorophenol, and 2.4 dichlorophenol in benzene) one may note the expected resulting radicals in this system are phenoxyl, 4-chlorophenoxyl and 2,4 dichlorophenoxyl, with 4-chlorophenoxyl as the most abundant. The dichlorinated product radical meets the condition for lowering its decomposition energy (i.e., one *ortho*-H atom moiety is present), relative to the balance, making the phenoxyl and 4 chlorophenoxyl radicals most resistant to decomposition in this work. Non-chlorinated dibenzofuran was consistently produced in the largest amounts[77] suggesting nonsubstituted phenoxyl radical coupling, followed by enolizaton and condensation, was energetically favored over the alternatives. Wiater et al.[75] have shown using slow combustion (500-600 C) the phenoxyl radical prefers to dimerize at its *para*-sites, a site unavailable in the 4-chlorophenoxyl case due to steric hindering by the chlorine atom. While the decomposition energies for phenoxyl and *para*-chlorophenoxyl are 62.9 and 63.6 kcal-mol^{-1}, these calculations

along with experimental works demonstrate the phenoxyl radical would be most likely to dimerize considering the absence of steric hinderance (higher Arrhenius factor in dibenzofuran rate) at its *para*-carbon and its high decomposition energy.

Reference 77 is congruent with Wiater et al. when it also reports PCDF formation is favored radicals with chlorine substitutions at *meta*-positions 3 and 5, as opposed to at *ortho*-positions 2 and 4. This observation has also been explained by the preference phenoxyl radical dimerization has for its *ortho* and *para* sites[75], sites available for addition in 3,5 dichlorophenoxyl due to the absence of steric hinderance from chlorine atoms at these locations. With respect to the dichlorophenoxyl homologue pattern radical decomposition results, 3,5-dichlorophenoxy radical is least likely to decompose (into CO and a dichlorocyclopentadienyl radical), with one exception, giving it a greater lifetime in the gas-phase and greater probability for involvement in PCDF formation. It is not surprising that the 3,5 dichloro-isomer also has *ortho*-hydrogen moieties available for the condensation step. The exception (2,6 dichlorophenoxy) does not have an *ortho*-H atom available for the condensation step.

After separating those chlorinated radicals whose decomposition is facilitated by the presence of one *ortho*-H atom from this work, one may observe degree of chlorination correlates with the destabilization of the alpha-C-C bond in the balance of chlorinated phenoxyl radicals. Additionally, amongst each homologue pattern, it should be noted the presence of two *ortho*-arranged chlorine atoms makes these radicals the least likely candidates for decomposition.

Chlorinated phenoxyl radicals are also resonance stabilized and may behave similarly to phenoxyl radicals in oxidative environments.[79, 80] To address this issue, bimolecular reaction calculations between 2-, 3-, and 4-monochlorophenoxyl radicals and molecular oxygen were undertaken. High activation energies and positive free energies of reaction are similar to their

non-reactive phenoxyl analogue suggesting chlorinated phenoxyl radicals are virtually unoxidizable as well.

CHAPTER 2. QUANTUM CHEMICAL THEORY

All *ab initio* calculations were performed with the *Gaussian 98/03* system of programs[81] using both SuperMike (a 1024 cpu supercomputer, mike.cct.lsu.edu) and SuperHelix (a 256 cpu supercomputer, helix.bcvc.lsu.edu) which are both located in the Louisiana State University (LSU) Center for Computational Technology (www.cct.lsu.edu). Casper (casper.lsu.edu), a 14 node system (8 cpu/node), provided another resource and is located inside the LSU Department of Information Technology Services (www.lsu.edu/ocs).

2.1 The 6-31G(d,p) and 6-31++G(d,p) Basis Sets

Basis sets are pre-defined approximations and allow for the expression of molecular orbitals as linear combinations of one electron functions (or basis functions). An individual molecular orbital is defined as[30]

$$\Phi_i = \sum c_{ji} X_j$$

where c_{ji} are the molecular orbital expansion coefficients and X_j are the basis functions.

Gaussian (G03) uses gaussian-type atomic functions (primitive gaussians) as basis functions[82] which have the following form

$$X(\alpha,r) = cx^n y^m z^l \exp(-\alpha r^2)$$

G03 sums the primitive gaussians to approximate Slater-type orbitals (STOs) (Figure2). The sum of primitive Gaussians is termed a contracted gaussian function. This manipulation is done to circumvent the difficulty with integrating the two electron integral composed of STOs and increase computational speed. Speed takes place because the two electron integral of 2 contracted gaussian functions is another contracted gaussian function (Figure 3).[30]

The 6-31G(d,p) basis set[30] is described by a contraction of 6 primitive Gaussians for non-valence molecular orbitals (inner) and 2 types of functions for valence orbitals (outer). The best orbital exponents are commonly slightly greater than and lower than the optimal exponent of a minimal basis function (STO-3G)[30], and 2 functions for valence orbitals allow for greater flexibility (more orbital exponents and coefficients) in larger systems. Double Zeta polarization functions allow for adjustment of the valence orbitals' exponents (inner and outer) in a basis set by 2 scale factors (ζ' and ζ", respectively). Unfortunately, ammonia is planar when its polarization functions are only described in this manner. Polarization functions must also include virtual (higher angular quantum number) orbitals. The (d,p) term in both basis' used in this work indicates polarization functions (or d functions) have been added for first row elements (Li through Ne), and p orbitals have been added to hydrogen atoms. The "plus" sign term in the 6-31++G(d,p) basis indicates diffuse functions have been added into the expansion. Diffuse functions use smaller exponential coefficients and thus decay more slowly than a standard function. The double ++ term indicates diffuse functions have been added to heavy atoms as well as hydrogen atoms.

2.2 Hartree Fock Theory

Separation of variables may be employed for a 2 electron problem when the particles are non-interacting or independent. Initially, electron-electron coulombic repulsions are dismissed in Hartree Fock (HF) theory in order to arrive at a zeroth-order wave function. The Schrodinger equation for 2 independent electrons is[83]

$$(H_1 + H_2)\boldsymbol{\psi}(x_1,y_1,z_1,*,x_2,y_2,z_2,*) = (E_1 + E_2)\,\boldsymbol{\psi}(x_1,y_1,z_1,*,x_2,y_2,z_2,*)$$

$$* = \alpha\ (\uparrow) \text{ or } \beta\ (\downarrow) \text{ spin function}$$

a sum of individual Hamiltonian operators and energies. Each Hamiltonian in this sum includes electronic repulsions via its potential energy term thus allowing each electron

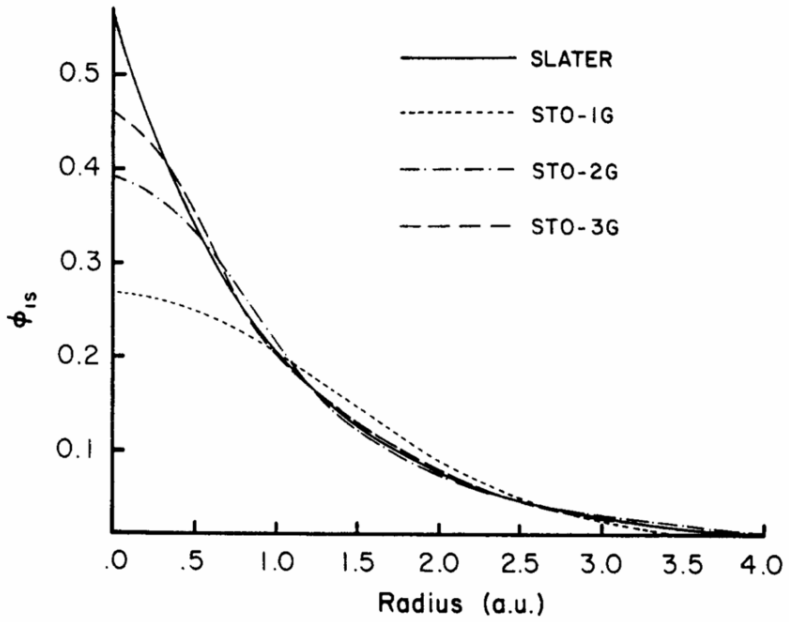

Figure 2: Comparison of the quality of the least-squares fit of a 1s Slater function (δ=1.0) obtained at the STO-1G, STO-2G, and STO-3G levels.

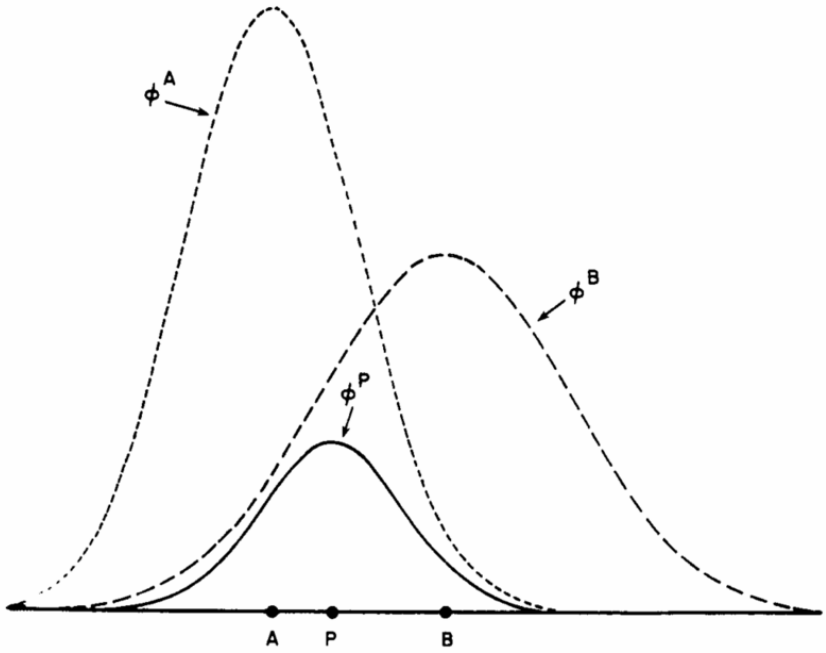

Figure 3: The product of two 1s Gaussians is a third 1s Gaussian.

to interact with the balance of n-1 electrons' positions. As a result, the repulsive portion of the potential energy (V) for each electron becomes a sum of n-1 terms, where n is the number of electrons. For example, the electron-electron interaction expansion for electron one becomes

$$V_1(r_1,\theta_1,\varnothing_1) = V_{1,2} + V_{1,3} + \ldots + V_{1,n-1}$$

Assuming the wave function $\boldsymbol{\psi}(x_1,y_1,z_1,*,x_2,y_2,z_2,*)$ is separable results in a total wave function (the Hartree product) which is a product of individual wave functions (zeroth-order).

$$\Psi = \boldsymbol{A}\ (g_1(r_1,\theta_1,\varnothing_1)\ g_2(r_2,\theta_2,\varnothing_2)\ldots\ g_N(r_N,\theta_N,\varnothing_N\ ))$$

$$\Psi = \begin{bmatrix} g_1(r_1,\theta_1,\varnothing_1) & \cdots & g_N(r_1,\theta_1,\varnothing_1) \\ \vdots & \ddots & \vdots \\ g_1(r_N,\theta_N,\varnothing_N) & \cdots & g_N(r_N,\theta_N,\varnothing_N) \end{bmatrix}$$

The HF method begins with a trial wave function not limited to a hydrogen-like function and searches for functions g_1, g_2, … which minimize the variational integral[30]

$$\frac{\int \Psi^* \hat{\mathbf{H}} \Psi \, dv}{\int \Psi^* \Psi \, dv}$$

Better approximate wavefunctions (g) are obtained by varying their parameters (coefficients and orbital exponents) until the electronic energy is minimized. The functions g

$$g(r, \theta,\varnothing,\alpha) = R(r)\ Y_l^m(\theta,\varnothing)\ \alpha$$

are a product of a radial function R(r), a spherical harmonic $Y_l^m(\theta,\varnothing)$, and a spin orbital ($\alpha$ or β) and are antisymmetric under interchange. That is, when 2 rows (or 2 electrons)

of Ψ are swapped, the sign of its determinant changes, in accordance with the Pauli principle.[30] Additionally, the determinant will vanish for the case of 2 swapped electrons (rows) which have the same set of quantum numbers.

The variational integral can be solved in space spanned by a set of orthonormal, normalized basis functions, its solution depends on the initial guess for these orbitals as this guess is refined iteratively (i.e., the self-consistent field approach), and its solution will converge to an energy greater than or equal to the ground state energy of the system. Using the Born Oppenheimer approximation (neglecting nuclear motion)[30], the electronic Hamiltonian ($\hat{\mathbf{H}}$) becomes a sum of a one electron operator, $\hat{H}(i)$, and a two electron operator, v(i,j).

$$\hat{\mathbf{H}}(i) = -\tfrac{1}{2}\,\mathrm{grad}(i)^2 - \sum_A \frac{Z_A}{r_{i,A}}$$

$$v(i,j) = 1/r_{i,j}$$

The one electron operator is composed of a kinetic term and an electron-nuclear attractive term, respectively. The two electron operator is composed of two parts: 1) a coulombic operator gives the interaction of eectron one with the average charge distribution of the other electrons and is referred to as "Hartree Fock mean field theory", and 2) an exchange operator which arises from the antisymmetric requirement of the wavefunction and resembles the coulombic term, except it switches or exchanges the spin orbitals. The exchange operator does not have a classical analog.[30]

2.3 Density Functional Theory

Density functional theory (DFT) also uses a variational treatment to arrive at the ground state energy of a system using the electronic density (ρ(r)) as the variable function, g.

$$\rho(r) = \int \psi(r)^* \psi(r) dr$$

$$N = \int \rho(r) dr$$

This simplification reduces 3N coordinates (spatial) to N density terms ($\rho(r)$) where N is the number of electrons.[30] As a result, the computational cost for DFT calculations is lowered significantly due to its increased speed.[84]

In 1964, Hohenberg and Kohn[85] showed for an N electron system the external potential ($V(r)$) is unique and completely fixes the Hamiltonian, thus N and $V(r)$ determine all the molecular properties of the ground state.

$$V(r) = \int \psi(r)^* V(r) \psi(r) dr$$

The variational integral then becomes a functional of a variation function (the density).

$$E_v[\rho(r)] = \int V(r) \rho(r) dr + F[\rho(r)]$$

It follows the independent kinetic (T) and interaction terms (U_{ee}), in the Hamiltonian, $F[\rho(r)]$, are calculated in a straightforward fashion from the wave function, a functional of the density.[85]

$$T = -\tfrac{1}{2} \int \text{grad } \psi(r)^* \text{ grad } \psi(r) dr$$

$$U_{ee} = \tfrac{1}{2} \int \psi(r)^* \psi(r')^* (1/|r-r'|) \psi(r') \psi(r) dr$$

In addition, $V(r)$ is termed the external potential since it is produced by charges external to the system of electrons. DFT treats the nuclear coordinates as fixed causing $V(r)$ to depend only on the electronic coordinates (x,y,z).

In DFT, HF exchange is replaced by a more general expression composed of 2 parts, the exchange-correlation functional. The electron-electron interaction term (U) now includes

correlation. The correlation energy (E_{corr}) is defined as $E_{corr} = E_{HF} - E_{exact}$. The goal in DFT is to mix various amounts of HF exchange (along with other approximations for exchange) with terms dealing with correlation such that the difference between E_{HF} and E_{corr} is exactly the energy of the system (E_{exact}). Specifically, B3LYP theory involves a three-parameter hybrid exchange functional containing Slater exchange, 20% HF exchange, and Becke's 1988 gradient corrections (i.e. B3).[86] The LYP portion of this theory indicates the gradient-corrected functionals of Lee, Yang, and Parr are included to adjust for correlation.[87] The half-and-half functional, or BHandHLYP theory, also designed by Becke, includes 50% Slater exchange along with 50% HF exchange. Since BHandHLYP gives more accurate barrier heights and since B3LYP is more accurate for deriving energies of reaction[26], we included both B3LYP and BHandHLYP in this work.

2.4 Moeller-Plesset Perturbation Theory

Møller-Plesset theory (MP2), or Many Body Perturbation Theory[30], is a post-Hartree Fock treatment that corrects the HF energy with a second-order correction term. The unperturbed HF Hamiltonian ($\hat{H}_o$) is extended by adding a small perturbation (V) where λ is an arbitrary parameter and controls the size of the perturbation. This perturbation represents the difference between the true molecular electronic Hamiltonian and the HF Hamiltonian.

$$\hat{H} = \hat{H}_o + \lambda V$$

If the perturbation is sufficiently small both the wave function and the energy can be expressed as a power series in λ

$$\Psi = \lim_{n \to 2} \sum^{n} \lambda^i \Psi^i$$

$$E = \lim_{n \to 2} \sum^{n} \lambda^i E^i$$

Substitution of these series into the time-independent Schrodinger equation gives[83]

$$(\hat{H}_o + \lambda V)(\sum_i^2 \lambda^i \Psi^i) = (\sum_i^2 \lambda^i E^i)(\sum_i^2 \lambda^i \Psi^i)$$

After equating like coefficients in λ, the solution of this equation to zeroth order (in λ) gives an energy which is the sum of the orbital energies (E^o for an unperturbed wave function). This solution to first order gives the HF energy ($E^o + E^1$) and a first-order perturbed wave function (Ψ^1). This solution to second order is the MP2 energy and corrects the HF energy with one term (E^2)

$$E^2 = \langle \Psi_n^{o*} | V | \Psi_n^1 \rangle$$

using the complex conjugate of the unperturbed HF wave function, the perturbation, and the first-order HF perturbed wave function.[83]

The second order energy correction term becomes more familiar after one finds an expression for the first order corrected wavefunction, Ψ_n^1, and substitutes it into the above equation. The first order corrected wave function is derived from (i) a first order perturbation expansion of the wave function Ψ_n (and eigenvalues) followed by (ii) equating terms in λ^1.

$$(H_o - E_n^o)\, \Psi_n^1 = (E_n^1 - V)\, \Psi_n^o$$

Multiplication by Ψ_m^o (a complex conjugate) and substitution for the conjugate transpose of a Hermitian matrix (H_o) gives

$$(E_m^o - E_n^o) \langle \Psi_m^o | \Psi_n^1 \rangle = E_n^1 \langle \Psi_m^o | \Psi_n^1 \rangle - \langle \Psi_m^o | V | \Psi_n^o \rangle$$

The first order correction to the energy, E_n^1, may be obtained[83] (which is also the HF energy) when m=n.

$$E_n^1 \delta_{mn} = = \langle \Psi_m^o \left| V \right| \Psi_n^o \rangle$$

For the other case of m≠n,

$$E_m^o - E_n^o \langle \Psi_m^o \left| \Psi_n^1 \right\rangle = - \langle \Psi_m^o \left| V \right| \Psi_n^o \rangle$$

one needs an expression for the first order corrected wavefunction. A first order corrected wave function Ψ_n^1 may be expressed as a linear combination of coefficients and unperturbed wave functions.

$$\Psi_n^1 = \sum_m a_m \Psi_m^o$$

and whose molecular orbital coefficients are

$$a_m = \langle \Psi_m^o \left| \Psi_n^1 \right\rangle$$

$$(E_m^o - E_n^o)\, a_m = - \langle \Psi_m^o \left| V \right| \Psi_n^o \rangle$$

$$a_m = \frac{\langle \Psi_m^o \left| V \right| \Psi_n^o \rangle}{E_n^o - E_m^o}$$

gives a first order corrected wave function which can be substituted into the E^2 expression, defined earlier.

$$\Psi_n^1 = \sum_m a_m \Psi_m^o = \sum_m \frac{\langle \Psi_m^o \left| V \right| \Psi_n^o \rangle}{E_n^o - E_m^o} \Psi_m^o$$

Since a_n is undefined in the former expression, $a_n = \langle \Psi_n^o \left| \Psi_n^1 \right\rangle = 0$ is set to zero using a condition called *intermediate normalization.* [83] Intermediate normalization requires one assume

the unperturbed wave function is normalized ($\langle \Psi_n^o | \Psi_n^o \rangle = 1$) and the perturbed wavefunction is not normalized ($\langle \Psi_n^o | \Psi_n \rangle = 1$) such that the sum of their product is 1.

$$\langle \Psi_n^o | \Psi_n \rangle = \langle \Psi_n^o | \Psi_n^o \rangle + \lambda^1 \langle \Psi_n^o | \Psi_n^1 \rangle + \; = 1$$

The previous normalization condition for the unperturbed wave function is repeated when the correction terms $\langle \Psi_n^o | \Psi_n^1 \rangle = 0$ are orthogonal. Substitution of Ψ_n^1 into the second order energy correction term (E^2)

$$E^2 = \sum_m \frac{\langle \Psi_m^o | V | \Psi_n^o \rangle \langle \Psi_n^o | V | \Psi_m^o \rangle}{E_n^o - E_m^o} \qquad m \neq n$$

and using the Hermitian nature of the perturbation V,

$$E^2 = \sum_m \frac{| \langle \Psi_n^o | V | \Psi_m^o \rangle |^2}{E_n^o - E_m^o}$$

the second order energy correction term becomes more familiar in terms of unperturbed wave functions and their energies.[83]

2.5 Configuration Interaction Theory

Configuration Interaction (QCISD(T)) is also a post-HF treatment.[30] Recalling when the first 2 electron system (helium) is expanded in terms of a zeroth-order wavefunction and in the absence of correlation in the Hamiltonian, the energy of this system is in error by 38%, relative to the sum of its 2 ionization energies.[83] After helium's zeroth-order energy is corrected to first order by considering correlation containing one excitation, the energy of this system is in error by only 5.3%. This means when excitations are included in the wave function the energy of a

system will begin to converge to its exact value. Practically, a wave function cannot contain an infinite number of terms, however, CI addresses this issue by expanding the wave function in terms of 2 or more parameters such that mixing from other excited electronic configurations occurs and accounts for the correlation energy. For example, a wave function of 2 variables may expanded by holding one variable fixed (x_2) where the expansion coefficients (a_i) are functions of x_2 .

$$\Phi(x_1,x_2) = \sum a_i(x_2) X_i(x_1)$$

Next, the expansion coefficients are expanded,

$$a_i(x_2) = \sum b_{ij} X_j(x_2)$$

and substituted into the original expression.

$$\Phi(x_1,x_2) = \sum b_{ij} X_i(x_1) X_j(x_2)$$

a process which can be extended for an N electron system

$$\Phi(x_1,x_2, \ldots, x_N) = \sum_{ij\ldots N} b_{ij\ldots N} X_i(x_1) X_j(x_2) \ldots X_N(x_N)$$

where $x_1,\ldots,x_N$ represent the spin and spatial coordinates of each electron and $X_1,\ldots,X_N$ represent the spin orbitals.

The Configuration Interaction (QCISD(T)) method writes the N electron basis functions, Φ, as substitutions or "excitations" from the Hartree-Fock "reference" determinant[30],

$$|\Psi\rangle = c_o |\Phi_o\rangle + \sum_{ra} c_a^r |\Phi_a^r\rangle + \sum_{a<b,r<s} c_{ab}^{rs} |\Phi_{ab}^{rs}\rangle + \sum_{a<b<c,r<s<t} c_{abc}^{rst} |\Phi_{abc}^{rst}\rangle$$

i.e. where $|\Phi_a^r\rangle$ represents the Slater determinant formed by replacing the occupied spin orbital a in $|\Phi_o\rangle$ with a virtual (or unoccupied) spin orbital r. The Configuration Interaction space in this work has been truncated at a triples' excitation level as to make these calculations tractable. Every N electron Slater determinant may be described by a set of N spin orbitals from which it is formed, and this set of orbital occupancies is termed a "configuration". The great strength of the Configuration Interaction method lies in its ability to include excited states in its application and thus give rise to energetics of open-shell systems displaced somewhat from their equilibrium geometries.

2.6 Potential Energy Surfaces

A plot of energy versus one or more reaction coordinates (degrees of freedom) for a molecule creates a potential energy surface (PES).

A minimum structure is located in the bottom of a valley on a PES, and from such a point motion in any direction leads to a higher energy. The first derivative of the energy (the gradient) for a minimum structure will be zero in all directions, and its force constants (or the second derivatives, k) as a result will each be greater than zero such that the curvature of the PES in all directions from this point are concave up.[82]

A transition structure (TS) is also a stationary point on a potential energy surface described by a zero gradient and a force constant matrix (the Hessian) which contains one negative value. These two considerations define a simple saddle point or TS. This means a TS is a local maximum along one and only one vector while being a local minimum in all other orthogonal directions. The vector associated with the direction which contains the maxima is termed the transition vector and is the eigenvector associated with the negative eigenvalue (ν).[82]

$$\nu = (1/2\pi)(k/\mu)^{1/2}$$

An activation energy (E_{act}) is defined as the minimum energy necessary for a reaction to occur and is mathematically expressed as

$$E_{act} = E_{TS} - E_{reactant}$$

In this work the energy of a transition state (E_{TS}) was found using several techniques. For unimolecular decomposition reactions, coarse relaxed PES scanning was employed which involves stretching one degree of freedom in a structure while plotting the energy. For the bimolecular reactions, van der Waals' reactant and product minima[88] were located prior to performing a coarse two-dimensional scan thus reducing the amount of computations needed to locate the TS. Once a maxima was located coarse scanning became complete, and a more refined scanning approach was undertaken.

The Synchronous Transit-Guided Quasi-Newton (STQN) method[82], integrated into the Gaussian suite of programs by Schlegel et al[89] is a transition state seeking procedure and requires input structures which lie near the quadratic, maximum region of a PES. Two input structures (reactant and product geometries) are required for the QST2 form of this method; three (reactant, product, and TS structures) are required for its QST3 form.

2.7 Choosing a Framework Model Chemistry

Initially, a synthesis reaction where 2 chlorophenoxy radicals combine to yield a dichloro-diketodimer was studied using 3 quantum chemical methods: Hartree-Fock (HF), Density Functional Theory (B3LYP), and Many-Body Perturbation Theory (MP2) and 2 basis sets (6-31G(d,p) and 6-31++G(d,p)). Table 1 contains the non-zero point corrected energetics (ΔErxn) for the above reaction in terms of theory versus basis set. Energies are given in kcal-mol^{-1}. The U- and R- prefixes refer to unrestricted or restricted wave functions[30], respectively.

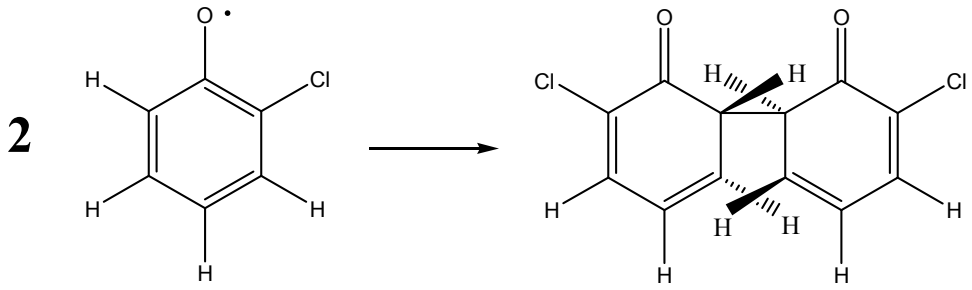

Figure 4: Two chlorophenoxyl radicals combine to form a dichlorodiketodimer.

Table 1: Reaction energies for the above synthesis reaction as a function of theory versus basis set.

Theory/Basis Set	6-31G(d,p)	6-31++G(d,p)
ROHF/RHF	-22.45	-20.58
B3LYP	-10.32	-7.87
UMP2	-78.29	-80.54
ROMP2	-28.56	NA

Given the Hartree Fock method does not contain any electron correlation (HF wave functions only satisfy the antisymmetry requirement of the Pauli principle when the wave function vanishes for 2 electrons with the same spin and spatial coordinates) and given previous DFT theoretical studies' results qualitatively order experiment values well, the less computationally expensive and faster DFT methods (relative to MP2 methods), were employed in the following calculations. The smaller 6-31G(d,p) basis set was chosen as the addition of diffuse basis functions (via 6-31++G(d,p)) was not necessary to qualitatively order the results.

Møller-Plesset theory (UMP2) was also dismissed due to its spin contamination, i.e. second-order corrected energetics are typically erroneous for systems with an unpaired electron.[90] Evidence of UMP2 spin contamination is observed for the doublet *ortho*-

chlorophenoxyl radical when one compares its expectation value for $\hat{S}^2$ with the other methods (Table 2). The Restricted Open-Shell MP2 (ROMP2) calculation maintains a fixed spin state for the chlorophenoxyl radical ($\hat{S}^2 = S(S+1) = 0.75$).

Table 2: $\hat{S}^2$ results for the 2-chlorophenoxyl radical as a function of theory and basis set.

Theory/Basis Set	6-31G(d,p)	6-31++G(d,p)
Hartree-Fock	0.75	0.75
B3LYP	0.79	0.79
UMP2	1.30	1.29
ROMP2	0.75	0.75

CHAPTER 3. GAS-PHASE REACTION OF HYDROXYL RADICAL AND MOLECULAR CHLORINE*

3.1 Reaction Rate Measurements

All rate constant determinations for Reactions 1-3:

$OH\bullet + Cl_2 \rightarrow$ Products (Reaction 1)

$OH\bullet + CH_4 \rightarrow$ Products (Reaction 2)

$OH\bullet + C_3H_8 \rightarrow$ Products (Reaction 3)

were studied using Pulsed Laser Photolysis-Pulsed Laser Induced Fluorescence (PLP-PLIF) and pseudo-first order conditions[88] ($[Cl_2]$, $[CH_4]$, $[C_3H_8] >> [OH\bullet]$). Previous investigations of the rate coefficient for Reaction 1 have not exceeded 354 K[11-15] As a result the uncertainty in the temperature dependent portion (E_{act}/R) of the rate constant is relatively large.[11] We have undertaken this study over an extended temperature range (231 to 826 K) in order to improve on the accuracy of previously determined rate coefficients for this reaction.

To firmly establish the rate coefficient for Reactions 1-3, experiments must be conducted with very low initial concentrations of OH• such that secondary reactions are minimized. Initial OH• radical concentrations in the detection zone were in the range of $1.0x10^{10} – 3.0x10^{11}$ molecules/cm^3, at least two orders of magnitude smaller than the lowest molecular substrate concentration. Initial OH• concentrations were estimated using the UV absorption coefficient of N_2O (ε)[91], our experimental evaluation of the absorption cross-section of N_2O (at 193 nm and different temperatures), the stoichiometry given in the photolysis mechanism of N_2O, and the

laser intensities (I) before and after filling the reactor with N_2O. I_o is obtained under conditions when $[N_2O] = 0$; I is obtained when $[N_2O]$ is non-zero. We used the Beer-Lambert law[88]

$$\ln(I/Io) = -\varepsilon nl$$

which becomes

$$(I_o - I) = I_o (\varepsilon nl)$$

when $\varepsilon nl << 1$. The energy absorbed by N_2O after filling the reactor with N_2O is $(I_o - I)$ or ΔE_{abs}. The number of photons absorbed by N_2O then is

$$\frac{\Delta E_{abs}}{h\upsilon} = \frac{I_o (\varepsilon nl)}{h\upsilon} = \text{number of absorbed photons by } N_2O$$

The number of absorbed photons is assumed equal to the number of N_2O molecules which have been excited. Each excited N_2O molecule produces 2 OH• radicals according to the photolysis mechanism.

$$N_2O + h\upsilon\ (193\ nm) \rightarrow O(^1D) + N_2$$

$$O(^1D) + H_2O \rightarrow 2\ OH\bullet$$

As a result, the initial concentration of OH• radicals is somewhat overestimated and must be understood as an upper limit for $[OH\bullet]_o$. The PLP-PLIF technique has excellent sensitivity to OH• (detection limit < 10^{11} molecules/cm^3), allowing one to make rate measurements with the necessary low initial concentrations.[24]

The temporal profile of OH• in the reactor was monitored by measuring its LIF signal, S_{OH}, as a function of reaction time t. The LIF signal followed the first order differential equation:

$$-d[OH\bullet]/dt = (k_{bi}[X][OH\bullet] + k_d[OH\bullet]) = k'[OH\bullet]$$

$$d[OH\bullet]/[OH\bullet] = -k'dt$$

$$\ln [OH]_t/[OH]_o = -k't$$

$$\ln [OH]_t = -k't + \ln[OH]_o$$

$$k' = k_{bi}[X] + k_d$$

where X is the molecular substrate, k_{bi} is the bimolecular rate coefficient, k' is the effective first order rate coefficient ($k' = k_{bi}[X]+k_d$), and k_d is the first order rate coefficient for loss of OH• in the absence of X due to reaction with impurities in the bath gas (He) and diffusion out of the detection zone. Slow-flow conditions were employed in order to minimize k_d. The effective first order rate coefficient, k', for Reaction 1 was found by plotting ln S_{OH} vs time (sec) (Graph 1).

Graph 2 displays isothermal least squares lines through data where the concentration of Cl_2 is constant. The bimolecular rate constant, k_{bi}, was determined from the slope of the least squares lines drawn through the k' versus [X], including the point (0, k_d).

The first order rate coefficient, k_d, for loss of OH• due to secondary reactions and diffusion out of the detection zone was derived from an OH• temporal profile in the absence of the molecular substrate. For each set of experiments the difference between the value of k_d measured in the absence of the molecular substrate (see line1 in Graph 1) and k_d found from the intercept of the least squares line in ([X], k') coordinates (see Graph 2) was small when compared to the experimental uncertainty in k_d. A typical initial reaction time of not less than 0.2 ms followed each photolysis pulse and was assumed sufficient for allowing complete

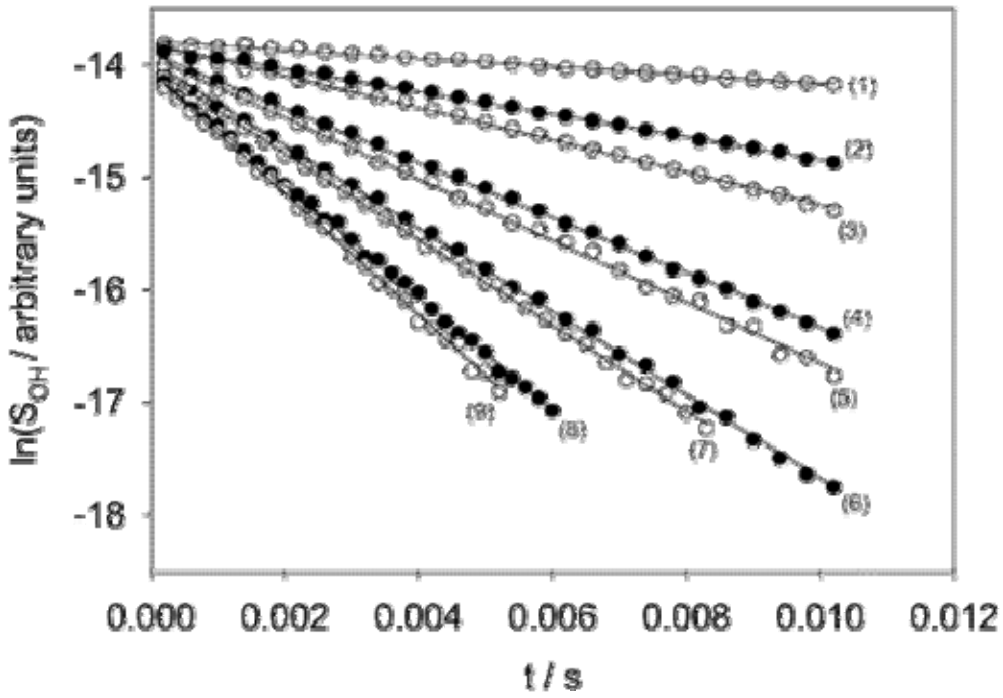

Graph 1: Examples of relative OH• temporal profiles obtained under the following conditions: He buffer gas, total pressure P=20.10 kPa (150.8 torr), temperature T=365K, $[N_2O]=3.8x10^{13}$ cm^{-3}, $[H_2O]=1.59x10^{15}$, $[X]=[Cl_2]= 0.0, 5.11x10^{14}, 9.09x10^{14}, 1.54x10^{15}, 1.76x10^{15}, 2.38x10^{15}, 2.52x10^{15}, 3.42x10^{15}, 3.75x10^{15} cm^{-3}$ for profiles 1-9, respectively.

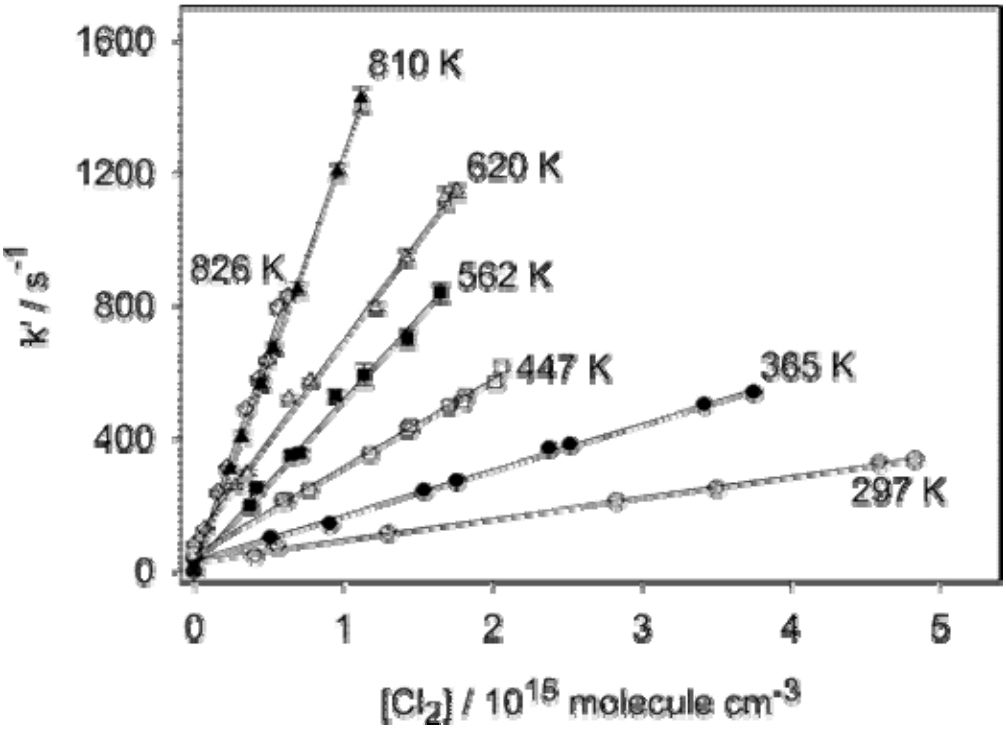

Graph 2: Examples of experimentally obtained k' vs $[Cl_2]$ dependences.

vibrational and rotational relaxation of excited OH• radicals into a Boltzmann type distribution[92] while minimizing the time for OH• radicals to diffuse outside the detection zone.

$$\frac{n_j}{n_i} = e^{-\Delta E/kT} \quad \text{where} \quad \Delta E = E_j - E_i$$

$$\frac{n_j}{n_t} = \frac{e^{-\Delta Ej/kT}}{\Sigma_j e^{-\Delta Ei/kT}}$$

Previous studies[93-97] have determined the rate coefficient for the following reaction

$$OH\bullet + CH_4 \rightarrow \text{Products} \qquad \text{(Reaction 2)}$$

using PLP-PLIF and similar experimental conditions with experimental temperature regions that overlap. We also studied Reaction 2 in order to validate our experimental technique. We find excellent agreement between our results and determinations of other researchers. In addition, Tully and Ravishankara[97], Tully and Dunlop[96], and Vovelle et al.[95] use a three-parameter expression[98] to fit their measured rate coefficients well. Graph 3a displays curves for Reaction 2 (k' versus $[CH_4]$) prepared in the same manner as for Reaction 1.

We studied Reaction 3 in order to validate our experimental technique as well.

$$OH\bullet + C_3H_8 \rightarrow \text{Products} \qquad \text{(Reaction 3)}$$

Reaction 3 was chosen due to its relatively fast reaction rate, as compared to Reaction 2. Previous studies[99-101] have determined the rate coefficient for Reaction 3, and our measurements of k' versus $[C_3H_8]$ are given in Graph 3b. We observe excellent agreement between our results and the determinations of other researchers with respect to Reaction 2 and 3.

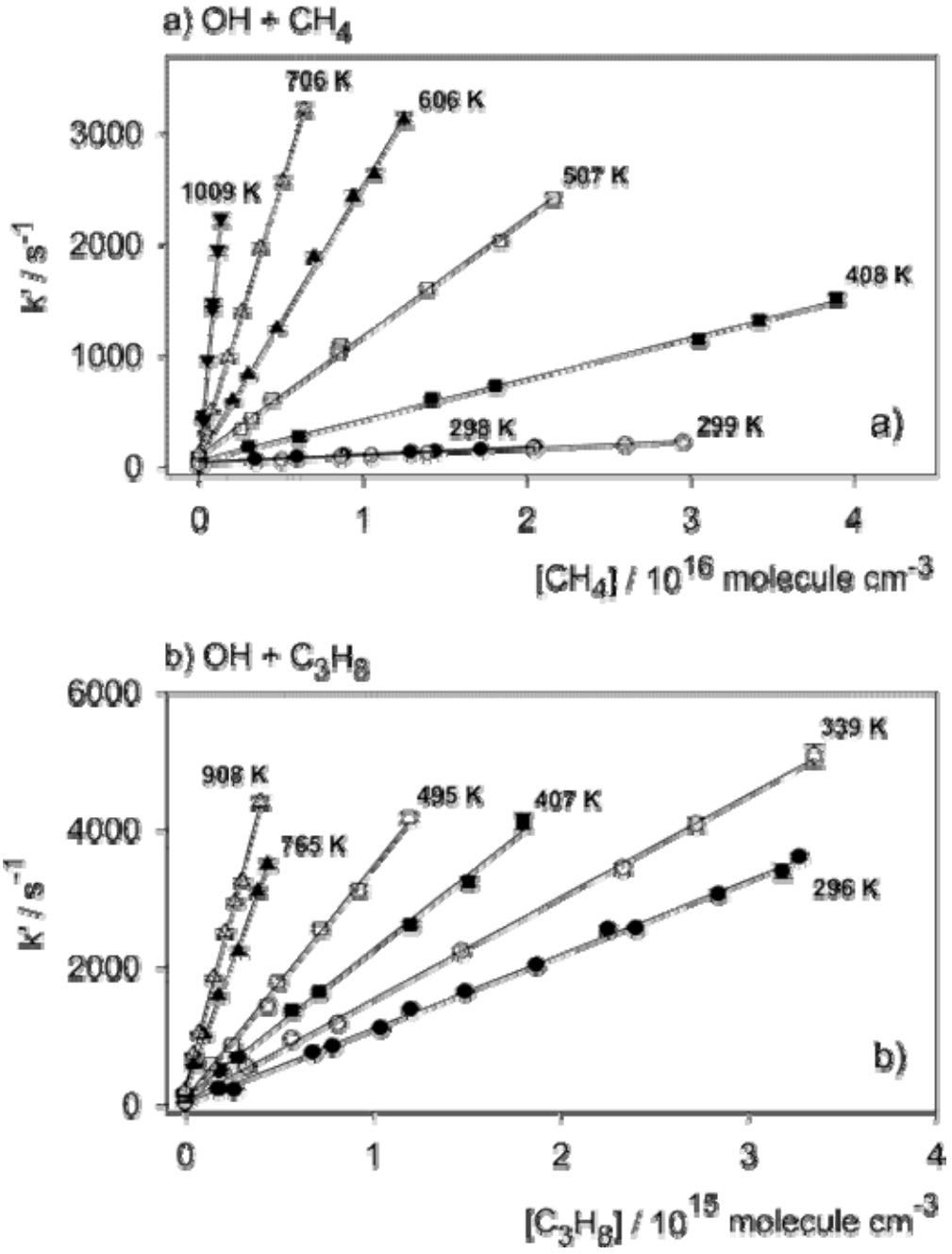

Graph 3: Examples of experimentally obtained k' vs $[CH_4]$ (part a) and k' vs $[C_3H_8]$ (part b) dependences.

3.2 Experimental

A schematic of the experimental apparatus and the optical test cell (reactor) are depicted in Figures 5a and b, respectively. This experimental system is similar to the one described in

reference 102. The PLP-PLIF system contains a dual laser system for generating and probing OH• radicals, an electronic time delay system between the lasers, a heating system for the reactor, a gas delivery system, and a photo-multiplier tube (PMT) for signal detection. The dual laser system consisted of an ArF excimer laser (Lambda Physik: Compex 102) and a Nd:YAG (Quanta Ray: DR-2a) pumped, frequency-doubled, tunable pulsed dye laser (Quanta Ray: PDL-3) which were employed to generate the pump and probe beams, respectively.

Pulsed, unfocused 193 nm radiation (10Hz pump frequency) from the excimer laser was passed through two iris diaphragms (D_1 and D_2), through a fluorescence-free UV fused silica window (W_1), and into a quartz tubular six-way cross where photolysis takes place. The pump (photolysis) beam was responsible for creation of the hydroxyl radicals.

Hydroxyl radicals were produced by photolyzing N_2O/ H_2O.[103] The photolysis mechanism can be described as

$$N_2O + h\upsilon\ (193\ nm) \rightarrow O(^1D) + N_2$$

$$O(^1D) + H_2O \rightarrow 2\ OH\bullet$$

where $h\upsilon$ is the photonic energy for laser photolysis to break the bond between N_2O. Excited $O(^1D)$ atoms result and rapidly react with water producing OH•.

In the presence of CH_4 or C_3H_8, OH• radicals may also be formed by reaction of $O(^1D)$ with these substrates. In selected high temperature (T>750K) experiments the initial OH• concentration was produced from the direct photolysis of water only

$$H_2O + h\upsilon\ (193\ nm) \rightarrow OH\bullet + H\bullet$$

to avoid possible effects from the thermal decomposition of N_2O at high temperatures. The OH• concentrations were found to be independent of the method of OH• generation. It should be added however exact knowledge of the initial OH• concentration is not needed for rate coefficient determination, due to pseudo-first order conditions and the experimental technique.

After the pulse of the excimer laser, the pulse of the probe laser causes excitation of the hydroxyl radicals. OH• was excited at approximately 282 nm via the $A^2\sum^+ \leftarrow X^2\prod$ ($1\leftarrow0$) transition followed by observation of fluorescence from the (1-1) and (0-0) bands at 308-316 nm, respectively. Fluorescent radiation was monitored using a photomultiplier tube (Electron Tubes Limited: P10N-01W) and a UV bandpass filter (308 nm peak transmission) to reduce scattered light. The signal from the PMT was amplified (Electron Tubes Limited: Transimpedance Amplifier A1) and recorded by an oscilloscope (Textronic TDS 714L Digitizing Oscilloscope). The oscilloscope was triggered when the probe beam signal was received by photodiode, Ph1. The oscilloscope allows one to obtain an averaged integrated voltage across for a desired number of laser pulses (typically 150) in one time delay. The signal, S(t), received from the voltage signal is the sum of two components: the fluorescence of excited OH• radicals, S_{OH}, and the scattered light, S_{SC}. The averaged integrated voltage for Ssc was measured directly in the absence of OH•. For this measurement the pump laser was not triggered during the accumulation of scattered light. Kinetic information (OH• temporal profiles) was obtained by varying the time delay between pulses of the pump and the probe lasers in the desired time interval. We used a pulse generator (Stanford Research Systems DG535 Digital Delay/Pulse Generator) to trigger the excimer laser and the Nd:YAG laser with different time delays. Photodiodes (Ph1, Ph2) were used to measure and calibrate the time delay between pulses.

The typical limits of integration (for the best signal-to-noise ratio, S_{OH}/S_{SC}) were 180 and 860 ns after the probe laser pulse.

Pulsed, unfocused radiation (10 Hz probe pump frequency) from the probe laser was directed using two flat laser (UV enhanced, aluminum coated) mirrors (M_1 and M_2), passed through two iris diaphragms (D_3 and D_4), and passed through a fluorescence-free UV fused silica window, (W2) which was placed at a Brewster angle into the detection zone of the optical test cell.

A program was written using *Visual Basic 6.0* for gathering the OH• temporal profile automatically. Kinetic data S(t) values with corresponding reaction time delays t were collected in the computer for subsequent data processing. S*sc* was found not to vary from experiment to experiment (at 100 ms) and was subtracted from S(t) at all reaction time delays and one fixed concentration of molecular substrate in order to obtain a relative OH• concentration temporal profile.

$$S_{OH} = S(t) - Ssc.$$

The systematic uncertainty in the experimentally obtained S_{OH} values (deviation from linearity) was defined using characteristics of the accuracy stated by the manufacturers for the photomultiplier, amplifier, and oscilloscope. The maximum of the systematic deviation of the OH• concentration detection system from linearity has been estimated as 3.0%.

The program controlled both pulse generation (the pulse generator) and data collection (the oscilloscope) through a GPIB port (National Instruments). The program prompts the user for data input such as 1) the number of points, 2) averaging for each point, 3) time steps between points, and 4) number of repetitions of the kinetic curve obtained for each concentration of molecular substrate. Kinetic data was collected in a computer for subsequent data analysis. S_{SC}

was subtracted from S(t) measured at different reaction time delays and one fixed concentration of molecular substrate in order to extract the signal, $S_{OH}(t)$. The detection sensitivity of OH• radicals ranged from $1x10^8 – 5x10^8$ molecules/cm^3 depending on averaging, pressure, temperature of the detection zone, and concentration of the molecular substrate.

Helium (He) was used as the carrier gas in this work. Four separate gas flow metering devices were used to prepare the reaction gas mixtures (He, N_2O/He, H_2O/He, X). The flow of N_2O/He ranged from 1:200 - 1:1000; the flow of H_2O/He was prepared by bubbling He through water vapor at a pressure and temperature controlled with a thermo-stabilized saturator (maintained at a temperature of ~2K below ambient temperature). Three calibrated mass-flow controllers (Sierra Instruments, Inc. Model 810C) with appropriate flow ranges provided stable gas flows. We checked each gas flow by measuring the rate of pressure increase in a calibrated volume located immediately before the optical test cell (reactor). The pressure measurements were performed with capacitance manometers (MKS Instruments Model 626A13TAE, range 1000 torr or Model 622A12TAD, range 100 torr.installed with a Type 660B Power Supply/Digital Readout; precision of the readings is 0.01 torr). The detected instability in the sum of the gas flows did not exceed 2%. The flow of molecular substrate, X, was regulated with a metering valve (Swagelok Type SS-SS4). The flow of X was also determined after measuring the rate of pressure increase in a calibrated volume before and after each OH• temporal profile was obtained. The difference in these measurements did not exceed 3% for each OH• temporal profile. An arithmetic average of these two measurements (before and after) was taken in order to calculate the molecular substrate concentration in the reaction zone. The independence of the measured flows on the surface-to-volume ratio of the calibrated volume was verified to ensure the absence of interference from heterogeneous absorption and desorption processes on the walls

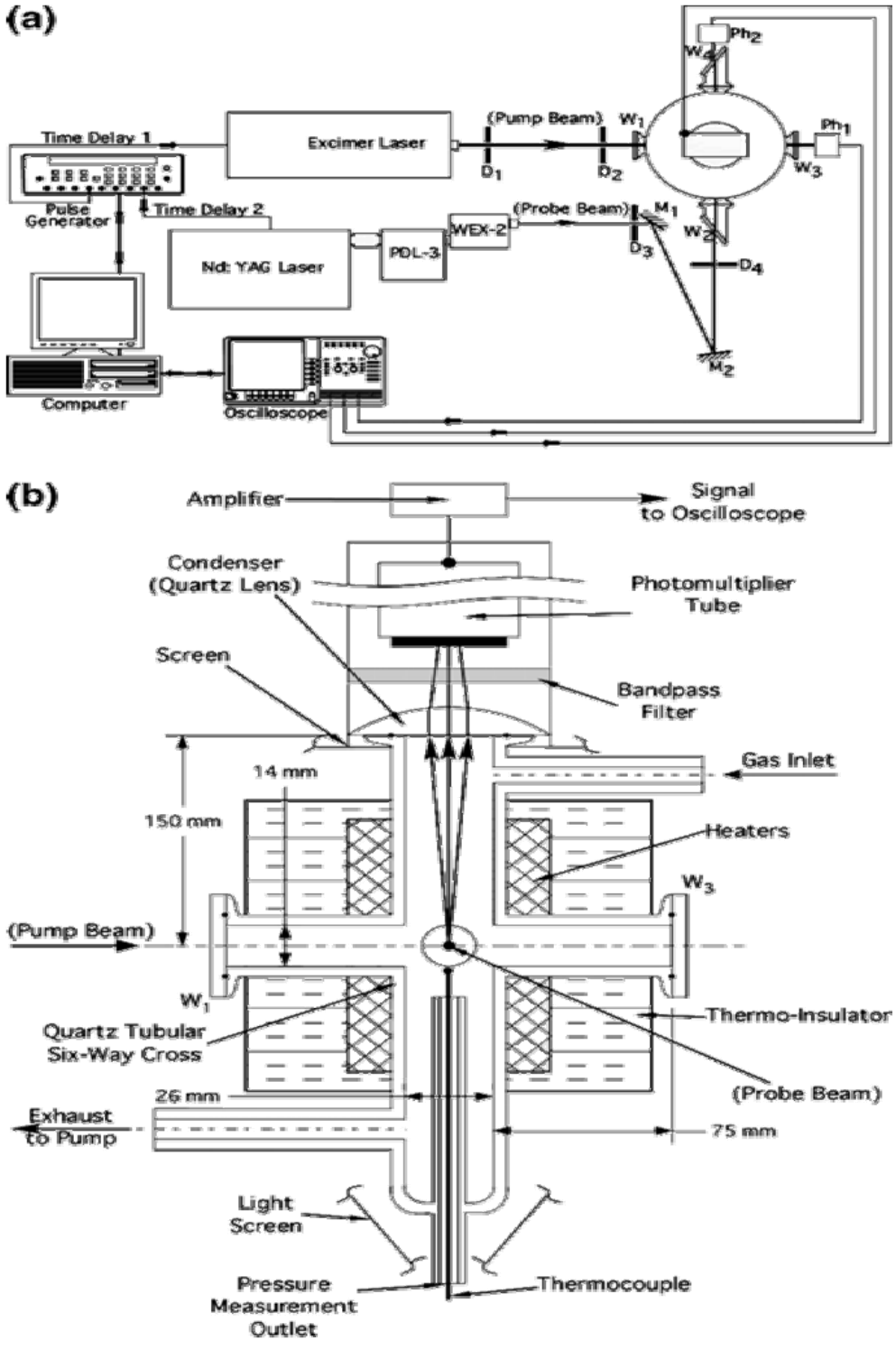

Figure 5a: Schematic drawing of the experimental apparatus. 5b. Two-dimensional schematic drawing of the optical test cell (reactor). The probe beam is perpendicular to the plane of the figure and intersects the pump (photolysis) laser beam in the center of the reactor.

of this volume. All flows were pre-mixed prior to flow through the reactor. The total flow ranged from 5.0 to 25 cm^3/sec at standard temperature and pressure. The value of the total flow was adjusted depending on the total pressure and temperature in the reaction zone in order to ensure slow-flow conditions, i.e. each photolysis pulse initiated reaction within a locally fresh gas mixture eliminating potential complications that might result from accumulation of photolysis or reaction products. The composite flow conditioned the reactor for several minutes prior to data collection, thereby minimizing any effects due to reactant adsorption on the reactor walls and stabilizing the established experimental conditions. The maximum systematic uncertainty in the ratio of the measured flow of X/total flow has been evaluated at 1.5% of this value.

Pressure in the reactor was monitored with capacitance manometers described earlier. A pressure measurement inlet (see Figure 1b) was located on the main axis, ~15 mm downstream from the photolysis zone in the quartz tubular six-way cross. The pressure difference between the pressure measurement inlet and the static pressure in the detection zone was negligible. We installed a large deviation pressure control system downstream of the reactor to keep the total gas pressure constant in the detection zone. This pressure controlling system consisted of a manually regulated needle valve (Swagelok SS-1KS8) along with an electrical servo-valve (Edwards DM20) controlled by pressure (Edwards 1501C). This system allows one to maintain a stable pressure in the detection zone.

The reactor was resistively heated. A heater, a thermo-insulator, 2 temperature controllers (series CN77000), and two Chromel-Alumel thermocouples were supplied by Omega Engineering, Inc. The first 0.813 mm diameter thermocouple was fixed on the main axis, ~5 mm downstream from the photolysis zone (see Figure 1b). The temperature field

inside the heated zone with the desired temperature in the detection zone was measured (calibrated) with the second movable 0.508 mm diameter thermocouple and referenced to the readout of the first. The uniformity of the temperature field in the reactor did not vary more than $\pm$2 Kelvin. The maximum total uncertainty in the measurements of the reaction temperatures did not exceed 0.5% and was considered a systematic source of error based on the $\pm$2K variations revealed during calibration and experiment.

The concentration of each reactant in the reaction zone was calculated by multiplying three values: 1) the total concentration of all molecules in the reaction zone (derived from measured pressure and temperature using the ideal gas law), 2) the partial concentration of reactant in the flow, and 3) the ratio of the flow carrying the reactant to the total gas flow. The concentration of water in the flow was found using the vapor pressure of water (as a function of temperature and pressure) and an assumption that He had been completely saturated with water while passing through the bubbler. Typical reaction mixtures were (in molecules/cm^3):

N_2O	$(3.6x10^{12} – 1.5x10^{14})$ or 0.0
H_2O	$4.0x10^{14} – 2.1x10^{15}$
He	$5.06x10^{17} – 3.99x10^{18}$
Cl_2	$0.0 – 5.07\ x10^{15}$
CH_4	$0.0 – 3.89\ x10^{16}$
C_3H_8	$0.0 – 3.49\ x10^{15}$

The chemicals used in this study had the following minimum stated purities (and were supplied by): (1) He, 99.999% (BOC Gases), (2) Cl_2, 99.999% (Matheson), (3) CH_4, 99.999% (Matheson), (4) C_3H_8, 99.993% (Matheson), (5) N_2O, 9.98% mixture of 99.99% purity in 99.999% He (BOC Gases), (6) H_2O, ACS Reagent Grade (Aldrich). Helium was further purified by passing it through liquid N_2 cooled traps. Analyses of Cl_2, CH_4,

and C_3H_8 samples detected only trace levels of impurities, and these small concentrations had a negligible effect on the observed OH• decay rates.

3.3 Results

The kinetic study of OH• radicals with Cl_2, CH_4, and C_3H_8 was performed in the following temperature and pressure ranges:

	Temperature(K)	Pressure(kPa)
Reaction 1: OH• + Cl_2	297-826	6.70-21.46
Reaction 2: OH• + CH_4	298-1009	6.71-24.15
Reaction 3: OH• + C_3H_8	296-908	6.68-24.13

The initial concentration of OH• varied as a result of varying the photolyzing excimer laser intensity and the concentration of the photolyte, N_2O. Experimental conditions and results for Reactions 1-3 along with calculated rate coefficients are given in Tables 3 and 4.

The rate coefficients demonstrate independence with respect to pressure and the initial OH• concentration. This pressure independence was expected as the mechanism of Reactions 1-3 involves atom abstraction, i.e. the number of molecules in the reaction mixture remains constant over time. The rate coefficient independence with respect to the initial OH• concentration indicates the absence of any influential secondary reactions, as can be expected by the low values of $[OH•]_o$ ($1.0x10^{10}$-$3.0x10^{11}$ molecules/cm^3). Similarly, the observed absence of any correlation between the measured rate coefficients and the photolysis laser intensity indicates the potential effects of reactions between OH• and photolysis products (from the substrates) are negligible. At the highest temperatures

used in this study (in Reaction 1), the absence of effects from the potential decomposition of Cl_2 was verified by measuring the rate coefficient at different pressures and bulk flow velocities.

Temperature dependences of the rate coefficients for Reactions 1-3 are presented in Arrhenius coordinates (1000/T, log k) in Graphs 4 and 5. Due to the curvature in each

Table 3: Conditions and Results of Experiments to Measure Rate Coefficients of the Reaction of OH• with Molecular Chlorine (Reaction 1).

$OH\bullet + Cl_2 \rightarrow$ Products

No.[a]	T/K	P/kPa	$[Cl_2]$ range/ 10^{14} molecule cm^{-3}	I^b/mJ $pulse^{-1}$ cm^{-2}	$[OH]_o/10^{10}$ molecule cm^{-3}	$k_1{}^c/10^{-14}$ $molecule^{-1}$ cm^3 s^{-1}
1	297	13.41	4.84-50.7	13	30	6.25±0.31
2	297	13.40	4.05-48.3	2.6	6.0	6.38±0.21
3	330	6.70	4.58-41.7	12	19	9.25±0.67
4	330	6.72	4.63-33.1	2.8	4.4	9.28±0.26
5	365	20.10	5.11-37.5	11	9.6	13.72±0.44
6	404	13.41	3.05-49.1	11	17	19.72±0.33
7	404	13.40	3.11-19.1	2.6	4.0	19.00±0.38
8	447	13.41	5.94-20.6	11	12	26.32±0.96
9	447	13.41	5.93-20.7	2.6	2.8	25.2±1.3
10	501	13.41	3.71-43.5	11	7.0	35.7±1.7
11	501	13.42	3.21-20.2	11	7.3	36.9±2.3
12	562	6.70	3.76-16.5	12	4.3	49.7±3.0
13	562	6.70	3.79-16.3	12	4.3	50.7±4.0
14	620	13.40	2.78-17.6	4.3	5.9	60.3±2.6
15	620	13.39	3.18-16.8	12	16	59.0±3.6
16	719	13.42	1.44-10.1	13	19	87.1±4.0
17	719	13.42	1.43-10.7	2.6	3.8	87.7±5.0
18	810	10.74	2.4-11.2	10	16	125.8±2.5
19	810	10.74	2.39-11.1	2.1	3.4	124.7±7.4
20*	825	10.73	1.19-5.68	13	3.8	131.0±7.9
21*	825	21.46	3.79-10.9	13	7.6	121.5±4.1
22*	826	13.39	0.71-6.3	12	4.4	131.3±6.9

[a] Experiment number. $[N_2O] = 0$ was in experiments marked with *. [b] Photolysis laser intensity. [c] Error limits represent 2□ statistical uncertainties only. Maximum estimated systematic uncertainty is 5% of the rate coefficient value.

Table 4: Conditions and Results of Experiments to Measure Rate Coefficients of the Reactions of OH• with Methane (Reaction 2) and Propane (Reaction 3).

$OH + CH_4 \rightarrow$ Products (Reaction 2)

No.[a]	T/K	P/kPa	$[CH_4]$ range/ 10^{15} molecule cm^{-3}	I^b/mJ $pulse^{-1}$ cm^{-2}	$[OH]_o/10^{10}$ molecule cm^{-3}	$k_2{}^c/10^{-15}$ $molecule^{-1}$ cm^3 s^{-1}
1	298	13.46	3.41-20.5	11	6.1	6.48±0.19
2	298	13.43	3.51-20.7	3.6	2.0	6.29±0.34
3	299	13.43	5.04-29.5	11	27	6.75±0.12
4	299	13.43	5.11-29.9	4.1	10	6.78±0.14
5	341	6.71	5.86-18.7	10	8.5	15.19±0.57
6	341	6.71	6.05-19.1	2.6	2.2	15.22±0.62
7	408	13.43	3.02-38.9	10	7.7	36.7±1.2
8	408	13.43	3.00-38.1	4.3	3.3	37.1±1.3
9	507	13.43	2.55-21.6	12	7.3	108.5±3.7
10	507	13.43	2.56-21.7	3.3	2.0	106.9±3.6
11*	606	24.15	2.05-12.5	13	2.5	243.7±8.7
12	706	13.41	0.422-6.47	13	11	482±12
13	706	13.41	0.427-6.41	3.3	2.9	481.9±7.5
14*	807	13.43	0.121-4.00	14	3.2	803±19
15*	908	13.41	0.271-2.70	11	16	1246±42
16*	908	13.41	0.271-2.70	2.6	3.8	1232±43
17*	961	6.71	0.333-1.26	13	6.3	1421±43
18*	1009	21.46	0.230-1.33	11	12	1687±72
19*	1009	21.46	0.236-1.33	3.6	3.8	1670±62

(table continued)

OH + C_3H_8 → Products (Reaction 3)

No.[a]	T/K	P/kPa	$[C_3H_8]$ range/ 10^{14} molecule cm^{-3}	I[b]/mJ $pulse^{-1}$ cm^{-2}	$[OH]_o/10^{10}$ molecule cm^{-3}	k_3[c]/10^{-12} $molecule^{-1}$ cm^3 s^{-1}
1*	296	12.07	3.78-20.3	8.6	1.0	1.083±0.055
2	296	12.01	1.73-32.7	13	3.7	1.081±0.024
3	339	12.09	3.28-33.5	13	6.7	1.487±0.034
4	339	12.09	3.25-39.4	4.1	2.1	1.453±0.044
5	407	6.71	1.86-18.0	12	2.1	2.156±0.092
6	495	12.05	1.34-11.9	8.9	2.7	3.37±0.15
7	605	6.71	1.17-4.69	4.8	2.4	4.91±0.22
8	705	12.05	0.460-2.88	13	3.0	6.65±0.20
9	765	6.68	0.453-4.39	14	7.7	7.41±0.30
10	765	6.68	0.482-3.83	4.8	2.6	7.37±0.38
11	805	24.13	0.498-3.65	13	2.7	8.37±0.20
12*	908	12.05	0.429-4.00	12	15	10.23±0.31
13*	908	12.05	0.408-4.12	2.9	3.6	10.36±0.19

[a] Experiment number. $[N_2O] = 0$ was in experiments marked with *.[b] Photolysis laser intensity.[c] Error limits represent 2σ statistical uncertainties only. Maximum estimated systematic uncertainty is 5% of the rate coefficient value.

Arrhenius plot, the temperature dependence of the rate constant was modeled using the generalized three-parameter expression.[98] Deviation from linearity occurs in a two-parameter

$$k(T) = A\ T^{\alpha}\ \exp^{(-Eact/RT)}$$

Arrhenius expression when activation energy is a function of temperature.

$$k = A \exp(-E_{act}/RT)$$

$$y = \ln k = \ln A - E_{act}/RT = \ln A - E_{act}(x)/R \qquad \text{where } x = 1/T$$

$$y' = dy/dx = d \ln k/d(1/T) = -E_{act}/R$$

$$E_{act} = -R\,(dy/dx) = -R\ d \ln k/d(1/T)$$

$$y'' = d^2 \ln k/d(1/T)^2 = (-1/R)(dE_{act}/d(1/T)) = T^2 dE_{act}/RdT = \delta T^2 \text{ where } \delta = dE_{act}/RdT$$

If E_{act} increases with temperature ($dE_{act}/dT>0$) the plot of ln k versus 1/T will appear concave up. If E_{act} decreases with temperature ($dE_{act}/dT<0$) the plot of ln k versus 1/T

will appear convex down. As a consequence, one can see the curvature (or sign of the second derivative, y") in a 2-parameter Arrhenius expression is a function of the first derivative of activation energy with respect to temperature and whose magnitude is also controlled by the T^2/R term.

The three parameter expression, $k(T) = AT^{\alpha}exp^{(-Eact/RT)}$, follows from statistical mechanical approach.[92] Using a canonical ensemble, the total internal energy for a linear or non-linear system can be expressed in two equivalent forms

$$\langle E \rangle = \Sigma E_j(V,N)\exp(-\beta E_j(V,N))/Q \text{ where } Q = \Sigma\exp(-\beta E_j(V,N))$$

and it follows

$$\langle E \rangle = kT^2(\partial \ln Q/\partial T)_{N,V} = NkT^2(\partial \ln q/\partial T)_V$$

after all the independent, indistinquishable particles' contributions q (translational, rotational, vibrational, and electronic) in the system partition function Q are included, operated upon, and summed in the above expression. N is the number of particles (N=moles N_a). Once these operations are complete, one may arrive at the total internal energy of 1 mole ($N/N_a=1$) system ($R=N_ak$).

$$\langle E \rangle = \frac{3RT}{2} + \frac{3RT}{2} + \left[\frac{R\theta_v}{2} + \frac{R\theta_v}{(\exp(\theta_v/T)-1)}\right] - N_aD_e$$

Beginning from the left, $\langle E \rangle$ represents the average internal energy for a system, 3RT/2 represents the average translation energy, 3RT/2 represents the average rotational energy (for a non-linear system), the third term represents the zero-point vibrational energy where θ_v is the vibrational temperature (hv/k), and the fourth term is the electronic energy

relative to zero (2 separated atoms resting at their ground states). Taking the first derivative of the above expression with respect to temperature for the transition state (≠), the 2 reactants (A and B), and substituting these 3 equations into the first derivative (let $x= \theta_v/T$) gives

$$\frac{dE_{act}}{dT} = \left[3R/2 + 3R/2 + R\Sigma\left[\frac{x^{\neq 2}\exp^{x\neq}}{(\exp^{x\neq}-1)^2}\right]\right] - \left[3R/2+R+R\Sigma\left[\frac{x^{2A}\exp^{xA}}{(\exp^{xA}-1)^2}\right]\right] - \left[3R/2 + R+R\Sigma\left[\frac{x^{2B}\exp^{xB}}{(\exp^{xB}-1)^2}\right]\right]$$

$$dE_{act}/dT = -2R + R\sum^{3(4)-6}\left[\frac{x^{\neq 2}\exp^{x\neq}}{(\exp^{x\neq}-1)^2}\right] - R\sum^{3(2)-5}\left[\frac{x^{2A}\exp^{xA}}{(\exp^{xA}-1)^2}\right] - R\sum^{3(2)-5}\left[\frac{x^{2B}\exp^{xB}}{(\exp^{xB}-1)^2}\right]$$

when a non-linear transition state and diatomic reactants are used, as is the case for Reaction 1 ($OH\cdot + Cl_2 \rightarrow$)

For the case of low temperature and high frequencies, the vibrational terms each approach zero ($\exp^x >> 1$), and

$$dE_{act}/dT = -2R < 0, \quad \text{convex down}$$

Alternatively, for the case of high temperature and low frequencies, the vibrational terms each approach one, and

$$dEact/dT = -2R + R(6-1-1) = 2R > 0, \quad \text{concave up}$$

The positive curvature seen in Graphs 4 and 5 reveals Reactions 1-3 are described by activation energies which are increasing with temperature.

$$\delta = dE_{act}/RdT > 0$$

If δ is considered to be independent of temperature, then integration of

$$d^2 \ln k/d(1/T)^2 = \delta T^2 = \delta/(1/T)^2$$

yields a three parameter expression for k(T).[98]

$$\ln k(T) = -E_{act}/T + a - \delta \ln (1/T)$$

$$-\delta \ln (1/T) = \ln T^{\delta}$$

$$k(T) = A\ T^{\delta} \exp^{(-Eact/T)}$$

As a result, points (1000/T, ln k) in Graphs 4 and 5 were fit to the previous expression

$$y = \ln k(T) = \ln A + \delta \ln T - E_{act}/T$$

$$y = \ln k(T) = \ln A_1 + A_2 \ln(1000/x) - A_3\ (x/1000)$$

with a non-linear curve fitting algorithm[104] using three free parameters where A_1 is the Arrhenius parameter (A), A_2 is the temperature exponent (δ), and A_3 is the energy of activation (E_{act}) divided by R. The rate coefficients with their corresponding temperature ranges for Reactions 1-3 then become

Reaction 1: $k = 3.59 \times 10^{-16}\ T^{1.35} \exp^{(-745K/T)}\ cm^3\ molecule^{-1}\ sec^{-1}$ (I)

Reaction 2: $k = 3.82 \times 10^{-19}\ T^{2.38} \exp^{(-1136K/T)}\ cm^3\ molecule^{-1}\ sec^{-1}$ (II)

Reaction 3: $k = 6.64 \times 10^{-16}\ T^{1.46} \exp^{(-271K/T)}\ cm^3\ molecule^{-1}\ sec^{-1}$ (III)

The maximum deviation of the individual experimental rate coefficients from their complementary curve-fitted expressions was 7.0% (Reaction 1), 4.8% (Reaction 2), and 2.5% (Reaction 3).

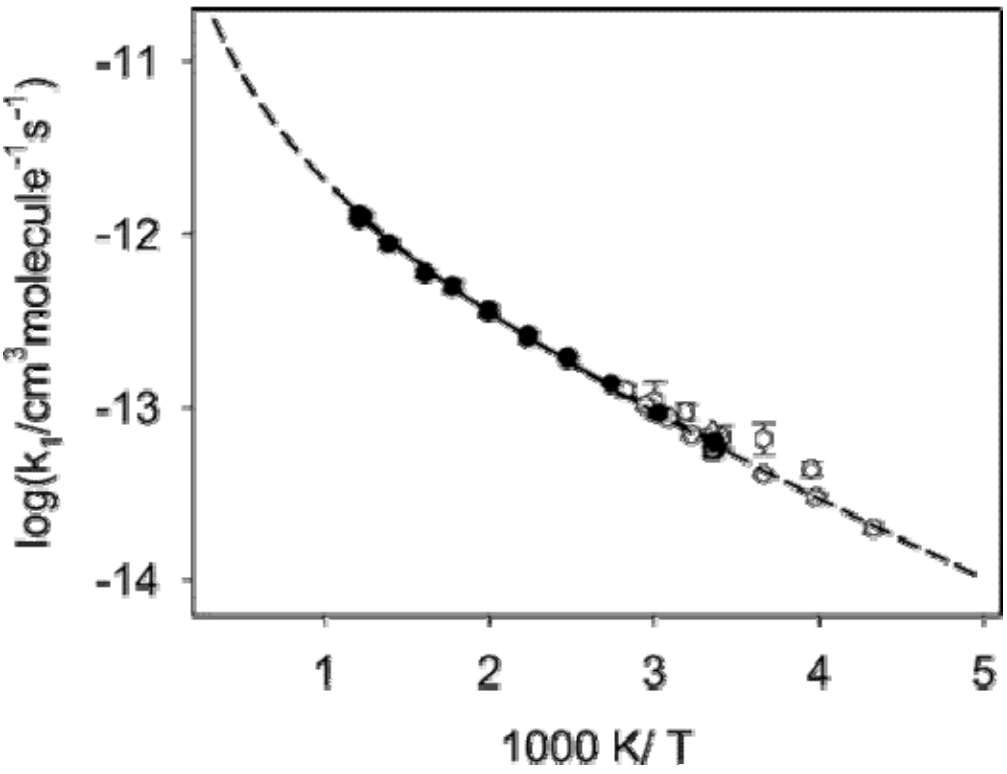

Graph 4: Temperature dependence of the rate coefficient for Reaction 1 displayed in Arrhenius coordinates. Closed circles represent the current experimental data; open squares represent reference 12; open triangle up represents reference 15; open diamonds represent reference 14; open hexagons represents reference 13; open circles represents reference 11. The solid line represents the modified Arrhenius fit of equation I; the dashed line represents equation VI found in reference 105.

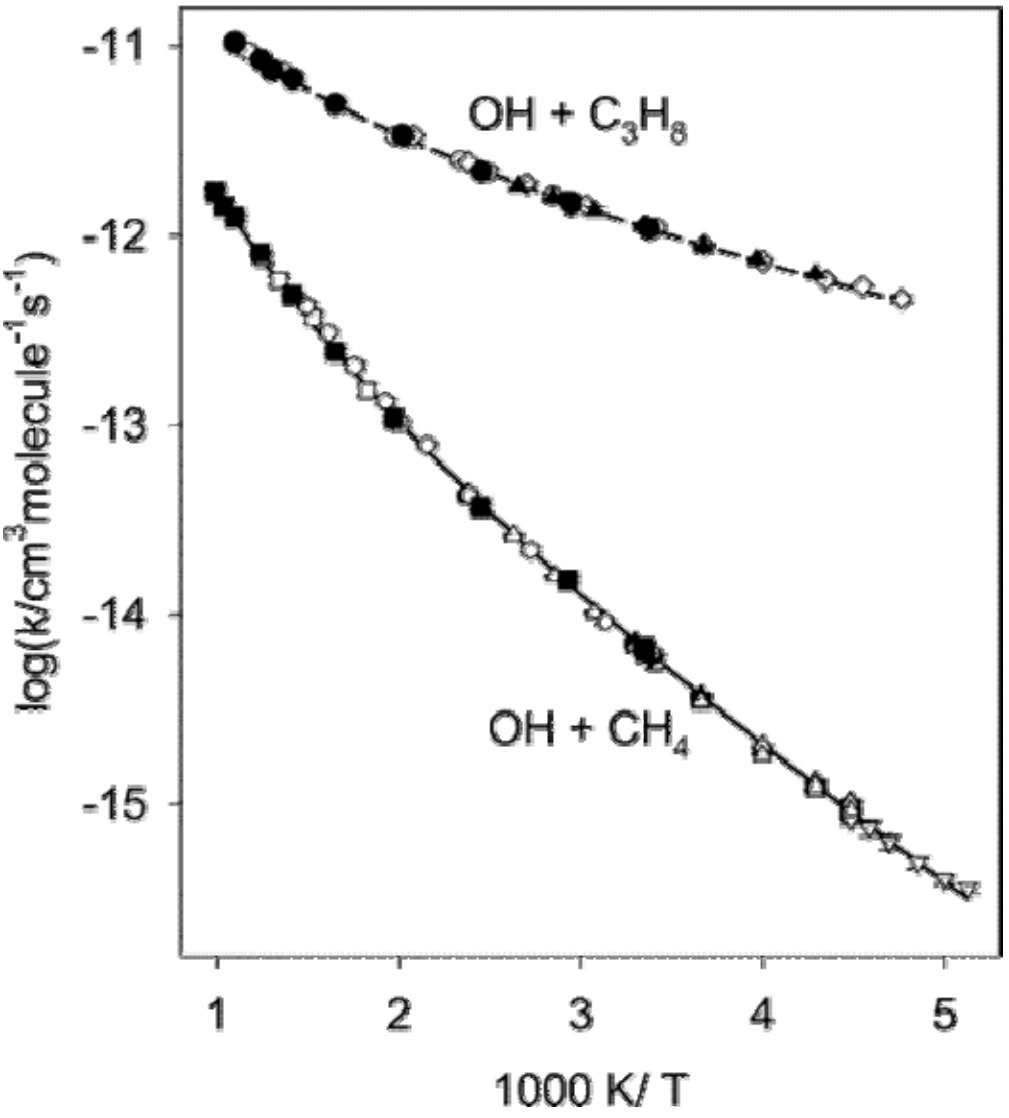

Graph 5: Temperature dependences of the rate coefficients for Reactions 2 and 3 displayed in Arrhenius coordinates. Reaction 2 ($OH\cdot+CH_4\rightarrow$): Closed squares represent the current experimental data; open triangles up represent reference 93; open squares represent reference 96; open triangles down represent reference 94; open hexagons represent reference 95; the solid line represents the result of the fit of the current experimental data only (equation II). Reaction 3 ($OH\cdot+C_3H_8\rightarrow$): closed circles represent the current experimental data; open circles represent reference 99; closed triangles up represent reference 100; open diamonds represent reference 101. The dashed line represents the result of the fit of the current experimental data only (equation III).

Sources of error in the measured experimental parameters such as error in the total flow rate, the flow rate of the molecular substrate, ratios of the calibrated volumes, pressure, temperature, reaction time, and signal values were separated into statistical and systematic sources of error using experimental observations. The evaluation of potential systematic error was based on the finite accuracies given with each calibrated, certified piece of equipment. The uncertainties for the measured experimental parameters were propagated to the final value of the uncertainty in k(T) using the following generic expression for propagation of error.[106]

$$Q = f(q_1, q_2, \ldots, q_n)$$

$$dQ = (\partial f/\partial q_1)\Delta q_1 + (\partial f/\partial q_2)\Delta q_2 + \ldots + (\partial f/\partial q_n)\Delta q_n$$

Assuming the partial derivatives are independent of one another, fractional percent (dQ/Q) systematic uncertainty was approximated by summing the squared contributions, taking the square root of the sum, and dividing by Q. The systematic uncertainty reaches a maximum of 5% of the rate coefficient values. The error limits of the experimentally obtained rate coefficients reported in Tables 1 and 2 were found with a 95% level of confidence and represent two standard deviations (random) of uncertainty only.

3.4 Thermodynamics and Potential Energy Surface Study

- **Thermodynamics**

Reaction 1 has the potential for exhibiting diverse behavior through a multiplicity of product channels. They are:

$OH\bullet + Cl_2 \rightarrow HCl + OCl\bullet$ (Reaction 1a)
$OH\bullet + Cl_2 \rightarrow HOCl + Cl\bullet$ (Reaction 1b)
$OH\bullet + Cl_2 \rightarrow H\bullet + OCl_2$ (Reaction 1c)

Table 5 provides non-zero point corrected reaction energies (ΔE_{rxn}) and enthalpies (ΔH_{rxn}) for Reactions 1a-1c calculated with B3LYP/6-31G(d,p). Energetic units are given in kcal mol^{-1}.

Table 5: Energies and Enthalpies of Reaction for Reactions 1a-1c using B3LYP/6-31G(d,p). Energetic quantities in parentheses were derived using the NIST Computational Chemistry Comparison and Benchmark Database and an identical model chemistry.[107] Enthalpies of reaction in brackets were derived using experimentally determined gas phase thermodynamic data from the NIST Chemistry WebBook database.[108]

Reaction	ΔE_{rxn}	ΔH_{rxn}
1a	-9.19 (-9.19)	-9.89 [-7.19]
1b	-4.19 (-4.19)	-2.34 [1.87]
1c	62.58 (62.58)	58.84 [63.78]

The potential energy surface (PES) of Reaction 1a was chosen for study initially given this reaction is thermodynamically favored.

- **Potential Energy Surface Study**

An attempt was made to locate a transition state (a PES saddle point) for the reaction channel which leads directly to HCl + OCl• (products) from OH• + Cl_2 (reactants). In these calculations a two-dimensional PES scan (Cl-Cl and O-H, starting from the reactant van der Waals minima) and a three-dimensional scan (Cl-Cl, O-H, and O-Cl, starting from the reactant van der Waals minima) at the BHandHLYP/6-31G(d,p) level were performed. The searched-for transition state could not be found. These scans both produced a ridge without a saddle point separating the reactant and the product van der Waals minimums.

Given the earlier mentioned PES scan revealed a transition state does not lie between the reactant and product van der Waals minimums with respect to Reaction 1a, a different approach using BHandHLYP/6-31G(d,p) and QCISD(T)/6-31G(d,p) was undertaken. Two dimensional scanning with respect to Reaction 1b located an energy barrier (TS1) and two shallow van der

Waals minima on both the reactant (VDW1) and the product (VDW2) sides of the barrier (-3.4 kcal relative to the reactants and -2.5 kcal relative to the products).

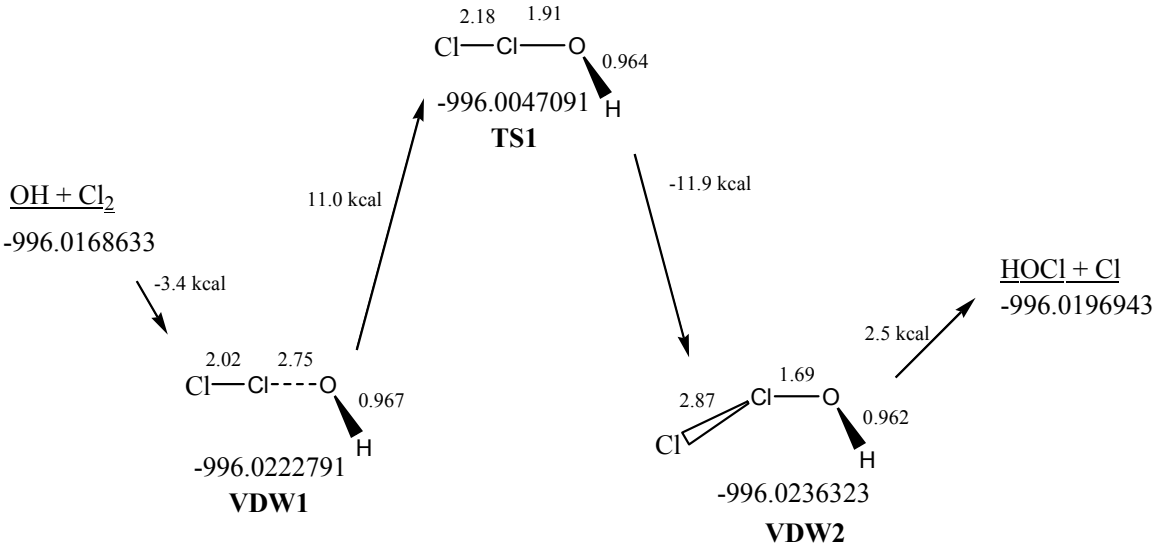

Figure 6: Potential energy surface for Reaction 1b using BHandHLYP/6-31G(d,p). Energies for each structure are given in hartrees.

The energy barrier height (7.6 kcal mol^{-1} above the reactants) is overestimated with BHandHLYP/6-31G(d,p) as can be seen by comparing this value with the 2.8 kcal mol^{-1} experimental activation energy obtained when the experimental k(T) dependence is fit with a two-parameter Arrhenius expression. The use of the higher level QCISD(T)/6-31G(d,p) model chemistry reduces the barrier height to more realistic value of 5.4 kcal mol^{-1}.

Table 6: Activation and reaction energies (kcal mol^{-1})[a] for Reaction 1b using BHandHLYP/6-31G(d,p) and QCISD(T)/6-31G(d,p).

Model Chemistry	Transition State, TS1	HOCl + Cl•
BHandHLYP/6-31G(d,p)	7.6	-1.8
QCISD(T)/6-31G(d,p)	5.4	-7.2

[a]Energies (non zero-point corrected) are relative to the reactants, OH• + Cl_2.

A reaction path leading from the product van der Waals minima (VDW2 in Figure 6) to HCl + OCl• was found using BHandHLYP/6-31G(d,p). This path (in Figure 7) leads from VDW2, through products HOCl + Cl•, through a transition state (TS2), and through another van derWaals complex (VDW3) which resembles HCl + OCl• .

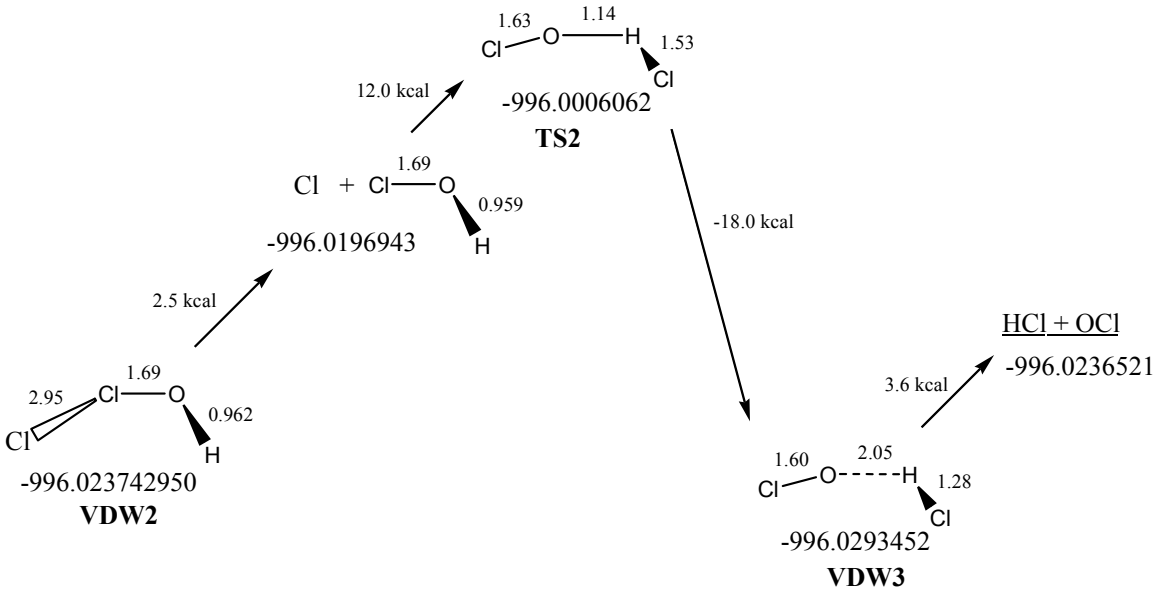

Figure 7: Potential energy surface for the pathway leading from HOCl + Cl• to HCl + OCl• using BHandHLYP/6-31G(d,p). Energies for each structure are given in hartrees.

The TS1 structure, in Figure 6, represents a tight transition state ($\Delta S^{\neq}<0$)[109] or a dynamic bottleneck for Reaction 1b. Further, chemical transformation of the van der Waals complex (VDW2) is expected to favor dissociation into HOCl and Cl• via consideration of its very large, loose nature and a positive ΔS for this step. In addition, the energy of tight transition state (TS2) in Figure 7 leading to HCl + OCl• is higher than that of the HOCl + Cl• products by 12.0 kcal mol^{-1} indicating the potential formation of the HCl + OCl• products can be neglected in the OH• + Cl_2 reaction.

CHAPTER 4. AB-INITIO STUDY OF THE FORMATION AND DEGRADATION REACTIONS OF SEMIQUINONE AND PHENOXYL RADICALS

4.1 Computational Procedures

Density Functional Theory (DFT) is a common computational procedure despite known deficiencies.[25, 26] DFT calculations have been previously used to study radical reactions[110-113] and have shown phenoxyl radical decomposition thermodynamics and activation barriers are in good agreement with experiment.[45] A variety of studies have demonstrated that DFT calculations can accurately reproduce the relative differences in bond dissociation energies between similar compounds. Studies of transition state properties have shown that the BHandHLYP[26, 114] level of theory is reasonably accurate. Therefore, calculations herein have used the B3LYP, BHandHLYP, and as a check on the quality of the DFT energies, QCISD(T)//BHandHLYP model chemistries. All calculations in this chapter were performed with the 6-31G(d,p) basis set. In this work, we are interested in the relative activation energies and reaction energies of a series of similar molecules and therefore have used different DFT model chemistries to assess the accuracy of our calculations. For a group of closely related compounds (e.g. substituted phenols) reliable differences in BDEs (ΔBDEs) can be carried out using calculated absolute E values due to the cancellation of error.[66] We compared B3LYP/6-31G(d,p), BHandHLYP/6-31G(d,p), and QCISD(T)/6-31G(d,p)//BHandHLYP/6-31G(d,p) for selected reactions (see Figure 8) and found that all 3 methods gave the same relative ordering of activation energies and reaction thermodynamics.

Stationary points were characterized as either a local minimum structure (no imaginary frequency) or a transition state (one imaginary frequency) by analytical evaluation of the Hessians. The energies used in the calculations are unscaled and zero-point corrected. The absolute enthalpies and free energies (as well as reaction enthalpies and free energies) are

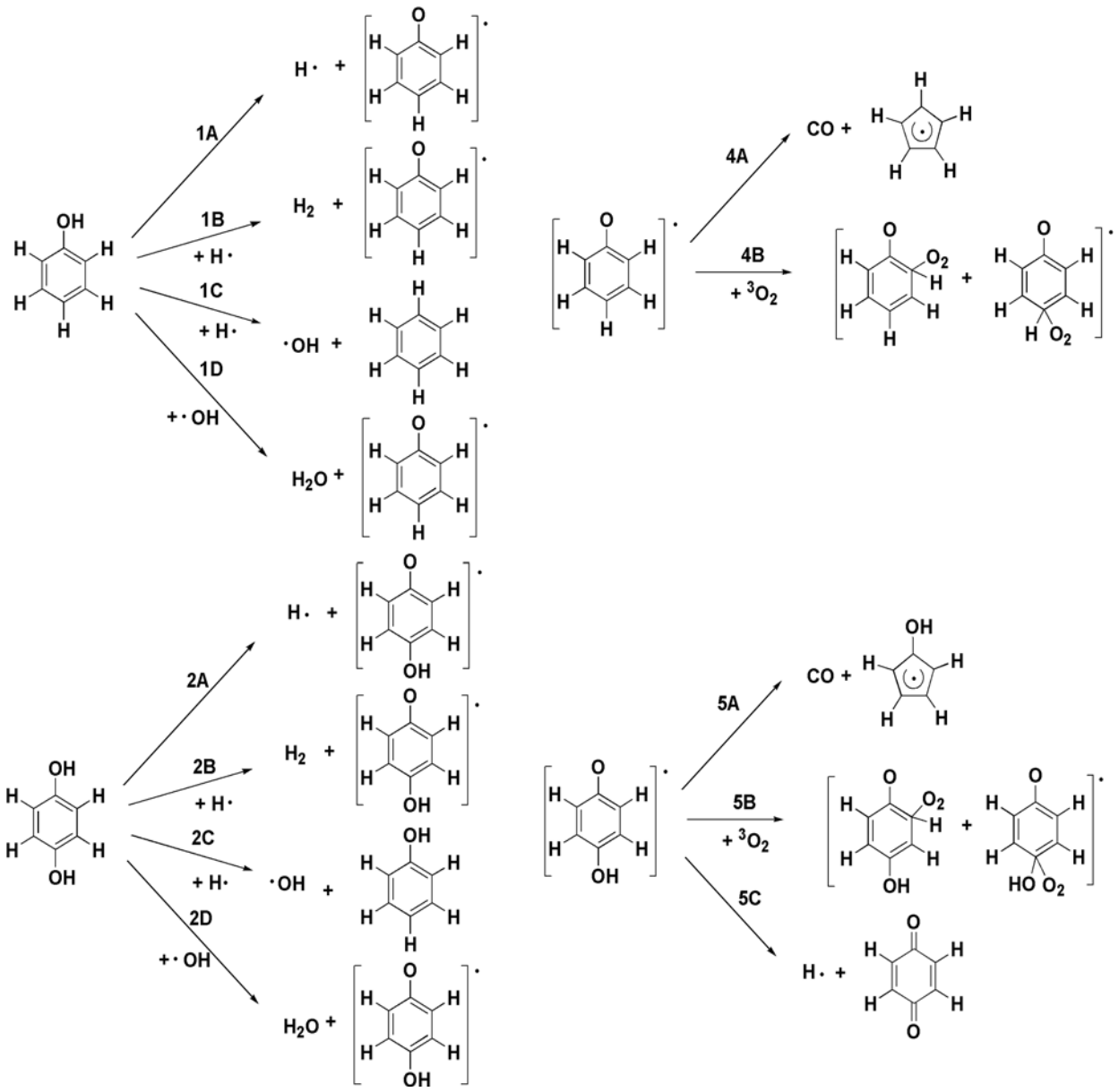

(figure continued)

Figure 8: Reactions of phenol, hydroquinone, catechol, phenoxyl radical, *p*-semiquinone radical, and *o*-semiquinone radical. The schemes on the left-hand side are the reactions of the parent molecular species, some of which form the radical. The schemes on the right-hand side include the decomposition and reaction with molecular oxygen of the resulting radical.

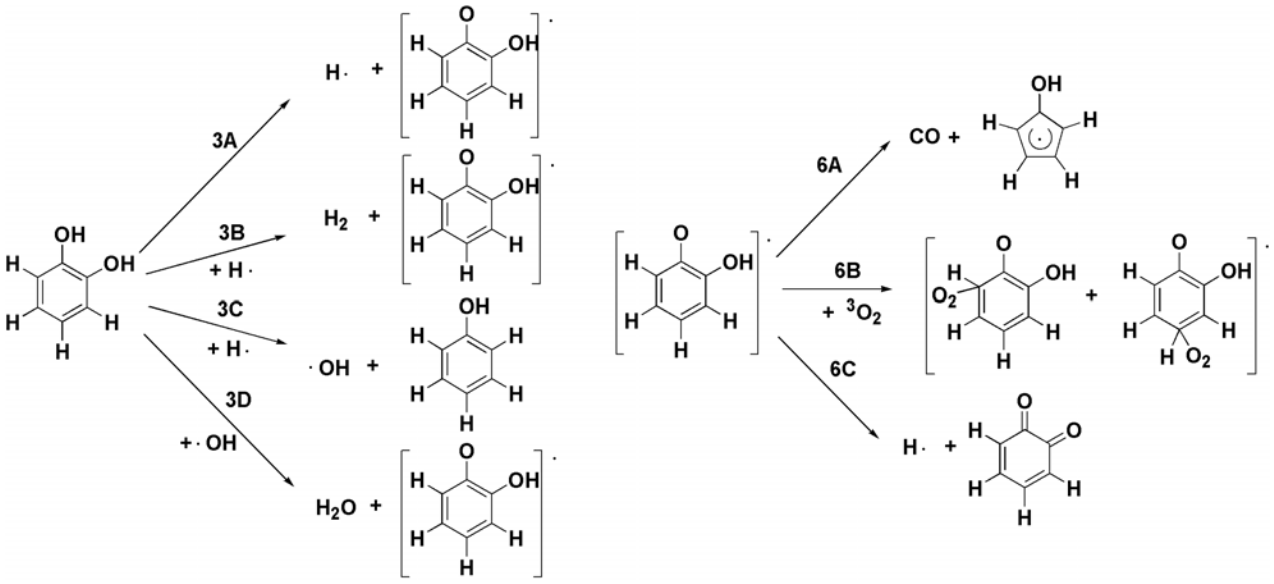

calculated at 298 K and 1 atmosphere of pressure and included both thermal effects and the effects of changes in molecularity. When more than one isomer for particular species existed, the most stable isomer was used in these calculations. Reaction energies (ΔE_{rxn}) were computed using the first law of thermodynamics[115]

$$\Delta E_{rxn} = \Sigma n E_{\text{products}} - \Sigma m E_{\text{reactants}}$$

where *n* and *m* are the coefficients in the balanced chemical equation.

Using BHandHLYP, the search for transition states for Channels 1A-3A, which form two radicals, were studied using unrestricted open-shell methods, using the GUESS=ALTER option in *Gaussian 03* to create the proper open-shell singlet state; no transition states could be found. Since we constrained the system to a singlet spin-state, our results are for adiabatic (fixed spin

state) reactions only (similarly for reactions 4B-6B and the reaction of the phenyl radical with triplet oxygen discussed below). A search for a triplet transition state for reactions 1A-3A yielded activation energies greater than the change in energy for the reaction and thus non-adiabatic reactions are unlikely to contribute significantly to the kinetics of these reactions.

The transition states for Channels 1D-3D were found by performing a two-dimensional scan of these reactions' surfaces. In each case, a van der Waals minimum was found on both the product and reactant sides of the transition state, and each transition state energy was very close, relatively speaking, to its van der Waals reactant minimum. IRC (Intrinsic Reaction Coordinate)[116] calculations were performed for each of these 3 transition states in the forward and reverse directions, and each IRC calculation confirms the transition state as valid. Below, Figure 9 depicts a two-dimensional contour plot for Channel 1D where the upper left and lower right corners are the van der Waals reactant and product minimums, respectively. Figure 10 depicts the absolute energies for each structure involved in determining the activation and reaction energies for this channel, and Figure 11 depicts the IRC calculated energies used for the confirmation of the Channel 1D transition state.

In all 3 cases (Channels 1D-3D), the energy difference between the transition state and its respective van der Waals reactant minima was less than or equal to 6.3 kcal/mol (BHandHLYP/6-31G(d,p) meaning the transition states for these reactions are more reactant-like than product-like (ΔE_{rxn} = -26.6 kcal/mole).

Transition states for Channels 4A-6A used a previous computational work[45] for phenoxyl radical decomposition as a model for the location of the rate-limiting transition state structure. In the first step of phenoxyl radical decomposition, its planar C_{2v} ground state (a global minimum)

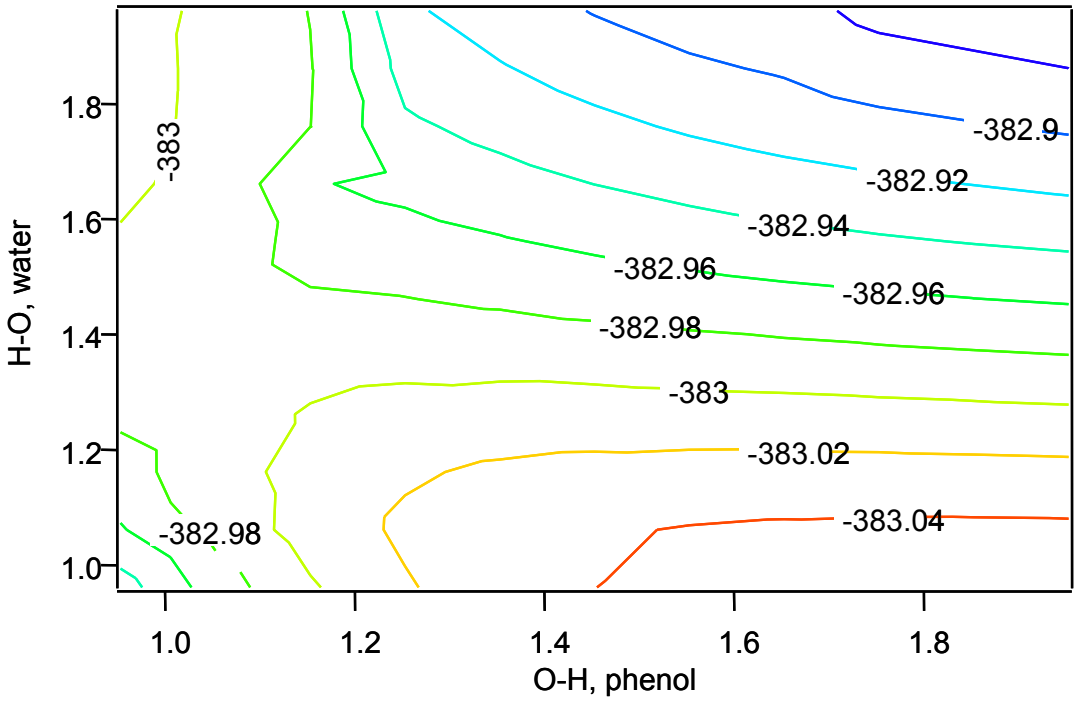

Figure 9: BHandHLYP contour plot for Channel 1D. The upper left and lower right corners represent the van der Waals reactant and product minimums, respectively.
Absolute energies are given in hartrees.

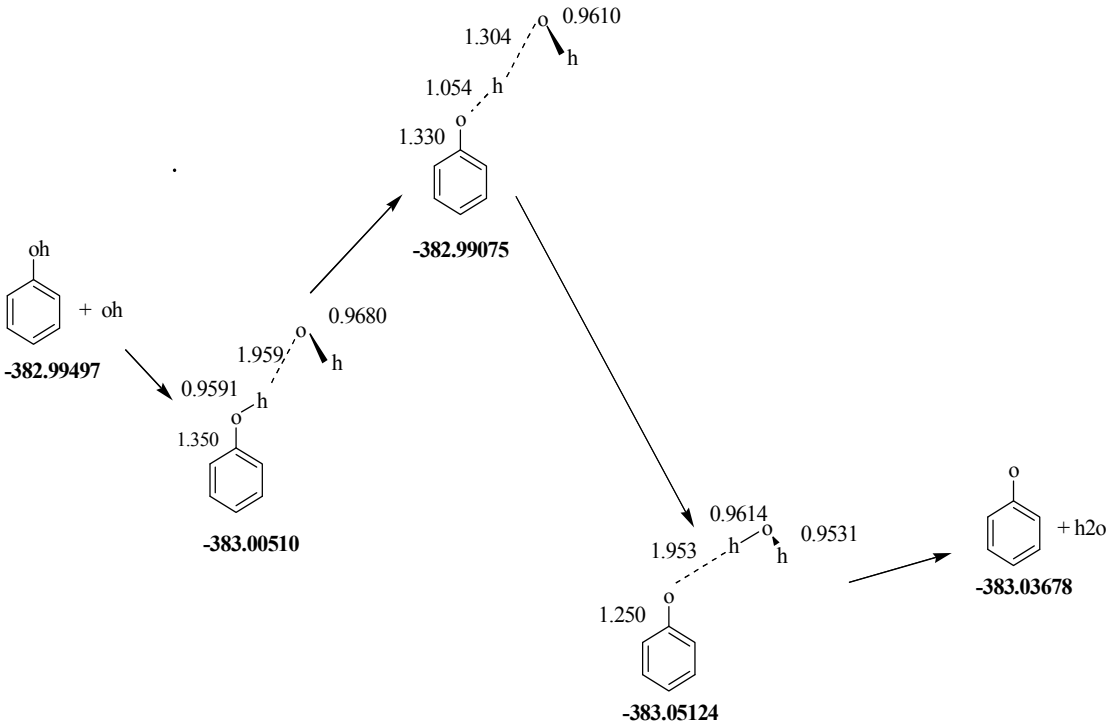

Figure 10: Channel 1D BHandHLYP PES which depicts the absolute energies in hartrees (left to right) for the reactants (phenol and the hydroxyl radical), the reactant van der Waals minimum, the transition state, the van der Waals product minimum, and the products (water and the phenoxyl radical).

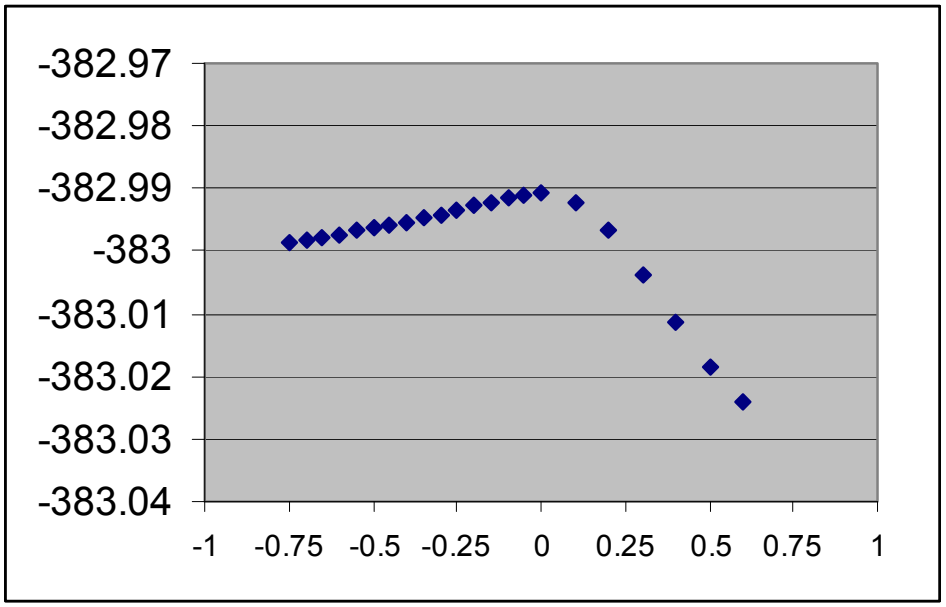

Figure 11: Channel 1D BHandHLYP/6-31G(d,p) IRC calculation results in hartrees versus reaction coordinate.

isomerizes into a C_s symmetry after proceeding through a vertical excitation and a transition state which is not rate-limiting. The C_s symmetry phenoxyl structure is a local minimum (no imaginary frequency) and is depicted in Figure 12.

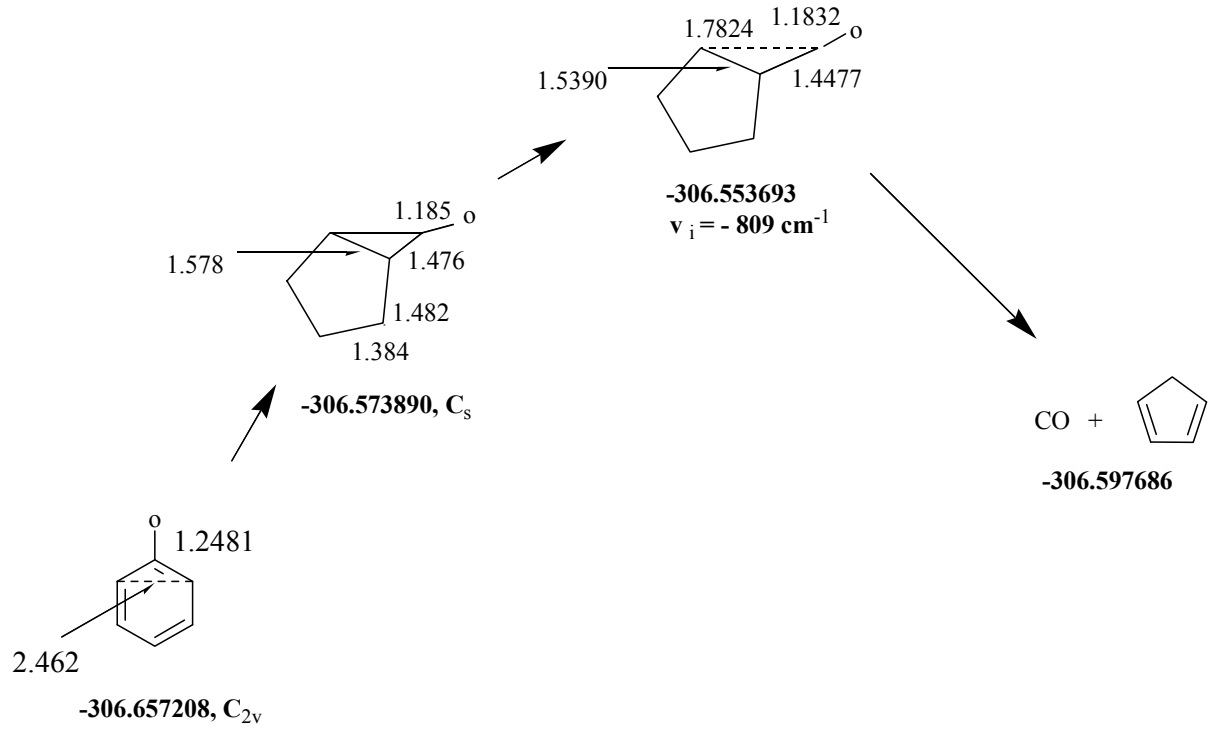

Figure 12: Channel 4A PES which depicts the absolute energies in hartrees (left to right) for the reactant (the phenoxyl radical in its ground state, C_{2v}), a local minimum (C_s), the rate-limiting transition state, and the products (carbon monoxide and a cyclopentadienyl radical).

After Channel 4A passes through its rate-limiting transition state another local minima is found prior to decomposition to the products, CO and the cyclopentadienyl radical.[45] This minimum structure has been confirmed in this work using a BHandHLYP/6-31G(d,p) model chemistry whose absolute energy is -306.59037 hartrees. With this information in mind, one would not expect the IRC forward (to products) and reverse (to reactants) calculations to precede through -306.59037 or -306.57389 hartrees, respectively.

IRC calculations confirm the rate-limiting structures for the decomposition of phenoxyl, *p*-semiquinone, and *o*-semiquinone radicals (Channels 4A-6A) are valid. Figure 13 depicts the IRC calculated energies for the confirmation of the Channel 4A transition state.

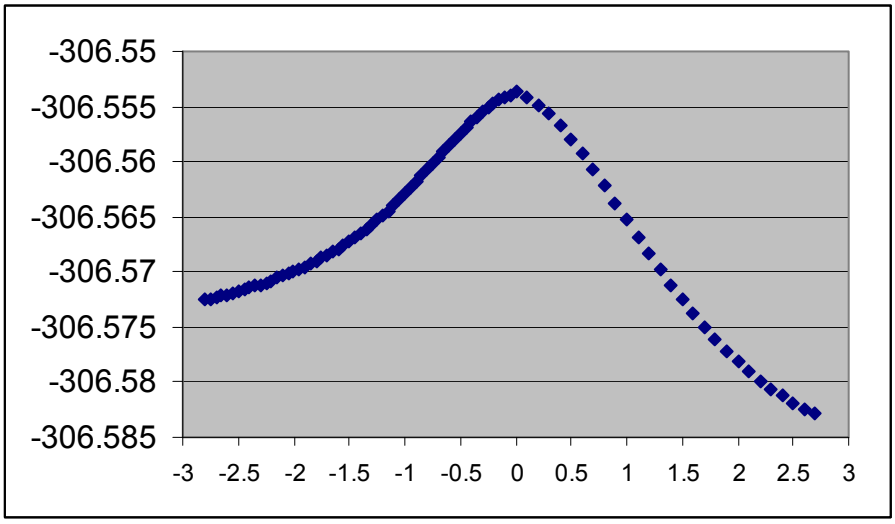

Figure 13: Channel 4A BHandHLYP IRC calculation results, hartrees versus reaction coordinate.

The six transition states for oxidative Channels 4B-6B were found by performing one-dimensional scans of the carbon-oxygen bond distances (Angstroms), i.e. extending the carbon-oxygen bond (of each adduct or product) while plotting the absolute energy as a function of this distance. Figures 14 and 15 depict this one-dimensional scan and the reactants', transition state, and product structures for the *ortho*-case of Channel 4B, respectively. These oxidative reactions (radical and $^3O_2$) were studied in the doublet state based on a previous study of the reaction between phenyl and $^3O_2$.[46]

IRC calculations for each oxidative channel have confirmed these transition states are valid. For the *ortho*-case of Channel 4B, IRC calculated results are given in Figure 16.

The transition states for the loss of the hydroxyl hydrogen atom from the *ortho*- and *para*-semiquinone radicals (Channels 5C-6C) were found by first performing a one-dimensional scan

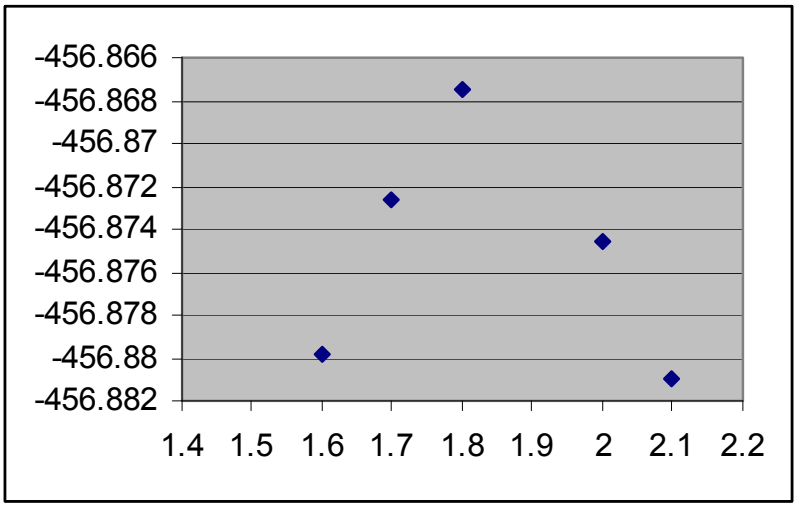

Figure 14: BHandHLYP/6-31G(d,p) scan of carbon-oxygen bond in the *o*- O_2-phenoxyl product given in hartrees versus Angstroms.

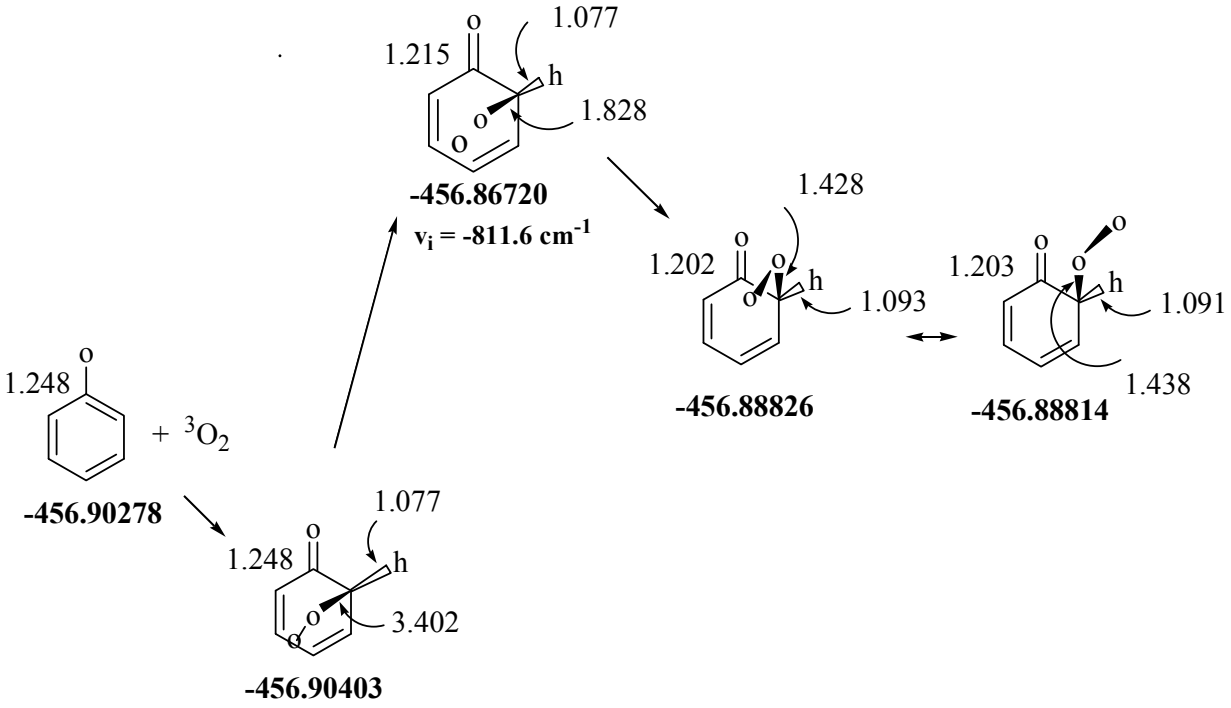

Figure 15: Channel 4B PES (the *ortho*-case) which depicts the BHandHLYP/6-31G(d,p) absolute energies in hartrees (left to right) for the reactants (phenoxyl and $^3O_2$), a local minima, the transition state, and 2 isomers of the product.

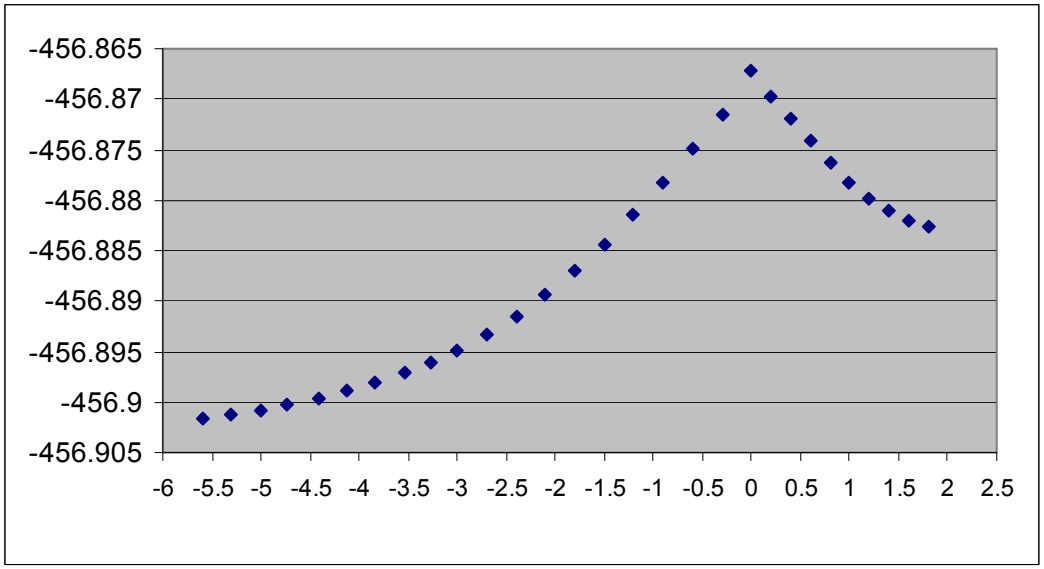

Figure 16: Channel 4B (*ortho*-addition) BHandHLYP IRC calculation results, hartrees versus reaction coordinate.

of each of these radicals' hydroxyl bond. For example, the one-dimensional scan for *p*-semiquinone appears in Figure 17.

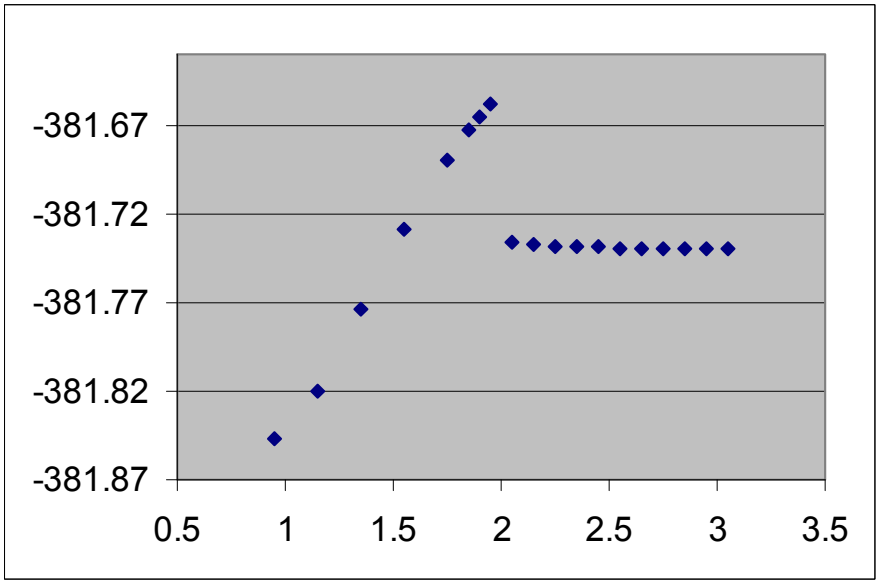

Figure 17: One-dimensional BHandHLYP/6-31G(d,p) scan of hydroxyl bond in *p*-semiquinone given in hartrees versus Angstroms.

The one-dimensional scans were followed by implementation of the STQN method integrated into the suite of programs inside *Gaussian 03*. Figure 18 depicts the reactant, the transition state, and products' structures for Channel 5C. IRC calculated results appear in Figure 19 and confirm the transition in Figure 18 as valid.

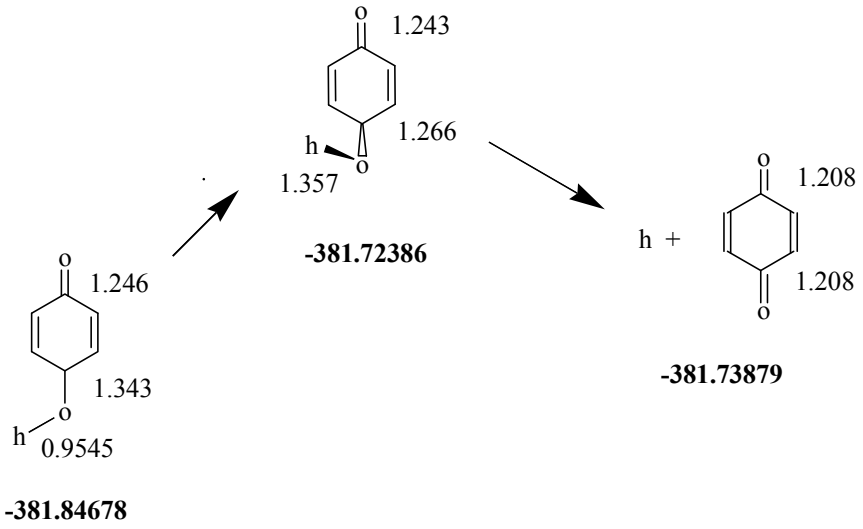

Figure 18: Channel 5C PES which depicts the BHandHLYP/6-31G(d,p) energies in hartrees (left to right) for the reactant (*p*-semiquinone), the rate-limiting transition state, and the products (hydrogen atom and *p*-benzoquinone).

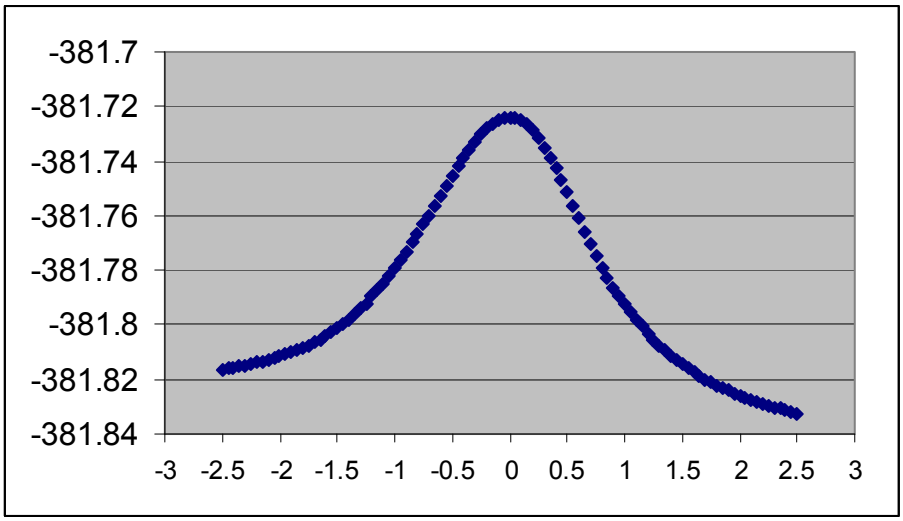

Figure 19: Channel 5C BHandHLYP IRC calculation results, hartrees versus reaction coordinate.

4.2 Results

The reaction internal energies (ΔE), reaction enthalpies (ΔH), and reaction Gibbs free energies (ΔG) for each reaction in Figure 8 are given in Table 7. Activation energies were calculated for the key unimolecular radical decomposition (Channels 4A-6A and 5C-6C), bimolecular radical - $^3O_2$ consumption reactions (Channels 4B-6B) as well as hydroxyl radical abstraction reactions with the molecular precursors (Channels 1D-3D).

Figure 8 summarizes the reactions of phenol, catechol, hydroquinone, phenoxyl radical, o-semiquinone radical, and p-semiquinone radical studied in this work. These reactions can be characterized as follows:

4.2.1 Radical Formation

- Unimolecular decomposition of the parent species via phenoxyl-hydrogen bond rupture (Channels 1A, 2A, and 3A)
- Bimolecular reaction of the parent species with a hydrogen atom
    - Abstraction of a phenoxyl hydrogen (Channels 1B, 2B, and 3B)
    - Displacement of a hydroxyl group (Channels 1C, 2C, and 3C)
- Bimolecular reaction of the parent species with a hydroxyl radical
    - Abstraction of a phenoxyl hydrogen (Channels 1D, 2D, and 2C)

Unimolecular decomposition involving a phenoxyl-hydrogen bond with dissociation energies between 73 and 80 kcal mol^{-1} (BHandHLYP/6-31G(d,p)) is expected to contribute to radical formation under oxidative and pyrolytic conditions.[109] Hydrogen atoms are the dominant reactive species under pyrolytic conditions and the hydroxyl radical is the dominant reactive species under oxidative conditions[57] and these species should contribute strongly to radical formation under pyrolytic and oxidative conditions, respectively.

The BHandHLYP calculations yield a 7.3 kcal mol^{-1} difference in the energies of reaction (activation energy) of the radical from the parent molecular species via unimolecular decomposition (Channels 1A, 2A, and 3A). Despite using unrestricted, open-shell DFT with orbital transpositions, no transition states could be found for reactions 1A-3A. The ΔE for formation of phenoxyl (Channel 1A) is consistent with previously reported hydroxyl bond dissociation energies for phenol[117-120], hydroquinone, and catechol.[121-123]

The experimental rate constants (at 1000 K) for H• abstraction and OH• displacement by H• (Channels 1B-3B and 1C-3C)[124] are similar with the rate constant for phenol decomposition.[125]. Assuming an H• concentration[126] of 10^{13} to 10^{14} atoms-cm^3 and a temperature of 1000K results in a predicted rate (mole/L-sec) for these 2 reactions greater than the rate for unimolecular decomposition under pyrolytic conditions. Further, the calculated ΔE_{rxn} results (Table 7) for Channels 1B-3B and 1C-3C show that thermodynamics favors the formation of phenoxyl over the formation of benzene. Formation of molecular species by hydroxyl displacement (Channels 1C-3C) may compete with radical formation (Channels 1B-3B), but hydroxyl reactions (Channels 1D-3D) with phenol, catechol, and hydroquinone are all calculated to have low or negative activation energies, information which is consistent with analogous bimolecular hydroxyl reactions with aromatics.[73 113, 127-132] Using rate constant information and these and these calculations the oxidative pathway, i.e. H• abstraction by OH• (Channels 1D-3D), are expected to be the dominant pathway, a radical forming pathway.

The kinetic and thermodynamic differences for the radical formation channels may be of little practical consequence in combustion systems as the reactions of the molecular precursors with hydrogen atoms and hydroxyl radicals (Channels 1B-3B, 1C-3C, and 1D-3D) are all exothermic

($\Delta H_{rxn} \leq$ -7.4 kcal-mol^{-1}, BHand HLYP) and are expected to have very similar activation energies resulting in similar radical formation yields. Our calculations show similar trends in ΔE_{rxn} for the formation of *o*- and *p*-semiquinone, and as a result, we expect similar trends in reaction rates for their precursors. Under the conditions present in this experiment, these radical formation calculations demonstrate that unimolecular or bimolecular processes at combustion temperatures all readily form the radicals. The radical consumption energetics are more revealing.

4.2.2 Radical Consumption

- Thermal Decomposition via concerted elimination of carbon monoxide (Channels 4A, 5A, and 6A)
- Bimolecular reaction with ground state molecular oxygen ($^3O_2$) (Channels 4B, 5B, and 6B)
- Unimolecular bond scission of the second hydroxyl hydrogen to form a quinone (Channels 5C and 6C)

Unimolecular thermal decomposition via elimination of carbon monoxide with reaction enthalpies in the 27-33 kcal mol^{-1} (BHandHLYP/6-31G(d,p)) range may contribute to radical consumption under oxidative or pyrolytic conditions.[109] Hydrogen atom reactions (Channels 5C-6C) were included in analogy to the reactions of the molecular species in radical formation. Bimolecular reaction with $^3O_2$ was included as it is the highest concentration reactive species in the atmosphere and the known principal route of consumption of most organic radicals under oxidative conditions.

4.2.3 Radical Stability

Phenoxyl, *p*-semiquinone, and *o*-semiquinone radicals (Channels 4A, 5A, and 6A) are resistant to thermal decomposition by elimination of carbon monoxide to form

Table 7: BHandHLYP/6-31G(d,p), B3LYP/6-31G(d,p), and QCISD(T)/6-31G(d,p)//BHandHLYP/6-31G(d,p) Results for Each Channel in Figure 8. (B3LYP results precede QCISD(T)/6-31G(d,p) results in parentheses). The QCISD(T)/6-31G(d,p) results are calculated at BHandHLYP/6-31G(d,p) optimized geometries. Reaction enthalpies and free energy changes were calculated at 298 K and 1 atmosphere of pressure.

Channel	E_{act}	ΔE	ΔH	ΔG
1A	N.A.	80.2(81.3, 89.4)	81.5(82.7)	73.2(74.3)
2A	N.A.	76.3(76.4, 85.0)	77.5(77.6)	69.4(69.5)
3A	N.A.	72.9(71.6, 80.7)	73.9(72.7)	66.1(64.8)
1B		-23.1(-24.0,-16.4)	-22.6(-23.5)	-23.9(-24.8)
2B		-27.0(-28.9,-20.9)	-26.7(-28.6)	-27.8(-29.7)
3B		-30.4(-33.7,-25.2)	-30.2(-33.5)	-31.0(-34.3)
1C		-7.7(-2.3, -6.2)	-7.8(-2.4)	-10.7(-5.3)
2C		-9.5(-4.0, -7.8)	-9.7(-4.3)	-12.4(-7.0)
3C		-7.3(-2.0, -5.4)	-7.4(-2.2)	-10.2(-4.9)
1D	1.0 (,6.9)	-26.6(-30.4,-26.5)	-26.5(-30.2)	-27.4(-31.2)
2D	-0.6(,6.0)	-30.6(-35.3,-31.0)	-30.6(-35.3)	-31.2(-36.0)
3D	-1.0( )	-34.0(-40.1,-35.3)	-34.1(-40.2)	-34.5(-40.6)
4A	62.9(56.4,56.4)	29.0(29.6, 22.9)	30.6(31.3)	18.1(18.8)
5A	65.1(59.9,59.3)	27.2(27.8, 20.5)	28.4(29.0)	16.6(17.3)
6A	74.4(70.0,68.3)	32.8(34.6, 27.2)	34.2(36.0)	22.1(23.9)
4B				
o-addition	23.5(13.7,14.6)	12.3(9.3, 1.8)	11.7(8.8)	22.1(19.1)
p-addition	20.7(10.8,11.1)	8.4(6.2, -2.0)	7.8(5.7)	18.5(16.2)
5B				
o-addition	22.4(13.1,13.1)	13.7(12.0, 3.2)	13.1(11.5)	23.3(21.7)
p-addition	19.6(10.8, 9.3)	11.3(10.7,-0.5)	10.7(10.3)	21.5(20.6)
6B				
o-addition	26.4(18.1,18.6)	16.4(15.4, 6.9)	15.9(15.0)	26.4(25.3)
p-addition	21.3(12.5,7.6)	11.8(11.3, 2.6)	11.2(10.8)	21.9(21.2)
5C	72.9(63.8,71.4)	60.9(57.8,54.7)	62.3(59.2)	54.5(51.4)
6C	79.8(71.6,79.0)	74.3(71.6,68.2)	75.8(73.2)	67.6(64.9)

cyclopentadienyl (from phenoxyl) and hydroxycyclopentadienyl (from catechol and hydroquinone) radicals with activation energies (BHandHLYP/6-31G(d,p)) ranging from 62.9 kcal mol^{-1} for phenoxyl to 74.4 for *o*-semiquinone. Qualitatively, our calculations do indicate that *o*-semiquinone is more resistant to decomposition than phenoxyl or p-semiquinone, which may be significant. *o*- and *p*-semiquinone (Channels 5C and 6C)

may also decompose by the loss of the second phenoxyl hydrogen which is not possible in phenoxyl. These reactions are highly endothermic with calculated activation energies of 72.9 and 79.8 kcal mol^{-1} (BHandHLYP/6-31G(d,p)) for *p*- and *o*-semiquinone, respectively. In fact, the calculated activation energy for the loss of the second hydroxyl hydrogen is actually 6.9 kcal mol^{-1} greater than the activation energy for the loss of the first hydrogen in the *o*-semiquinone/catechol system. The large activation energies for loss of the second hydrogens are again indicative of the stabilities of the radicals. Since the activation energies for reaction of the radicals with molecular oxygen were so similar and the semiquinone radicals have a decomposition channel that phenoxyl radical does not have, our results suggest that phenoxyl may be slightly more stable than the *o*- and *p*-semiquinone radicals.

4.2.4 Radical Reactivity

Calculations for reaction energies here indicate that the addition of molecular oxygen to the oxygen atom of phenoxyl is highly endothermic (ΔH_{rxn} = +72.8 kcal mol^{-1}, UHF/6-31G(d,p)) making production of an ozonide (ROOO•) unlikely (Figure 21). Additionally, no transition state could be located for reaction at an oxygen center and this reaction is believed to be infeasible.

Attempts to optimize the UHF ozonide structure with B3LYP and BHandHLYP were

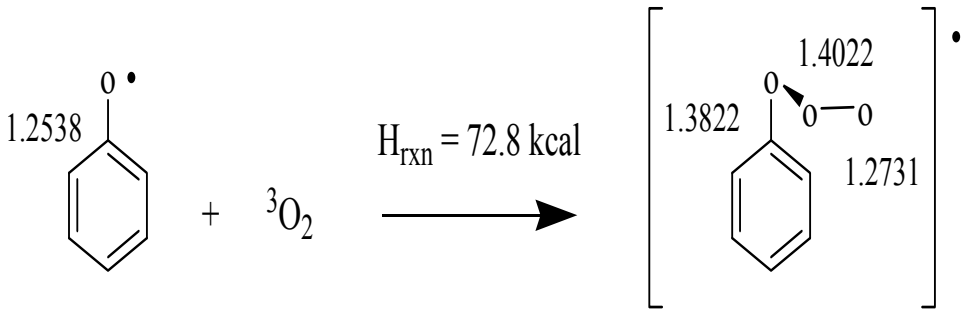

Figure 21: Addition of molecular oxygen and the phenoxyl radical producing an ozonide (ROOO•) via UHF/6-31(d,p).

unsuccessful and hence addition of molecular oxygen to the oxygen atom is not included in Table 7 and not a possibility further considered. This ozonide product suggests addition of molecular oxygen with the oxygen-center of the semiquinones would be highly endothermic as well. Our calculations also indicate $^3O_2$ addition to the *ortho-/para-* carbon atoms of phenoxyl (Channel 4B) are unlikely with calculated activation energies are 23.5/20.7 and ΔEs of 12.3/8.4 kcal mol^{-1} (BHandHLYP/6-31G(d,p)). An important result is the lower activation energies of 19.6-21.3 kcal-mol^{-1} (BHandHLYP/6-31G(d,p)) for reaction at the more reactive *para*-position of each radical with molecular oxygen . Furthermore, equilibrium does not favor these reactions, i.e. ΔGrxn = 18.5-26.4 kcal-mol^{-1}. Based on these calculations, this reaction should not occur for any of these radicals. This finding is consistent with the literature, i.e. these radicals are stable in oxidative environments allowing them to engage rather in radical-radical or radical-precursor combinations.[10, 20, 58-61, 63, 74-77, 133-138] Addition of molecular oxygen was also considered at the radicals' *ortho*-positions, but the activation energies are 2.8-5.1 kcal-mol^{-1} higher than at the *para*-position.

Because our calculations indicated semiquinone and phenoxyl radicals were exceptionally resistant to oxidation, for comparison, we also performed calculations on a phenyl radical that is known to be very reactive with $^3O_2$ (Figure 22). [46-52, 139] For this reaction, an experimental activation energy of -0.32 kcal/mole has been previously measured[52], and a ΔGrxn of -32.3 kcal mol^{-1} has been previously calculated using B3LYP/6-311+G(d,p)//B3LYP/6-31G(d)).[46] The experimental exothermicity for this reaction is -37 kcal-mol^{-1}.[46] A one-dimensional scan of the carbon-oxygen bond in the adduct is shown in Figure 23. These calculations also indicate this reaction is barrierless with a ΔHrxn and ΔGrxn (B3LYP/6-31G(d,p)) of -46.2 and -34.8 kcal-mol^{-1}, respectively.

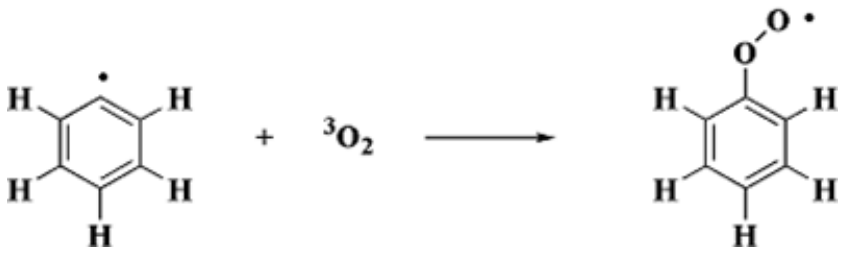

Figure 22: The addition reaction of the phenyl radical with molecular oxygen which produces the phenylperoxy radical.

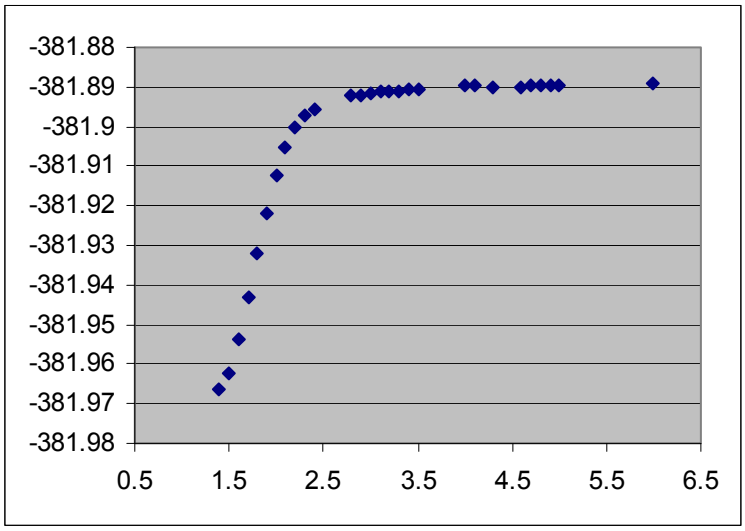

Figure 23: B3LYP/6-31G(d,p) one-dimensional scan of the phenylperoxy carbon-oxygen bond distance.

The reaction between the phenoxyl radical and $^3O_2$ (Channel 4B) has also been experimentally studied, and it was found that the room temperature reaction rate was on the order of 10^{-18} to 10^{-21} cm^3/molecule-sec.[79, 80] This is very slow compared to the reaction of $^3O_2$ with phenyl radical which is 10^{-11} to 10^{-13} cm^3/molecule-sec[49, 50, 52] and further supports the results of our calculations for *o*- and *p*-semiquinone radicals as well as phenoxyl.

An additional calculation that is useful for assessment of the reactivity of the radicals is the Bader Valence Electron Density.[140] The results of these calculations, which assign the valence

electron density to individual atoms, can be used to determine the amount of valence electron density that is oxygen-centered and carbon-centered. The results presented in Table 8 indicate that *o*-semiquinone and *p*-semiquinone are both 37 % oxygen-centered and phenoxyl is 22 % oxygen centered. Since earlier UHF/6-31G(d,p) calculations (Figure 21) indicate molecular oxygen may not react at the oxygen center of phenoxyl to form an ozonide (ROOO•) but may react at a carbon-center to form a peroxide (ROO•) (BHandHLYP/6-31G(d,p)), the greater carbon electron density found in phenoxyl (25 % higher than the semiquinone radicals) becomes a factor. This suggests that the pre-exponential factor for reaction of phenoxyl radical with molecular oxygen will be higher than for either of the semiquinone radicals. This effect, to some extent, counters the effect of the high activation energy for the reaction of molecular oxygen with phenoxyl radical.

Table 8: Bader Valence Electron Density Analysis using a BHandHLYP/6-31G(d,p)) model chemistry.

Radical	% Carbon	% Hydrogen	% Oxygen
o-semiquinone	52.2	10.6	37.2
p-semiquinone	49.8	13.4	36.8
phenoxyl	63.6	14.8	21.6
phenyl	82.2	17.8	na

CHAPTER 5. AB-INITIO STUDY OF THE FORMATION AND DEGRADATION REACTIONS OF POLY-CHLORINATED PHENOXYL RADICALS

5.1 Computational Procedures

All reaction and kinetic calculations in Chapter 5 have been performed using unscaled, zero-point corrected energies and the following model chemistries: B3LYP/6-31G(d,p), BHandHLYP/6-31G(d,p), and QCISD(T)/6-31G(d,p)//BHandHLYP/6-31G(d,p). As a check on the relative ordering of the results, the monochlorophenols' decomposition reaction energies have also been calculated with the BHandHLYP/6-311++G(d,p) model chemistry. The transition states for the radical decomposition and oxidative channels have been IRC confirmed and are similar to those given in Chapter 4.

5.2 Results

5.2.1 Radical Formation

5.2.1.1 Unimolecular Decomposition of the Chlorophenols

Despite the importance of the role of the 19 congeners of chlorophenol in gas-phase PCDD/F formation, this is the first study to focus undertake all of their OH bond dissociation energies (BDE) in computational fashion. Previous experimental pyrolytic studies have been limited to the mono-, di-, or tri-chlorophenol precursors and their products with an aim for developing a PCDD/F formation mechanism[56-58, 73, 74, 77, 78, 134, 136-138] and some have used the OH bond dissociation energy of phenol in their models. Previous computational studies have also been limited to only the mono- or dichloro-phenols' OH bond dissociation energies.[64-71]

In comparison to the non-substituted case, a mono-hydroxylated aromatic ring is more likely to undergo electrophilic (E+) substitution at its *ortho* and *para* carbon sites due to the electron-donating properties of a hydroxyl substituent.[141] Specifically, after an E+ adds (at an *ortho* or

para carbon atom) the positive charge can be delocalized into 3 locations, one of which is near the carbon-hydroxyl bond. In this case, the hydroxyl group may stabilize the carbocation with its electron-donating character.

An experimental study, using EPR[142] has shown the terminal group on passing from phenols (R-OH) to phenoxyl radicals (R-O•) changes its electronic properties from electron-donating to strongly withdrawing when an electron-donating chloro-substituent is in its *para*-position. This is confirmed by the absolute energies here (Table 9), i.e. amongst the monochlorophenols, the *para*- isomer is highest in energy and amongst the monochloro-phenoxyl radicals, the *para*-isomer is the lowest in energy.

Table 9: BHandHLYP/6-311++G(d,p) zero-point corrected absolute energies (in hartrees) for the monochlorinated phenols and monochlorinated phenoxyl radicals.

ortho-chlorophenol	-766.882553
meta-chlorophenol	-766.881398
para-chlorophenol	-766.880766
ortho-chlorophenoxyl	-766.252099
meta-chlorophenoxyl	-766.252752
para-chlorophenoxyl	-766.254632

ortho-chlorophenol was expected to be the most stable isomer of monochlorophenol due to its internal hydrogen bond.

Destabilization of the OH bond in *para*-chlorophenol is easily observed here with BHandHLYP/6-311++G(d,p) relative to phenol (Table 10) and is consistent with this experimental finding.[142] *ortho- and meta*-chlorophenol were expected to exhibit higher OH bond dissociation energies, relative to phenol, a result of their internal hydrogen bonding, and their OH bond dissociation energies are also consistent with those reported in earlier computational works.[65, 67, 70, 71]

Table 10: BHandHLYP/6-311++G(d,p) reaction energies in kcal-mol^{-1}.

	ΔE_{rxn}
phenol → H + phenoxyl radical	80.6
ortho-chlorophenol → H + *ortho*-chlorophenoxyl radical	82.7
meta-chlorophenol → H + *meta*-chlorophenoxyl radical	81.6
para-chlorophenol → H + *para*-chlorophenoxyl radical	80.0

Another experimental study uses the 3 mono-chlorophenols and 4 dichlorophenols as precursors to understand chlorinated-dibenzofuran formation where the conditions were both pyrolytic and oxidative.[138] For the 3 mono-chlorophenols and pyrolytic conditions, these authors report *para*-chlorophenol decomposes most readily while *ortho*-chlorophenol is most resistant to decomposition (based on unreacted precursor amounts in identical experiments). This experimental finding is also consistent with OH bond dissociation energies reported in Tables 10 and 11.

The dichlorophenols used in this experimental study were 2,3-, 2,4-, 2,5-, and 2,6-DCP. Expected tetrachlorinated furans, based on a previously reported mechanism[75] which involves *ortho-ortho* radical dimerization, enolization, followed by condensation, were produced in the largest yield in each experiment. The 2,6-DCP did not give rise to any furans, as expected, as the radical product of this precursor does not have an *ortho*-H atom moiety available for the final condensation step. The oxidative experiments where $[O_2]$ = 8% did not change the product distributions or amounts indicating molecular oxygen is zeroth order with respect to the rate of formation of furans.

While Han et al.[72] have computationally studied the 19 congeners of chlorophenol, their focus was only their relative energetics and geometries. They observed that degree of chlorination can be correlated with an increasing OH bond distance, and as a result, they argue the acidity of the chlorophenols will increase with degree of chlorination. While we observe degree of

chlorination correlates with increasing OH bond distance (Table 12), we do not find a similar trend for the chlorophenols homolytic bond dissociation energies (BDE). Rather, we observe the lowest energy congener in a homologue pattern has the greatest OH BDE (taking into account the substituent effects on the ground state and radical energies), with one exception. Amongst the tetrachlorophenols, the lowest energy congener is its 2,3,5,6- isomer and the 2,3,4,5- isomer has the greatest OH BDE.

Table 11: ΔE_{rxn} for unimolecular decomposition of the chlorophenols producing a hydrogen atom and a chlorinated phenoxyl radical.

	B3LYP	BH&HLYP	QCISD(T)//BH&HLYP
Phenol	81.3	80.2	89.4
2-chlorophenol	83.1	82.5	91.1
3-chlorophenol	82.4	81.4	90.6
4-chlorophenol	80.7	80.1	89.0
2,3 dichlorophenol	83.8	83.2	
2,4 dichlorophenol	82.3	82.1	
2,5 dichlorophenol	83.9	83.5	
2,6 dichlorophenol	81.9	81.8	
3,4 dichlorophenol	81.7	81.2	
3,5 dichlorophenol	83.5	82.6	
2,4,6 trichlorophenol	81.0	81.3	
2,3,4 trichlorophenol	82.9	82.9	
2,3,5 trichlorophenol	84.6	84.3	
2,3,6 trichlorophenol	82.3	82.4	
2,4,5 trichlorophenol	83.0	83.0	
3,4,5 trichlorophenol	82.6	82.2	
2,3,4,5 tetrachlorophenol		83.9	
2,3,5,6 tetrachlorophenol		82.9	
2,3,4,6 tetrachlorophenol		82.0	
pentachlorophenol		82.6	

Table 12: Hydroxyl Bond Distance (BHandHLYP/6-31G(d,p)) in Angstroms as a function of increasing degree of chlorination for the 19 congeners of chlorophenol.

	R(O-H), Angstroms	Homologue Mean R(O-H)
o-chlorophenol	0.9564	0.9546
m-chlorophenol	0.9538	
p-chlorophenol	0.9536	
2,3-dichlorophenol	0.9566	0.9557
2,4-dichlorophenol	0.9565	
2,5-dichlorophenol	0.9567	
2,6-dichlorophenol	0.9568	
3,4-dichlorophenol	0.9539	
3,5-dichlorophenol	0.9540	
2,4,6-trichlorophenol	0.9567	0.9562
2,3,4-trichlorophenol	0.9567	
2,3,5-trichlorophenol	0.9565	
2,3,6-trichlorophenol	0.9569	
2,4,5-trichlorophenol	0.9567	
3,4,5-trichlorophenol	0.9540	
2,3,4,5-tetrachlorophenol	0.9569	0.9570
2,3,5,6-tetrachlorophenol	0.9571	
2,3,4,6-tetrachlorophenol	0.9570	
Pentachlorophenol	0.9571	0.9571

After performing a one-dimensional relaxed PES scan of the hydroxyl torsional angle in both the 2,3,5,6- and 2,3,4,5- tetrachlorophenols (Figure 24a-b), it appears this exception may be partially explained by the presence of 2 *ortho* chlorine atoms (in 2,3,5,6-) which facilitate rotation for its hydroxyl H atom, relative to the alternative case of where there is only one *ortho* chlorine atom (in 2,3,4,5-). Specifically, the rotational barriers (BHandHLYP/6-31G(d,p)) for the hydroxyl H atom are 4.8 and 5.7 kcal-mol^{-1} for 2,3,5,6- and 2,3,4,5-, respectively.

After the hydroxyl rotational energies are subtracted from the calculated OH bond dissociation energies for 2,3,4,5- and 2,3,4,6-tetrachlorophenol, one may observe (in Table 13) the energy necessary for OH bond scission is virtually identical.

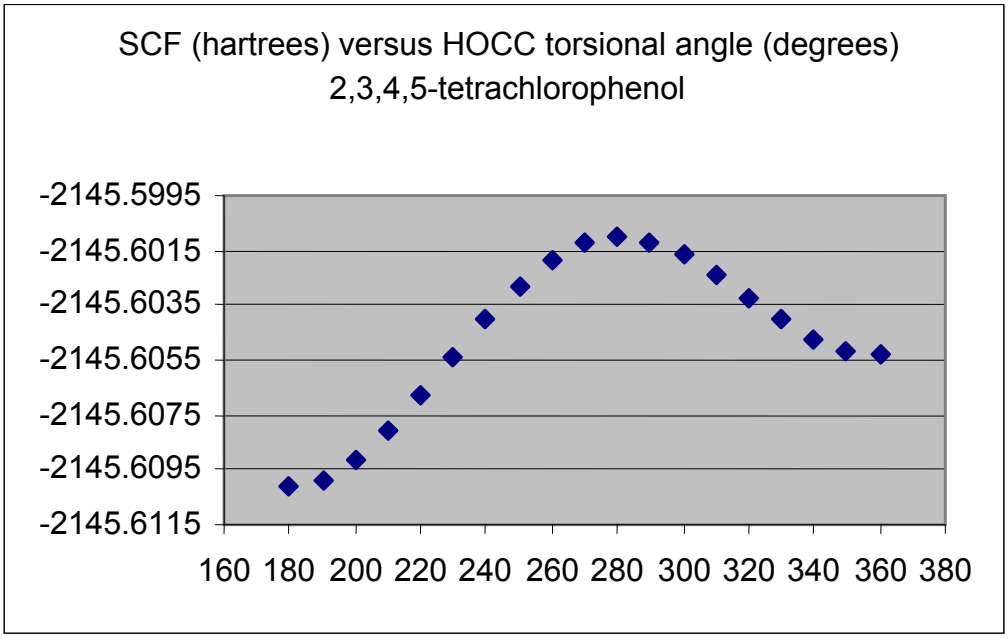

Figure 24a : One-dimensional relaxed PES scan of the hydroxyl H torsional angle in 2,3,4,5-tetrachlorophenol using BHandHLYP/6-31G(d,p).

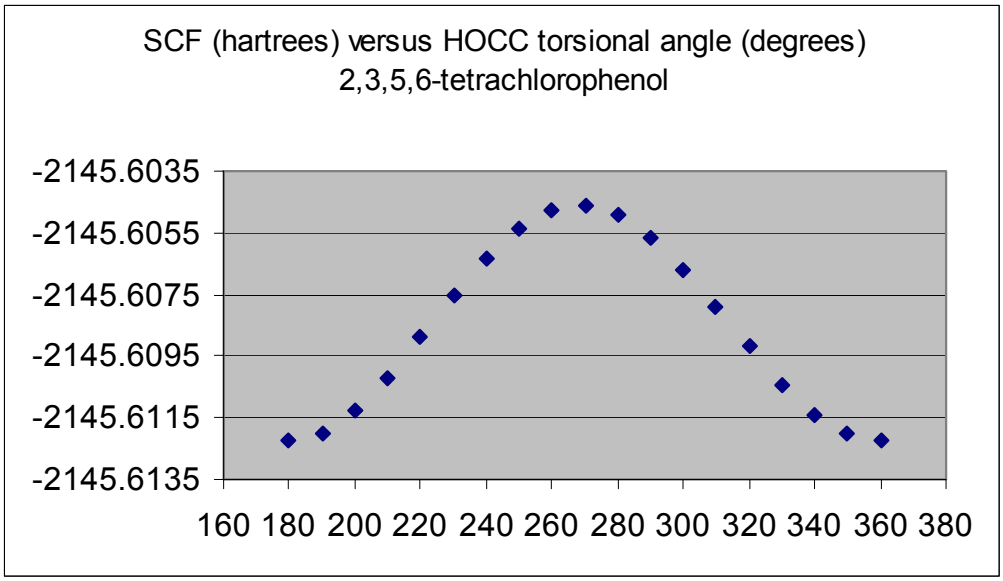

Figure 24b: One-dimensional relaxed PES scan of the hydroxyl H torsional angle in 2,3,5,6-tetrachlorophenol using BHandHLYP/6-31G(d,p).

Table 13: BHandHLYP/6-31G(d,p) OH bond dissociation energies (BDE) after rotational energies (kcal-mol^{-1}) are subtracted, for 2,3,4,5- and 2,3,5,6-tetrachlorophenol.

	OH BDE
2,3,4,5- tetrachlorophenol → H + 2,3,4,5-tetrachlorophenoxyl	78.2
2,3,4,6- tetrachlorophenol → H + 2,3,4,6-tetrachlorophenoxyl	78.1

This observation may be extended to the other homologue groups. In general, amongst each homologue pattern, those congeners which contain *one* internal H bond (with Cl) are described by higher OH bond dissociation energies than the balance. Chlorophenols with *two ortho*-chlorine atoms facilitate hydroxyl H atom rotation making OH bond dissociation energies lower; in addition, these tetrachlorophenol precursors are not expected to give rise to a predicted furan.[75] The 3 remaining chlorophenol congeners (3,4-DCP, 3,5-DCP, 3,4,5-TCP), i.e. those with 2 *ortho*-H atoms are, in general, most easily decomposed amongst the dichloro- and trichloro-homologue groups, respectively. These 3 precursors are also important for their product radicals also meet the conditions for forming the predicted chloro-dibenzofurans, i.e. these radicals may *ortho-ortho* dimerize, enolize, and condense producing 2,3,7,8-tetra-, 1,3,7,9-tetra-, and 1,2,3,7,8,9-hexa-chlorinated dibenzofurans.

5.2.1.2 Bimolecular Reactions with Hydrogen Atoms

Neither experimental nor computational rate information for the abstraction of H (the hydroxyl H) by H from a chlorophenol is available. Dehydroxylation by a H atom, on the other hand, was studied in the gas-phase by Manion and Louw.[143] Theses authors report this reaction proceeds via an addition/*ipso* substitution method and experimentally find the dehydroxylation rate constants (by H) for the 3 mono-chlorophenols are similar in magnitude to the analogous reaction for phenol. Specifically, these experimental rate constants' ratios were 1.08, 0.75, and 0.88 for 2-, 3-, and 4-monochlorophenol after making the analog (phenol) unity. Based on these similarities (analogous pyrolytic

dehydroxylation of the monochlorophenols by H) we use the experimental gas-phase rate constant for dehydroxylation of phenol by H[124] along with a H atom concentration of 10^{-13} to 10^{-14} atoms-cm^{-3} [126] to arrive at a predicted rate for the analogous reactions with the array of chlorophenols. Bimolecular reaction rates with H atoms are expected to be 2 orders of magnitude faster than the rate of unimolecular decomposition for the chlorophenols.

The reaction thermodynamics' (ΔErxn) in Table 14a and 14b are similar to the results for the pyrolytic channels (Channels 1B-3B and 1C-3C) in Chapter 4 which also suggests the bimolecular reactions of chlorophenols with H atoms will also favor production of chloro-phenoxyl radicals, as opposed to chlorobenzenes.

Table 14a: ΔErxn for bimolecular reaction with a hydrogen atom producing H_2 and a chlorinated radical

	B3LYP	BH&HLYP	QCISD(T)//BH&HLYP
Phenol	-24.0	-23.1	-16.4
2-chlorophenol	-22.2	-20.8	-14.7
3-chlorophenol	-22.9	-21.8	-15.2
4-chlorophenol	-24.6	-23.2	-16.9
2,3 dichlorophenol	-21.5	-20.0	
2,4 dichlorophenol	-23.0	-21.1	
2,5 dichlorophenol	-21.4	-19.8	
2,6 dichlorophenol	-23.4	-21.5	
3,4 dichlorophenol	-23.7	-22.1	
3,5 dichlorophenol	-21.8	-20.7	
2,4,6 trichlorophenol	-24.3	-22.0	
2,3,4 trichlorophenol	-22.4	-20.4	
2,3,5 trichlorophenol	-20.7	-19.0	
2,3,6 trichlorophenol	-23.0	-20.9	
2,4,5 trichlorophenol	-22.3	-20.3	
3,4,5 trichlorophenol	-22.7	-21.1	
2,3,4,5 tetrachlorophenol		-19.4	
2,3,5,6 tetrachlorophenol		-20.4	
2,3,4,6 tetrachlorophenol		-21.3	
pentachlorophenol		-20.7	

Table 14b: ΔErxn for bimolecular reaction with a hydrogen atom producing OH and chlorobenzene

	B3LYP	BH&HLYP	QCISD(T)//BH&HLYP
Phenol	-2.3	-7.7	-6.2
2-chlorophenol	-1.5	-7.0	-5.2
3-chlorophenol	-2.5	-7.9	-6.3
4-chlorophenol	-2.8	-8.2	-6.7
2,3 dichlorophenol	-4.6	-7.0	
2,4 dichlorophenol	-1.9	-7.4	
2,5 dichlorophenol	-1.5	-7.1	
2,6 dichlorophenol	-3.5	-9.0	
3,4 dichlorophenol	-2.9	-8.2	
3,5 dichlorophenol	-2.7	-8.0	
2,4,6 trichlorophenol	-3.8	-9.4	
2,3,4 trichlorophenol	-1.8	-7.3	
2,3,5 trichlorophenol	-1.6	-7.1	
2,3,6 trichlorophenol	-3.4	-9.0	
2,4,5 trichlorophenol	-2.0	-7.5	
3,4,5 trichlorophenol	-3.0	-8.4	
2,3,4,5 tetrachlorophenol		-7.4	
2,3,5,6 tetrachlorophenol		-9.1	
2,3,4,6 tetrachlorophenol		-9.2	
pentachlorophenol		-9.4	

5.2.1.3 Bimolecular Reaction with the Hydroxyl Radical

While there are several studies for the reaction of chlorophenols with the hydroxyl radical, these studies have been limited to aqueous solution, a form of waste water treatment. Gas-phase experimental rate constants are absent, i.e. for the bimolecular reactions between the chloro-phenols' hydroxyl site and a hydroxyl radical producing water and an appropriately chlorinated phenoxyl radical. As a result, the analogous reactions with benzene and phenol are used to draw comparisons here. With regard to the radical formation channels, oxidative conditions, and using

previous experimental and computational evidence for the analogues[113, 128, 129, 131], the gas-phase reaction between the chlorophenols and the hydroxyl radical is expected to dominate the scene.

For example, in an effort to study the phenol-OH adduct reactions with NO_x at temperatures 266-364 K, Berndt et al.[128] realized their hydroxyl generation mechanism was also a source of H atoms. In order to clarify the influence of the reaction between phenol and a H atom, these authors have found this reaction does not compete with the reaction of phenol and a hydroxyl radical.

Knispel et al.[131] have studied kinetically the bimolecular reactions of benzene, toluene, and phenol with OH (Figure 25) in terms of formation of their adducts (k_1), decomposition of their adducts (k_3), and abstraction of H by OH (k_2) at temperatures 298-374 K. For the reaction, phenol and OH, these authors find the addition channel dominates at 298 K, and the adduct decay channel dominates at 374 K. Although the phenol and OH addition channel is 2 times faster than the abstraction channel at high temperature (374 K), the high probability the adduct will dissociate back to the reactants makes the abstraction channel an important radical-producing channel at combustion temperatures. The reactions of benzene and toluene with OH were similar, i.e. addition dominated at low temperature and adduct decomposition dominated at high temperature; however, the abstraction rates for these reactions at high temperature remained small.

The addition reaction of benzene and OH is expected to dominate at 298 K based on the work of Knispel et al.[131] Calvert et al.[129] have compiled several researchers experimental works for this reaction and derive a rate coefficient of k_∞ (benzene+OH) ~ $3.8 \times 10^{-12}\ e^{(-300\ K/T)}$ cm^3-molecule^{-1}-sec^{-1} for T=240-350 K. The energy of activation in this expression, after conversion from K, is 0.6 kcal-mol^{-1}. A recent computational study has found the exothermicity (ΔH_{298}) for

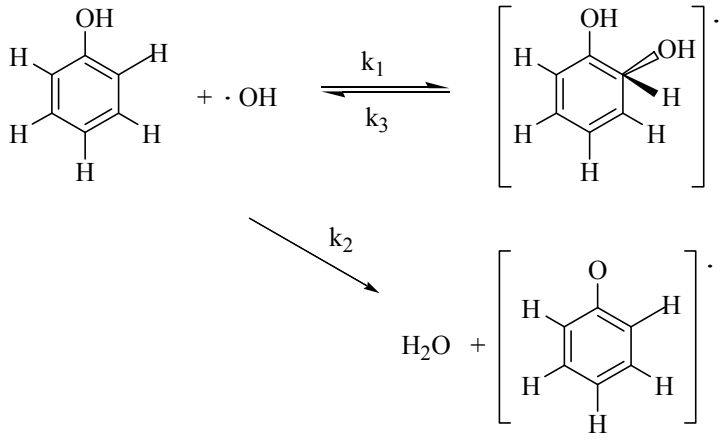

Figure 25: Bimolecular reaction of phenol and a hydroxyl radical. Equilibrium adduct formation (k_1), its unimolecular decay (k_3), and H abstraction (k_2).

the addition channel is -2.5 kcal-mol^{-1}, and the barrier for the abstraction channel is 4.8 kcal-mol^{-1} [113], using B3LYP/6-31G(d,p) optimized geometries and composited methods. Please recall the k_3 rate coefficient (the abstraction channel) for this reaction remains small at high temperature (or 374K).[131]

With regard to the reaction between phenol and OH, addition dominates at 298 K and abstraction effectively begins to dominate at 339 K[131] due to the rapid decomposition of the adduct into reactants and the increase in the abstraction rate constant. Calvert et al.[129] have also compiled consistent experimental works for this reaction and derive a rate coefficient of k_∞ (phenol+OH) = 1.73 x 10^{-12} e$^{(840K/T)}$ cm^3-molecule^{-1}-sec^{-1} for T=290-380 K. The energy of activation in this expression, after conversion from K, is -1.7 kcal-mol^{-1}. Calculations here for this abstraction barrier are lower, as expected, 1.0 kcal-mol^{-1} using BHandHLYP/6-31G(d,p). Formation of the adduct (after OH addition to carbon) is expected to be exothermic (at 298 K) for this channel as well.[127-129, 131, 132]

Additionally, Olariu et al.[144] have experimentally studied OH + phenol at 298 K in NO_x. These authors find catechol (80.2%) is the produced in the largest yield followed by

p-benzoquinone (3.7%) and 2-nitrophenol (5.8%). Catechol reflects addition of OH occurred at the ortho-site of phenol and nearby hydrogen atom was lost. This experimental evidence is congruent with the work of Knispel et al.[131]

The DFT computational barriers for (i) benzene and OH, and (ii) phenol and OH are ordered with experimental findings, i.e. the abstraction channel for the latter begins to dominate at a lower temperature making the reaction of phenol and OH important in terms of its radical-producing nature. Due to the ordering of the computational energies of activation with the experimental work for these 2 analogues, benzene and phenol, we expect the abstraction reaction rates between 2-, 3-, and 4-chlorophenol (CP) and OH to take place in this order, 4-CP+OH > 3-CP+OH > 2-CP+OH (Table 15). In addition, the reaction thermodynamics in Table 15 for H atom abstraction from a chlorophenol by OH are similar as well to the analogous reaction with phenol.

Table 15: ΔErxn for bimolecular reaction with OH producing water and chlorinated radical

	B3LYP	BH&HLYP		QCISD(T)//BH&HLYP
	Erxn	Eact	Erxn	Erxn
Phenol	-30.4	1.0	-26.6	-26.5
2-chlorophenol	-28.6	3.9	-24.4	-24.9
3-chlorophenol	-29.3	1.7	-25.4	-25.4
4-chlorophenol	-31.0	1.0	-26.8	-27.0
2,3 dichlorophenol	-28.0		-23.6	
2,4 dichlorophenol	-29.4		-24.7	
2,5 dichlorophenol	-27.8		-23.3	
2,6 dichlorophenol	-29.9		-25.1	
3,4 dichlorophenol	-30.1		-25.7	
3,5 dichlorophenol	-28.2		-24.2	
2,4,6 trichlorophenol	-30.8		-25.5	
2,3,4 trichlorophenol	-28.8		-23.9	
2,3,5 trichlorophenol	-27.1		-22.6	
2,3,6 trichlorophenol	-29.4		-24.5	
2,4,5 trichlorophenol	-28.7		-23.8	
3,4,5 trichlorophenol	-29.2		-24.6	

(table continued)

2,3,4,5 tetrachlorophenol	-23.0
2,3,5,6 tetrachlorophenol	-23.9
2,3,4,6 tetrachlorophenol	-24.9
pentachlorophenol	-24.3

5.2.2 Radical Consumption

5.2.2.1 Radical Decomposition into Carbon Monoxide and a Chlorinated Cyclopentadienyl Radical

The zero-point corrected absolute energies for *ortho-, meta-,* and *para*-chlorophenoxyl (Table 16) radicals are as expected as the *para*-isomer as most stable and the *ortho*-isomer is least stable.

Table 16: BHandHLYP/6-31G(d,p) zero-point corrected absolute energies (hartrees).

ortho-chlorophenoxyl	-766.153455
meta-chlorophenoxyl	-766.153767
para-chlorophenoxyl	-766.155404

The resonance effect of chlorine in these monochlorinated phenoxyl radicals is weak as the carbon *2p* orbitals of the aromatic ring do not overlap well with the high angular momentum valence orbitals of chlorine.[141] On the other hand, the integration of resonance drawings and the inductive (electron-withdrawing) nature of chlorine explains the ordering in Table 16. The lone radical electron cannot be delocalized (stabilizing) through the carbon-chlorine bond of *meta*-chloro phenoxyl as its 4 resonance structures (Figure 26) reveal. While with both *ortho*- and *para*-chlorophenoxyl radicals resonance drawings allow for better distribution of the radical effect, *ortho*-chlorophenoxyl is the least stable as a result of the local proximities of 2 electro-negative atoms, oxygen and chlorine (a repulsive interaction).

Using a mechanism for phenoxyl decomposition and the rate-limiting transition state, developed by Liu et al.[45], the activation barriers for the decomposition of the 19 congeners of the

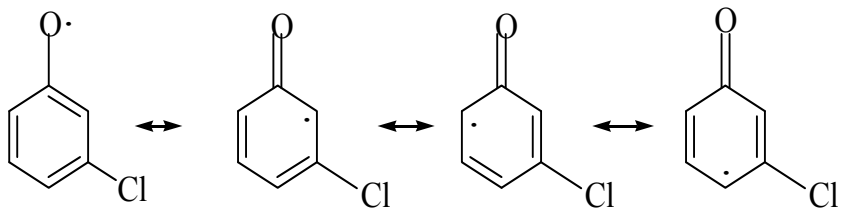

Figure 26: Resonance structures for *meta*-chlorophenoxyl radical.

chlorophenoxyl radical are calculated (in Table 17). Amongst the monochlorinated phenoxyl radicals, the decomposition energies correlate well with radical stability. The decomposition energies for the balance of the chlorinated phenoxyl radicals must be understood in terms of their resonance drawings, the proximities of 3 or more electronegative atoms, stabilities, and the radical effect.

Table 17: Activation and Reaction energies for chlorophenoxyl radical decomposition to CO and a chlorinated cyclopentadienyl radical

	B3LYP		BHandHLYP		QCISD(T)//BHandHLYP	
	Eact	Erxn	Eact	Erxn	Eact	Erxn
phenoxyl	56.4	29.6	62.9	29.0	56.4	22.9
2-chlorophenoxyl	52.5	26.4	60.2	25.7	54.1	19.5
3-chlorophenoxyl	56.5	26.1	63.0	25.9	56.3	18.9
4-chlorophenoxyl	57.6	27.4	63.6	26.9	57.4	20.2
2,3 dichlorophenoxyl		24.3	59.0	23.5		
2,4 dichlorophenoxyl		24.7	61.1	24.0		
2,5 dichlorophenoxyl		23.6	59.8	23.1		
2,6 dichlorophenoxyl		26.6	64.0	25.4		
3,4 dichlorophenoxyl		25.0	62.0	24.4		
3,5 dichlorophenoxyl		22.8	62.4	22.9		

(table continued)

2,3,4 trichlorophenoxyl	22.2	57.9	21.1
2,3,5 trichlorophenoxyl	20.7	58.3	20.4
2,3,6 trichlorophenoxyl	23.9	62.7	22.6
2,4,5 trichlorophenoxyl	22.0	59.1	21.2
2,4,6 trichlorophenoxyl	24.3	64.7	23.2
3,4,5 trichlorophenoxyl	21.3	59.7	20.7
2,3,4,5, tetrachlorophenoxyl		55.4	17.3
2,3,5,6, tetrachlorophenoxyl		60.6	19.5
2,3,4,6, tetrachlorophenoxyl		60.9	19.9
pentachlorophenoxyl		57.1	16.3

Amongst the monochlorinated phenoxyl radicals, the decomposition energies correlate well with radical stability. The decomposition energies for the balance of the chlorinated phenoxyl radicals must be understood in terms of their resonance drawings, the proximities of 3 or more electronegative atoms, stabilites, and the radical effect.

Amongst each homologue pattern in Table 17, the presence of one *ortho*-H atom moiety in a chlorinated phenoxyl radical appears to facilitate radical decomposition. Amongst the di-, tri-, and tetrachloro-phenoxyl homologue patterns, the presence of 2 *ortho*-chlorine atoms makes decomposition the least likely. The balance of radicals, i.e. those with 2 *ortho*-H atoms (i.e. phenoxyl, 3-CP, 4-CP, 3,4-DCP, 3,5-DCP, and 3,4,5-TCP) are expected to have intermediate lifetimes in the gas phase, an environment where chlorinated dibenzofuran production is favored.[56, 57 63] These isomers', in most cases, *ortho*- and *para*-sites are available for radical-radical dimerization (due to absence of steric hinderance by chlorine), they may enolize and condense water. As a result, this work makes these isomers' important candidates for predicted furan production.

5.2.2.2 Bimolecular Reactions with Molecular Oxygen

Based on previous study which has shown reactivity occurs primarily at the *ortho*- and *para*-sites of phenoxyl[75], molecular oxygen ($^3O_2$) has been added to the *ortho*- and *para*-carbon atoms

of phenoxyl, 2-CP, 3-CP, and 4-CP in order to find each adduct. The adducts' carbon-oxygen bond distances were then scanned (extended), one-dimensionally, in order to find each transition state. The activation energies here are slightly higher than the barrier for the analogue, phenoxyl, with the meta-chlorinated isomer being the exception.

In terms of electrophilic substitution, all *meta*-substituents are deactivating which means *meta*-carbons relative to a substituent are less attractive (less electron rich) to a positively charged electrophile.[141] Molecular oxygen, on the other hand, has two electrons (a triplet) in 2 of its *2p* antibonding orbitals making it relatively electron rich, or more attractive to an electron deficient *meta*-carbon atom. As a result, the activation barriers were expected to be slightly lower for $^3O_2$ addition to a *meta*-carbon atom, i.e. *meta*- relative to chlorine. It is also observed steric hinderance increases the barrier heights, as expected.

Ryu et al.[77] have used a radical formation-and-consumptive model along with experiment to study the distribution and amounts of chlorinated dibenzofuran congeners produced over a temperature range of 500-800 C. The model did not include furan production dependence on the concentration of oxygen, and experimentally, the oxygen concentration ranged from 0-8 %. These authors find good agreement between their model and experiment (Figure 27), i.e. the furan congener distribution remained virtually constant while the yields increased at lower temperatures (600 C). The agreement between this model and experiment indicates molecular oxygen is zeroth-order with regard to chlorinated dibenzofuran production rates.

In another study which aims to understand PCDD/F formation via a simulation[145], effects of temperature and gas composition are evaluated using an assumption of homogenous gas-phase equilibrium and a free energy minimization technique ($\Delta G=0$ at equilibrium). The gas phase included 19 isomers of PCDD/F and 60 gas phase species

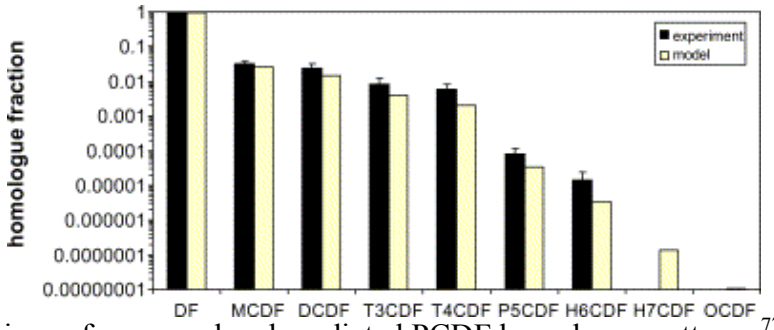

Figure 27: Comparison of measured and predicted PCDF homologue patterns.[77]

such as O_2, H_2, H_2O, Cl_2 and $C_xH_yO_z$ (where x=1-12, y=0-8, and z=0-4). The effect of varying the O_2 contribution from 0.0-0.6 moles was studied at 300 C (or 573 K) (Figure 28). This study shows increasing O_2 from 0.0-0.6 moles inhibits PCDD/F formation, i.e. equilibrium is shifted toward the reactants. This finding is consistent with the high activation barriers and free energies of reaction calculated in this work (Table 18a-b).

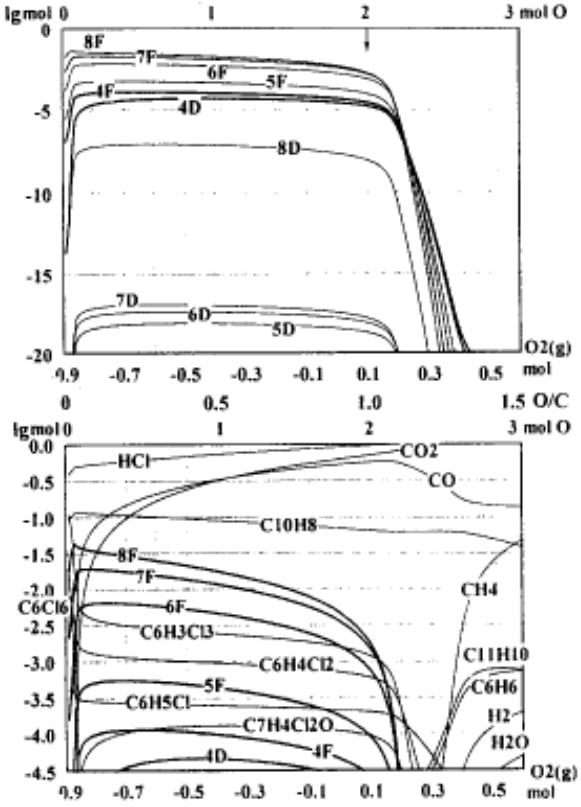

Figure 28: Effect of O_2 on the formation of PCDD/Fs. Temperature is 300 C. The 4- through 8-notation refers to the prefix for an isomer of dioxin or furan where 4 is tetra-, 5 is penta-, etc. The –D or –F notation refers to dioxin or furan, respectively.

Table 18a: Activation and Reaction energies for bimolecular radical-molecular oxygen ($^3O_2$) channels

	B3LYP		BH&HLYP		QCISD(T)//BH&HLYP	
ortho addition	Eact	Erxn	Eact	Erxn	Eact	Erxn
phenoxy	13.7	9.3	23.5	12.3	14.6	1.8
o-chlorophenoxy	14.9	11.5	24.3	13.6	15.5	3.0
o-chlorophenoxy *(chlorinated carbon)*	15.7	12.5	25.8	14.9	15.2	2.9
m-chlorophenoxy	13.2	9.0	23.2	11.6	14.0	0.7
m-chlorophenoxy *(alpha to chlorine)*	13.7	9.8	23.8	13.0	15.0	2.1
p-chlorophenoxy	14.6	11.3	24.2	13.9	15.2	3.4
para addition						
phenoxy	10.8	6.2	20.7	8.4	11.1	-2.0
o-chlorophenoxy	13.8	7.9	23.1	9.8	15.8	-0.5
m-chlorophenoxy	10.7	7.3	20.7	9.4	10.7	-1.9
p-chlorophenoxy	14.2	9.7	24.6	12.1	14.1	-0.1

Table 18b: Free Energies of Reaction using BHandHLYP/6-31G(d,p) (calculated at 298 K and 1 atmosphere of pressure)

ortho addition	ΔG_{rxn}
phenoxy	22.1
o-chlorophenoxy	23.6
o-chlorophenoxy *(chlorinated carbon)*	25.3
m-chlorophenoxy	21.6
m-chlorophenoxy *(alpha to chlorine)*	22.7
p-chlorophenoxy	23.7
para addition	
phenoxy	18.5
o-chlorophenoxy	19.9
m-chlorophenoxy	19.6
p-chlorophenoxy	22.4

CHAPTER 6. DISCUSSION

With regard to Chapter 1, Reactions 2 and 3 have been studied in the present work to validate the experimental apparatus employed for the first time after its construction. Hydrogen atom abstraction from hydrocarbons by hydroxyl radicals plays a fundamental role in the chemistry of the atmosphere and combustion processes; for this reason, Reactions 2 and 3 had been extensively studied previously. These earlier results are in general agreement with each other. Reviews of these data can be found in reference 95 for Reaction 2 and reference 101 for Reaction 3, and they are not repeated here. The rate coefficients obtained in the current study are in agreement with these earlier measurements (see Graph 5; data are exemplified by references 93-96 and 99-101 for Reactions 2 and 3, respectively. For example, over common temperature ranges, the maximum deviations between our calculated rate coefficient values using modified three-parameter Arrhenius expression and those calculated with expressions recommended in references 96 and 94 for Reaction 2 and in references 99 and 100 for Reaction 3 are the following: 5.4% and 2.5% for Reaction 2 and 5.1% and 1.3% (of the average rate coefficient value) for Reaction 3. Such good agreement with previously obtained data gives us confidence in the measurements performed with the experimental apparatus employed in this work.

All previous studies of the reaction of OH• + Cl_2 (Reaction 1) have been performed at low temperature (T_{max} = 354 K). Data reported in references 12 and 14 were measured at room temperature only, and they are in agreement with our data obtained at room temperature within experimental errors. Experimental temperature-dependent kinetic investigations of Reaction 1 were carried out in three works.[11, 13, 15] Our data are in

agreement with these studies over the common temperature ranges, within reported experimental errors.

The PES of Reaction 1 obtained in quantum chemical calculations demonstrates good agreement with experimental results. The QCISD(T)/6-31G(d,p) level energy calculations provide reasonable agreement with the experimental barrier height, a deviation of 2.6 kcal. The BHandHLYP/6-31G(d,p) level calculations provide reasonable agreement with the experimental reaction enthalpy, a deviation of 4.8 kcal.

Theoretical model predictions suggest OH• + Cl_2 → HOCl + Cl• (Reaction 1b) is the main channel for Reaction 1, in agreement with the room temperature branching ratio for the OH• reaction with Cl_2 found in the work of Loewenstein et al.[14] The agreement between the experimental and computational results provides support for further use of the computational techniques applied here for the treatment of other reactions of similar types.

With regard to Chapter 4, the detection of persistent, biologically active free radicals in airborne and combustion-generated particles raises the questions of their origin and nature. The EPR g-values for samples containing these radicals are typically greater than 2.003 and have been observed to be greater than 2.005.[35] These g-values are characteristic of oxygen-centered radicals or carbon-centered radicals with a nearby oxygen-containing functional group. Because the EPR spectral characteristics are consistent with those of semiquinone radicals and these radicals have been previously reported in cigarette tar, it has been presumed that the observed radicals are of the semiquinone-type.

Phenoxyl radicals in complex media yield EPR spectra similar to those of semiquinones, a motivation for this work. Our calculations indicate that the phenoxyl

radical is as stable and resistant to oxidation as *o*- and *p*-semiquinone. This non-favorable reaction prediction is consistent with experimental oxidation evidence, i.e. radical concentrations have been observed to increase after exposure to air.[35] Although formation via unimolecular decomposition from a parent phenol is not as energetically favorable as that of a semiquinone from catechol or hydroquinone, phenol is likely to be present in higher concentrations[42] than catechol or hydroquinone which suggests that phenoxyl may be the higher concentration radical in environmental samples.

The highly resonance stabilized *o*-semiquinone, *p*-semiquinone, and phenoxyl radical are all resistant to decomposition via the channels examined herein, which is not surprising. It was anticipated that they would be resistant to oxidation, but the activation energies and free energies of this reaction are surprisingly high, suggesting that they are virtually un-oxidizable by molecular oxygen. This result is actually consistent with available experimental evidence. As previously mentioned, semiquinone radicals have been reported in aged cigarette tar, supporting their extreme persistence. Recombination (dimerization) of phenoxyl radicals and their analogues have been proposed as a major pathway of formation of polychlorinated dibenzo-p-dioxins and dibenzofurans (PCDD/F) in combustion systems which indicates that these radicals survive in an oxidative environment at sufficiently high concentrations to undergo self-recombination.[59, 74, 75]

Elementary reaction kinetic data is not available for semiquinone radicals but has been obtained for phenoxyl radicals. Reported rates for reaction of phenoxyl radical with molecular oxygen are $k<2x10^{-18}$ and $<5x10^{-21}$ cm^3/molecule-sec.[79, 80] This is in contrast to reaction rates of common and typical organic radicals such as methyl, vinyl,

and phenyl which are 10^{-12}, 10^{-12}, and 10^{-11} to 10^{-13} cm^3/molecule-sec, respectively, which are ~6-10 orders of magnitude faster than the phenoxyl radical.[49, 50, 52-55, 103] We have calculated the ΔE_{rxn} of oxidation (B3LYP/6-31G(d,p)) for *para*-addition to the phenoxyl radical as 6.2 kcal/mol (9.3 for addition to the *ortho*- site) as compared to a negative 45.3 kcal mol^{-1} for the analogous reaction with phenyl. Barckholtz et al.[46] report a ΔH_{rxn} (for phenyl + $^3O_2$) using B3LYP/6-311+G(d,p)//B3LYP/6-31G(d) is a negative 43.3 kcal mol^{-1}. While addition of oxygen to common organic radicals such as methyl, vinyl, and phenyl is highly exothermic, it is highly endothermic for phenoxyl and semiquinone radicals. These calculations indicate that scavenging of phenoxyl and semiquinone radicals is neither kinetically nor thermodynamically a favorable reaction.

Our calculations were unable to find any path for molecular oxygen to react with any of these radicals at an oxygen-center, as formation of the ozonide is highly unfavorable (Figure 21). A metastable product could only be found if the reaction occurred at an *ortho*- or *para*-carbon. The high activation energies for oxidation of semiquinone and phenoxyl radicals appears to ensure that both types of radicals are equally unreactive with molecular oxygen.

These calculations demonstrate the expected stability and lack of reactivity of semiquinone radicals, but also suggest that phenoxyl radical is just as stable and unreactive. This in turn suggests that the phenoxyl radical must be considered as a candidate for the identity of the radicals observed to be associated with airborne fine particles and combustion-generated particles.[146, 147]

With regard to Chapter 5, experimental rate constant information for the analogous reactions with phenol have been used to draw conclusions due to the absence of

experimental rate information for chlorophenols' radical-producing channels. Based on the work of Knispel et al.[131], Olariu et al.[144], and the analogue, the OH + chlorophenol channels are expected to dominate at 298 K where addition to carbon is favored. It should be noted however, at combustion temperatures this adduct of addition is expected to decompose (back to reactants) making the abstraction of the hydroxyl H atom (by OH) the favored channel, a radical producing channel.

In terms of relative stabilities and hydroxyl bond dissociation energies, the agreement between experimental evidence and the computational results herein for the monochlorophenols[138, 142] lends confidence to the computational results for chlorophenols for which there are no experimental studies. Yang et al. also show, amongst the monochlorophenols, the pyrolytic burning of *p*-chlorophenol produces the largest amount dichlorodibenzofuran which is not surprising. That is, *p*-chlorophenoxyl is the most stable (or lowest energy) isomer of monochloro-phenoxyl and is also characterized by the largest activation energy for decomposition into carbon monoxide and a chlorinated cyclopentadienyl radical.

The high activation energies, energies of reaction, and large, positive free energies of reaction for the oxidative channels given in Chapter 5 also indicate these channels are thermodynamically unfavored at atmospheric conditions. This finding is consistent with the experimental works of Evans et al.[56, 57] and Yang et al.[138] which have shown dibenzofurans, relative to the pyrolytic case, are more produced more abundantly and at lower temperatures in an oxidative environment.

Recently, it has been realized monochlorinated phenoxyl radicals are isoelectronic with semiquinone radicals which are suspected to be responsible for much of the free radical damage incurred by cigarette smoke. The results in Chapter 5 also demonstrate the expected stability and

lack of reactivity (with O_2) of chlorophenoxyl radicals making them candidates for involvement in pollutant-forming mechanisms.[75] This work shows the likelihood of chlorinated dibenzofuran production may be correlated with radical stability.

REFERENCES

1. Dellinger, B., Rubey, W. A.; Hall, D. L., and Graham, J. L., Incinerability of Hazardous Wastes. *Hazardous Waste & Hazardous Materials* **1986,** 3, (2), 139-150.

2. Dellinger, B. and Taylor, P.H., Chemical Aspects of Combustion of Hazardous Wastes. *Centr. Eur. J. Publ. Hlth.* **1998,** 2, 79-87.

3. Vehlow, J., Bergfeldt, B., and Hunsinger, H., PCDD/F and related compounds in solid residues from municipal solid waste incineration - a literature review. *Waste Management and Research* **2006,** 24, (5), 404-420.

4. Van den Berg, M., Bimbaum, L., Bosveld, A., Brunstrom, B., Cook, P., Feeley, M., Giesy, J. P., Hanberg, A., Hasegawa, R., Kennedy, S.W., Kubiak, T., Larsen, J.C., Rolaf van Leeuwen, F.X., Djien Liem, A.K., Nolt, C., Peterson, R.E., Poellinger, L., Safe, S., Schrenk, D., Tillitt, D., Tysklind, M., Younes, M., Waern, F., and Zacharewski, T., Toxic Equivalency Factors (TEFs) for PCBs, PCDDs, PCDFs for Humans and Wildlife. *Env. Health Persp.* **1998,** 106, 775-792.

5. EPA Air Toxics Website. www.epa.gov/ttn/atw/orig189.html.

6. Jodkowski, J. T., Theoretical description of the kinetics of gas-phase reactions important in atmospheric chemistry. *Computational Chemistry* **2006,** 10, 139-227.

7. Atkinson, R., Kinetics and Mechanisms of the Gas-Phase Reactions of Hydroxyl Radical with Organic Compounds under Atmospheric Conditions. *Chem. Rev.* **1985,** 85, 69-201.

8. Sivaramakrishnan, R., Brezinsky, K., Vasudevan, H., Tranter, R.S., A shock-tube study of the high-pressure thermal decomposition of benzene. *Combustion Science and Technology* **2006,** 178, 285-305.

9. Knyazev, V. D., Computational study of the reactions of H atoms with chlorinated alkanes. isodesmic reactions for transition states. *Annual Meeting Archive-American Institute of Chemical Engineers* **2002**, 2531-6.

10. Ryu, J., Mulholland, J.A., Kim, D. H., and Takeuchi, M., Homologue and Isomer Patterns of Polychlorinated Dibenzo-p-dioxins and Dibenzofurans from Phenol Precursors: Comparison with Municipal Waste Incinerator Data. *Environ. Sci. Technol.* **2005,** 39, 4398-4406.

11. Gilles, M., Burkholder, J., and Ravishandara, A., Rate Coefficients for the Reaction of OH with Cl2, Br2, and I2 from 235-354 K. *Int. J. Chem. Kin.* **1999,** 31, 417-424.

12. Leu, M. T. and Lin, C.L., Rate Constants for the Reactions of OH with ClO, Cl2, and Cl2O at 298 K. *Geophysical Research Letters* **1979,** 6, 425-428.

13. Boodaghians, R. B., Hall, I. W., and Wayne, R. P., Kinetics of the Reactions of the Hydroxyl Radical with Molecular Chlorine and Bromine. *J. Chem. Soc., Faraday Trans. 2* **1987,** 83, 529-538.

14. Loewenstein, L. M. and Anderson, J. G., Rate and Product Measurements for the Reactions of OH with Cl2, Br2, and BrCl at 298 K. Trend Intrepretations. *J. Phys. Chem.* **1984,** 88, 6277-6290.

15. Ravishankara, A., Eisele, F., and Wine, P.H., The kinetics of the reaction of OH with ClO. *J. Chem. Phys.* **1983,** 78, 1140-44.

16. Chang, W. and Senkan, S.M., Detailed Chemical Kinetic Modeling of Fuel-Rich C2HCl3/O2/Ar Flames. *Environ. Sci. Technol.* **1989,** 23, 442-450.

17. Procaccini, C., Bozzelli, J.W., Longwell, J.P., Smith, K.A., and Sarofim, A.F., Presence of Chlorine Radicals and Formation of Molecular Chlorine in the Post-Flame Region of Chlorocarbon Combustion. *Environ. Sci. Technol.* **2000,** 34, 4565-4570.

18. Procaccini, C., Bozzelli, J.W., Longwell, J.P., Sarofim, A.F., and Smith, K.A., Formation of Chlorinated Aromatics by Reactions of Cl, Cl2, and HCl with Benzene in the Cool-Down Zone of a Combustor. *Environ. Sci. Technol.* **2003,** 37, 1684-1689.

19. Aizawa, T., Kamimoto, T., and Tamaru, T., Measurements of OH radical concentration in combustion environments by wavelength-modulation spectroscopy with a 1.55 um distributed-feedback diode laser. *Appl. Optics* **1999,** 38, (9), 1733-1741.

20. Wikstrom, E., Ryan, S., Touati, A., and Gullett, B.K., Key Parameters for de novo Formation of Polychlorinated Dibenzo-p-dioxins and Dibenzofurans. *Environ. Sci. Technol.* **2003,** 37, 1962-1970.

21. Gullett, B. K., Sarofim, A.F., Smith, K.A., and Procaccini, C., The role of chlorine in dioxin formation. *Process Safety and Environ Protection* **2000,** 78, 47-52.

22. Van Santen, R., Chlorine: World Outlook. *www.chemlink.com* **1998**.

23. Chlorine. *Chemical Week* **2002,** www.chemweek.com.

24. Kurylo, M. J. and Orkin, V. L., Determination of Atmospheric Lifetimes via the Measurement of OH Radical Kinetics. *Chem. Rev.* **2003,** 103, 5049-5076.

25. Johnson, B. G., Gill, P. M. W., and Pople, J. A., The performance of a family of density functional methods. *J. Chem. Phys.* **1993,** 98, (7), 5612-5626.

26. Lynch, B. J. and Truhlar, D.G., How Well Can Hybrid Density Functional Methods Predict Transition State Geometries and Barrier Heights? *J. Phys. Chem. A* **2001,** 105, 2936-2941.

27. Kang, J. K., and Musgrave, C.B., Prediction of transition state barriers and enthalpies of reaction by a new hybrid density-functional approximation. *J. Chem. Phys.* **2001,** 115, (24), 11040-11051.

28. Rice, B. M., Pai, S.V., and Chabalowski, C.F., Performance of Density Functional Theory on the Potential-Energy Surface of the H + OCS System. *J. Phys. Chem. A* **1998,** 102, 6950-6956.

29. Francisco-Marquez, M., Alvarez-Idaboy, J.R., Galano, A., and Vivier-Bunge, A., Theoretical study of the initial reaction between OH and isoprene in tropospheric conditions. *Phys. Chem. Chem. Phys.* **2003,** 5, 1392-99.

30. Szabo, A. and Ostlund, N.S., Modern Quantum Chemistry: Introduction to Advanced Electronic Structure Theory. *Dover Publications, Inc.* **1982**.

31. Dellinger, B.; Pryor, W. A.; Cueto, R.; Squadrito, G. L.; Hedge, V., Role of Free Radicals in the Toxicity of Airborne Fine Particulate Matter. *Chem. Res. Toxicol.* **2001,** 14, 1371-1377.

32. Squadrito, G. L.; Dellinger, B.; Cueto, R.; Deutsch, W. A.; Pryor, W. A., Quinoid Redox Cycling as a Mechanism for Sustained Free Radical Generation by Inhaled Airborne Particulate Matter. *Free Radical Biology & Medicine* **2001,** 31, 1132-1138.

33. Cormier, S. A., Lomnicki, S., Backes, W., and Dellinger, B., Origin and Health Impacts of Emissions of Toxic By-Products and Fine Particles from Combustion and Thermal Treatment of Hazardous Wastes and Materials. *Env. Health Persp.* **2006,** 114, (6), 810-7.

34. Hirakawa, K., Oikawa, S., Hiraku, Y., Hirosawa, I., and Kawanishi, S. , Catechol and Hydroquinone Have Different Redox Properties Responsible for Their Differential DNA-damaging Ability. *Chem.Res. Toxicol.* **2002,** 15, (1), 76-82.

35. Maskos, Z., Khachatryan, L., Cueto, R., Pryor, W.A., and Dellinger, B., Radicals from the Pyrolysis of Tobacco. *Energy and Fuels* **2005,** 19, 791-9.

36. Pryor, W. A., Prier, D.G., and Church, D.F., ESR Study of mainstream and sidestream cigarette smoke: Nature of free radicals in gas-phase smoke and in cigarette tar. *Environmental Health Perspectives* **1983,** 47, 345-355.

37. Church, D. and Pryor, W., Free-Radical Chemistry of Cigarette Smoke and its Toxicological Implications. *Environ. Health Perspect* **1985,** 64, 111-126.

38. Stone, K., Bermudez, E., Zang, L.Y., Carter, K.M., Queenan, K.E., and Pryor, W.A. , The ESR Properties, DNA Nicking, and DNA Association of Aged Solutions of Catechol versus Aqueous Extracts of Tar from Cigarette Smoke. *Archives of Biochemistry and Biophysics* **1995,** 319, 196-203.

39. Khachatryan, L., Adounkpe, J., Maskos, Z. and Dellinger, B., Formation of Cyclopentadienyl Radical from the Gas-Phase Pyrolysis of Hydroquinone, Catechol, and Phenol. *Environ. Sci. Technol.* **2006,** 40, (16), 5071-6.

40. Briois, C., Visez, N., Baillet, C., and Sawerysyn, J., Experimental Study on the thermal oxidation of 2-chlorophenol in air over the temperature range 450-900 C. *Chemosphere* **2006,** 62, 1806-16.113.

41. Wornat, M. J., Ledesma, E.B., and Marsh, N.D., Polycyclic aromatic hydrocarbons from the pyrolysis of catechol, a model fuel representative of entities in tobacco, coal, and lignin. *Fuel* **2001,** 80, 1711-26.

42. Ledesma, E. B., Marsh, N.D., Sandrowitz, A.K., and Wornat, M.J., An Experimental Study on the Thermal Decomposition of Catechol. *Proceedings of the Combustion Institute* **2002,** 29, 2299-2306.

43. Marsh, N. B., Ledesma, E.B., Sandrowitz, A.K., and Wornat, M.J., PAH Products of Catechol Pyrolysis: Temperature Effects. *Fuel Preprints* **2001,** 46, (1), 245-8.

44. Marsh, N. D., Ledesma, E.B., Sandrowitz, A.K., and Wornat, M.J., Yields of Polycyclic Aromatic Hydrocarbons from the Pyrolysis of Catechol: Temperature and Residence Time Effects. *Energy and Fuels* **2004,** 18, 209-17.

45. Liu, R., Morokuma, K., Mebel, A.M. and Lin, M.C., Ab Initio Study of the Mechanism for the Thermal Decomposition of the Phenoxy Radical. *J Phys Chem* **1996,** 100, 9314-9322.

46. Barckholtz, C., Fadden, M. J., and Hadad, C. M., Computational Study of the Mechanisms for the Reaction of O2 ($3\sum g$) with Aromatic Radicals. *J. Phys. Chem. A* **1999,** 103, 8108-8117.

47. Carpenter, B. K., Computational Prediction of New Mechanisms for the Reactions of Vinyl and Phenyl Radicals with Molecular Oxygen. *J. Am. Chem. Soc.* **1993,** 115, 9806-9807.

48. Mebel, A. M. and Lin, M. C., Ab Initio Molecular Orbital Calculations of C6H5O2 Isomers. *J American Chemical Soc* **1994,** 116, 9577-9584.

49. Sommeling, P. M., Mulder, P., Louw, R., Avila, D. V., Lusztyk, J. and Ingold, K. U., Rate of Reaction of Phenyl Radicals with Oxygen in Solution and in the Gas Phase. *J Phys Chem* **1993,** 97, (32), 8361-8364.

50. Tonokura, K., Norikane, Y., Koshi, M., Nakano, Y., Nakamichi, S., Goto, M., Hashimoto, S., Kawasaki, M., Andersen, M. P. S., Hurley, M. D., and Wallington, T. J., Cavity Ring-down Study of the Visible Absorption Spectrum of the Phenyl Radical and Kinetics of Its Reactions with Cl, Br, Cl2, and O2. *J. Phys. Chem. A* **2002,** 106, 5908-5917.

51. Tokmakov, I. V., Kim, G.S., Kislov, V.V., Mebel, A.M., Lin, M.C., The Reaction of Phenyl Radical with Molecular Oxygen: A G2M Study of the Potential Energy Surface. *J Phys Chem A* **2005,** 109, 6114-6127.

52. Yu, T. and Lin, M. C., Kinetics of the C6H5 + O2 Reaction at Low Temperatures. *J American Chemical Soc* **1994,** 116, 9571-9576.

53. Yu, C. L., Wang, C., and Frenklach, M., Chemical Kinetics of Methyl Oxidation by Molecular Oxygen. *J Phys Chem* **1995,** 99, 14377-14387.

54. Eskola, A. J. and Timonen, R.S., Kinetics of the reactions of vinyl radicals with molecular oxygen and chlorine at temperatures 200-362 K. *Phys Chem Chem Physics* **2003,** 5, (12), 2557-2561.

55. Mebel, A. M., Diau, E.W.G., Lin, M.C., Morokuma, K., Ab Initio and RRKM Calculations for Multichannel Rate Constants of the C2H3 + O2 Reaction. *J. Am. Chem. Soc.* **1996,** 118, 9759-9771.

56. Evans, C. S. and Dellinger, B., Mechanisms of Dioxin Formation from the High-Temperature Pyrolysis of 2-Chlorophenol. *Environ. Sci. Technol.* **2003,** 37, 1325-30.

57. Evans, C. S. and Dellinger, B., Mechanisms of Dioxin Formation from the High-Temperature Oxidation of 2-Chlorophenol. *Environ. Sci. Technol.* **2005,** 39, 122-7.

58. Fabian, W. M. F., and Janoschek, R., Thermochemical properties of stable intermediates and derived radicals for the gas-phase formation of 1,3,6,8- and 1,3,7,9-tetrachlorodibenzo-p-dioxins from 2,4,6-trichlorophenol: A Computational G3MP2B3 study. *Combustion and Flame* **2006,** 145, 282-9.

59. Louw, R. and Ahonkhai, S.I., Radical/radical vs. radical/molecule reactions in the formation of PCDD/Fs from (chloro)phenols in incinerators. *Chemosphere* **2002,** 46, 1273-1278.

60. Khachatryan, L., Burcat, A., and Dellinger, B., An elementary reaction-kinetic model for the gas-phase formation of 1,3,6,8- and 1,3,7,9-tetrachlorinated dibenzo-p-dioxins from 2,4,6-trichlorophenol. *Combustion and Flame* **2003,** 132, 406-21.

61. Khachatryan, L., Asatryan, R., and Dellinger, B., An Elementary Reaction Kinetic Model of the Gas-Phase Formation of Polychlorinated Dibenzofurans from Chlorinated Phenols. *J. Phys. Chem. A* **2004,** 108, 9567-72.

62. Stanmore, B. R., The formation of dioxins in combustion systems. *Combustion and Flame* **2004,** 136, 398-427.

63. Tuppurainen, K. A., Ruokojarvi, P. H., Asikainen, A.H., Aatamila, M., and Ruuskanen, J., Chlorophenols as Precursors of PCDD/Fs in Incineration Processes: Correlations, PLS Modeling, and Reaction Mechanisms. *Environ. Sci. Technol.* **2000,** 34, 4958-62.

64. Fu, Y., Liu, L., Mou, Y., Lin, B., and Guo, Q., Alfa and remote substituent effects on the homolytic dissociation energies of OH bonds. *Theochem* **2003,** 674, 241-9.

65. Klein, E., Lukes, V., Cibulkova, Z., and Polovkova, J., Study of N-H, O-H, and S-H bond dissociation enthalpies and ionization potentials of substituted anilines, phenols, and thiophenols. *Theochem* **2006,** 758, 149-59.

66. Klein, E. and Lukes, V., DFT/B3LYP study of O-H bond dissociation enthalpies of para and meta substituted phenols: Correlation with the C-O bond length. *Theochem* **2006,** 767, 43-50.

67. Himo, F., Eriksson, L., Blomberg, M., and Siegbahn, P., Substituent Effects on OH Bond Strength and Hyperfine Properties of Phenol, as Model for Modified Tyrosyl Radicals in Proteins. *Int. J. Quant. Chem.* **2000,** 76, 714-23.

68. Gomes, J. and da Silva, M., Gas-Phase Thermodynamic Properties of Dichlorophenols Determined from Density Functional Theory Calculations. *J. Phys. Chem. A.* **2003,** 107, 869-74.

69. Wu, Y. and Lai, D.K.W., A Density Functional Study of Substituent Effects on the O-H & O-CH3 Bond Dissociation Energies in Phenol and Anisole. *J. Org. Chem.* **1996,** 61, 7904-10.

70. Brinck, T., Haeberlein, M., and Jonsson, M., A Computational Analysis of Substituent Effects on the OH Bond Dissociation Energy in Phenols: Polar versus Radical Effects. *J. Am. Chem. Soc.* **1997,** 119, 4239-44.

71. Chandra, A. K., and Uchimaru, T., The OH Bond Dissociation Energies of Substituted Phenols and Proton Affinities of Substituted Phenoxide Ions: A DFT Study. *Int. J. Mol. Sci.* **2002,** 3, 407-22.

72. Han, J., Deming, R. L. and Tao, F., Theoretical Study of Molecular Structures and Properties of the Complete Series of Chlorophenols. *J. Phys. Chem. A* **2004,** 108, 7736-43.

73. Shaub, W. M. and Tsang, W., Dioxin Formation in Incinerators. *Environ. Sci. Technol.* **1983,** 17, 721-30.

74. Wiater-Protas, I. and Louw, R., Gas-Phase Chemistry of Chlorinated Phenols – Formation of Dibenzofurans and Dibenzodioxins in Slow Combustion. *Eur. J. of Org. Chem.* **2001**, 3945-3952.

75. Wiater, I., Born, J.G.P. and Louw, R., Products, Rates, and Mechanism of the Gas-Phase Condensation of Phenoxy Radicals between 500-840 K. *European Journal of Organic Chemistry* **2000**, 921-928.

76. Ahonkhai, S. I., Wiater, I. and Louw, R., Pathways to Dioxins in Incinerators. Role and Fate of Chlorophenols. *Organohalogen Compounds* **2000,** 46, 74-77.

77. Ryu, J., Mulholland, J.A., Oh, J., Nakahata, D.T. and Kim, D., Prediction of polychlorinated dibenzofuran congener distribution from gas-phase phenol condensation pathways. *Chemosphere* **2004,** 55, 1447-55.

78. Kim, D. H. and Mulholland, J.A., Temperature-Dependent Formation of Polychlorinated Naphthalenes and Dibenzofurans from Chlorophenols. *Environ. Sci. Technol.* **2005,** 39, 5831-36.

79. Berho, F., Lesclaux, R., The phenoxy radical: UV Spectrum and kinetics of gas-phase reactions with itself and with oxygen. *Chem Phys Letters* **1997,** 279, 289-96.
80. Platz, J., Nielsen, O.J., Wallington, T.J., Ball, J.C., Hurley, M.D., Straccia, A.M., Schneider, W.F., Sehested, J., Atmospheric Chemistry of the Phenoxy Radical: UV Spectrum and Kinetics of Its Reaction with NO, NO2, and O2. *J Phys Chem A* **1998,** 102, 7964-7974.

81. Frisch, M. J., Trucks, G.W., Schlegel, H.B., Scuseria, G.E., Robb, M.A., Cheeseman, J.R., Montgomery, Jr., J.A., Vreven, T., Kudin, K.N., Burant, J.C., Millam, J.M., Iyengar, S.S., Tomasi, J., Barone, V., Mennucci, B., Cossi, M., Scalmani,G., Rega, N., Petersson, G.A., Nakatsuji, H., Hada, M., Ehara, M., Toyota, K., Fukuda, R., Hasegawa, J., Ishida, M., Nakajima, T., Honda, Y., Kitao, O., Nakai, H., Klene, M., Li, X., Knox, J.E., Hratchian, H.P., Cross, J.B., Bakken, V., Adamo, C., Jaramillo, J., Gomperts, R., Stratmann, R.E., Yazyev, O., Austin, A.J., Cammi, R., Pomelli, C., Ochterski, J.W., Ayala, P.Y., Morokuma, K., Voth, G.A., Salvador, P., Dannenberg, J.J., Zakrzewski, V.G., Dapprich, S., Daniels, A.D., Strain, M.C., Farkas, O., Malick, D.K., Rabuck, A.D., Raghavachari, K., Foresman, J.B., Ortiz, J.V., Cui, Q., Baboul, A.G., Clifford, S., Cioslowski, J., Stefanov, B.B., Liu, G., Liashenko, A., Piskorz, P., Komaromi, I., Martin, R.L., Fox, D.J., Keith, T., Al-Laham, M.A., Peng, C.Y., Nanayakkara, A., Challacombe, M., Gill, P.M.W., Johnson, B., Chen, W., Wong, M.W., Gonzales, C., and Pople, J.A., Gaussian 03. *Revision C.02* **2004,** Gaussian, Inc., Wallingford, CT.

82. Foresman, J. B. and Frisch, A., Exploring Chemistry with Electronic Structure Methods, Second Edition. *Gaussian, Inc., CT* **1996**.

83. Levine, I. N., Quantum Chemistry, Fourth Edition. *Prentice Hall, Inc.; New Jersey* **1991**.

84. Parr, R. G. and Yang, W., Density-Functional Theory of Atoms and Molecules. *Oxford University Press; New York* **1989**.

85. Hohenberg, P. and Kohn, W., Inhomogenous Electron Gas. *Physical Rev.* **1964,** 136, (3B), B864-71.

86. Becke, A. D., Density-functional thermochemistry. III. The role of exact exchange. *J. Chem. Phys.* **1993,** 98, 5648.

87. Lee, C., Yang, W., and Parr, R.G., Development of the Colle-Salvetti correlation-energy formula into a functional of the electron density. *Phys. Rev. B* **1988,** 37, (2), 785-789.
88. Houston, P. L., Chemical Kinetics and Reaction Dynamics, First Edition. *McGraw-Hill Companies, Inc.* **2001**.

89. Peng, C., Ayala, P. Y., Schlegel, H. B., Frisch, M. J., Using Redundant Internal Coordinates to Optimize Equilibrium Geometries and Transition States. *Journal of Computational Chemistry* **1996,** 17, (1), 49-56.

90. Wollinski, K., and Pulay, P., Generalized Moller-Plesset perturbation theory: Second order results for two-configuration, open-shell excited singlet and doublet wave functions. *J. Chem. Phys.* **1988,** 90, (7), 3647-59.

91. Okabe, H., Photochemistry of Small Molecules, John Wiley and Sons. **1978**.

92. McQuarrie, D. A. and Simon, J.D., Physical Chemistry, A Molecular Approach. *University Science Books, Sausalito, CA* **1997**.

93. Vaghjiani, G. and Ravishankara, A., New measurement of the rate coefficient for the reaction of OH with methane. *Nature* **1991,** 350, 406-9.

94. Gierczak, T., Talukdar, R., Herndon, S., Vaghjiani, G., and Ravishankara, A., Rate Coefficients for the Reactions of Hydroxyl Radicals with Methane and Deuterated Methanes. *J. Phys. Chem. A* **1997,** 101, 3125-34.

95. Bonard, A., Daele, V., Delfau, J., and Vovelle, C., Kinetics of OH Radical Reactions with Methane in the Temperature Range 295-660 K and with Dimethyl Ether and Methyl-tert-butyl Ether in the Temperature Range 295-618 K. *J. Phys. Chem. A* **2002,** 106, 4384-89.

96. Dunlop, J. and Tully, F., A Kinetic Study of OH Radical Reactions with Methane and Perdeuterated Methane. *J. Phys. Chem.* **1993,** 97, 11148-50.

97. Tully, F. and Ravishankara, A., Flash Photolysis-Resonance Fluorescence Kinetic Study of the Reactions OH+H2-->H2O+H and OH+CH4-->H2O+CH3 from 298 to 1020 K. *J. Phys. Chem.* **1980,** 84, 3126-30.

98. Masgrau, L., Gonzales-Lafont, A., and Lluch, J., The curvature of the Arrhenius plots predicted by conventional canonical transition state theory in the absence of tunneling. *Theor. Chem. Acc.* **2003,** 110, 352-7.

99. Droege, A., and Tully, F., Hydrogen-Atom Abstraction from Alkanes by OH. 3. Propane. *J. Phys. Chem.* **1986,** 90, (9), 1949-56.

100. Talukdar, R., Mellouki, A., Gierczak, T., Barone, S., Chiang, S., and Ravishankara, A., Kinetics of the reactions of OH with alkanes. *Int. J. Chem. Kin.* **2004,** 26, (10), 973-90.

101. Kozlov, S., Orkin, V., Huie, R., Kurylo, M., OH Reactivity and UV Spectra of Propane, n-Propyl Bromide, and Isopropyl Bromide. *J. Phys. Chem. A* **2003,** 107, 1333-38.

102. Taylor, P., D'Angelo, J., Martin, M., Kasner, J., and Dellinger, B., Laser photolysis/laser-induced fluorescence studies of reaction rates of OH with CH3Cl, CH2Cl2, and CHCl3 over an extended temperature range. *Int. J. Chem. Kin.* **1989,** 21, (9), 829.

103. Atkinson, R., Baulch, D.L., Cox, R.A., Hampson, R.F., Kerr, J.A., Rossi, M.J., Troe, J., Evaluated kinetic, photochemical and heterogeneous data for atmospheric chemistry: supplement V, IUPAC subcommittee on gas kinetic data evaluation for atmospheric chemistry. *J Phys Chem Ref Data* **1997,** 26, (3), 521-1011.

104. 5.1.14, G., Grace Development Team, http://plasma-gate.weizmann.ac.it/Grace/. **1996-2004**.

105. Bryukov, M. G., Knyazev, V.D., Lomnicki, S.M., McFerrin, C.A. and Dellinger, B., Temperature-Dependent Kinetics of the Gas Phase Reactions of OH with Cl2, CH4, and C3H8. *J Phys Chem A* **2004,** 108, 10464-10472.

106. Barrante, J. R., Applied Mathematics for Physical Chemistry. *Prentice-Hall, Inc., New Jersey* **1974**.

107. National Institute of Standards and Technology Computational Chemistry Comparison and Benchmark Database, R., August 2005, NIST Standard Reference Database 101, http://srdata.nist.gov/cccbdb/.

108. National Institute of Standards and Technology Chemistry WebBook Database, J. R., NIST Standard Reference Database Number 69, http://webbook.nist.gov/chemistry/.

109. Benson, S. W., *Thermochemical Kinetics: Method for the Estimation of Thermochemical Data and Rate Parameters, Second Edition*. John Wiley and Sons, Inc.: 1976.

110. Speybrock, V. V., DeKimpe, N., and Waroquier, M.J., N-Alkenyl-2-aziridinylmethyl Radicals and N-Alkenylaminyl Radicals in Cascade Cyclizations to Pyrrolizidines and Indolizidines. *J. Org. Chem.* **2005,** 70, 3674-81.

111. Saeys, M., Reyniers, M.F., Marin, G.B., Van Speybrock, V., and Waroquier, M., Ab Initio Calculations for Hydrocarbons: Enthalpy of Formation, Transition State Geometry, and Activation Energy for Radical Reactions. *J. Phys. Chem A.* **2003,** 107, 9147-59.

112. Lee, J., Chen, C., and Bozzelli, J.W., Thermochemical and Kinetic Analysis of the Acetyl Radical (CH3CO.) + O2 Reaction System. *J. Phys. Chem A.* **2002,** 106, 7155-70.

113. Chen, C. and Bozzelli, J.W., Thermochemical Properties, Pathway, and Kinetic Analysis on the Reactions of Benzene with OH: An Elementary Reaction Mechanism. *J. Phys. Chem A.* **2004,** 108, 4632-52.

114. Durant, J. L., Evaluation of transition state properties by density functional theory. *Chem Phys Letters* **1996,** 256, 595-602.

115. Brown, T. L., LeMay, H.E., and Bursten, B.E., Chemistry: The Central Science, Eighth Edition, Prentice-Hall, Inc., New Jersey. **2000**.

116. Gonzales, C. and Schlegel, H.B., Reaction Path Following in Mass-Weighted Internal Coordinates. *J. Phys. Chem.* **1990,** 94, 5523-27.

117. Angel, L. A. and Ervin, K. M., Gas-Phase Acidities and O-H Bond Dissociation Enthalpies of Phenol, 3-Methylphenol, 2,4,6-Trimethylphenol, and Ethanoic Acid. *J. Phys. Chem A.* **2006,** 110, 10392-10403.

118. Angel, L. A., Ervin, K.M., Competitive Threshold Collision-Induced Dissociation: Gas-Phase Acidity and OH Bond Dissociation Enthalpy of Phenol. *J Phys Chem A* **2004,** 108, (40), 8346-8352.

119. da Silva, G., Chen, C., and Bozzelli, J.W., Bond dissociation energy of the phenol OH bond from ab initio calculations. *Chem. Phys. Lett.* **2006,** 424, 42-5.

120. Lovell, A. B., Brezinsky, K., Glassman, I., The Gas Phase Pyrolysis of Phenol. *Int. J. Chem. Kin.* **1989,** 21, 547-560.

121. Zhang, H., On the OH bond dissociation enthalpy of catechol. *New Journal of Chemistry* **2003,** 27, 453-4.

122. Thavasi, V., Leong, L.P. and Bettens, R.P.A., Investigation of the Influence of Hydroxyl Groups on the Radical Scavenging Ability of Polyphenols. *J. Phys. Chem A.* **2006,** 110, 4918-4923.

123. Cabral, B. J. C. and Canuto, S., Reply to comment on "The enthalpy of the OH bond homolytic dissociation: Basis-set extrapolated density functional theory and coupled cluster calculations" *Chem. Phys. Lett.* **2006,** 417, 570-2.

124. Baulch, D. L., Cobos, C.J., Cox, R.A., Esser, C., Frank, P., Just, T., Kerr, J.A., Pilling, M.J., Troe, J. Walker, R.W., Warnatz, J., Evaluated Kinetic Data for Combustion Modeling. *J. Phys. Chem. Ref. Data* **1992,** 21, (3), 411.

125. Bruinsma, O. S. L., Geertsma, R.S., Bank, P., Moulijn, J.A., Gas-phase pyrolysis of coal-related aromatic compounds in a coiled tube flow reactor. Benzene and derivatives. *Fuel* **1988,** 67, 327-333.

126. Horn, C., Roy, K., Frank, P., Just, T., Shock-Tube Study on the High-Temperature Pyrolysis of Phenol *27th Symposium (International) on Combustion, Combustion Institute* **1998**, 321-8.

127. Shamovsky, I. L., Riopelle, R.J. and Ross, G.M., Ab Initio Studies on the Mechanism of Tyrosine Coupling. *J. Phys. Chem A.* **2001,** 105, 1061-70.

128. Berndt, T. and Boge, O., Gas-phase reaction of OH radicals with phenol. *Phys. Chem. Chem. Phys.* **2003,** 5, 342-50.

129. Calvert, J. G., Atkinson, R., Becker, K.H., Kamens, R.M., Seinfeld, J.H., Wallington, T.J., and Yarwood, G. , The Mechanisms of Atmospheric Oxidation of Aromatic Hydrocarbons. *Oxford University Press, New York* **2002**.

130. Nadtochenko, V. and Kiwi, J., Dynamics of adduct formation of hydroquinone under oxidative conditions observed by laser spectroscopy. *Chem. Commun.* **1997**, 41-2.

131. Knispel, R., Koch, R., Siese, M., Zetzsch, C., Adduct Formation of OH Radicals with Benzene, Toluene, and Phenol and Consecutive Reactions of the Adducts with NOx and O2. *Ber. Bunsenges. Phys. Chem.* **1990,** 94, 1375-9.

132. Thuner, L. P., Bardini, P., Rea, G.J., and Wenger, J.C., Kinetics of the Gas-Phase Reactions of OH and NO3 Radicals with Dimethylphenols. *J. Phys. Chem A.* **2004,** 108, 11019-11025.

133. Asatryan, R., Davtyan, A., Khachatryan, L., and Dellinger, B., Molecular Modeling Studies of the Reactions of Phenoxyl Radical Dimers: Pathways to Dibenzofurnans. *J. Phys. Chem A.* **2005,** 109, 11198-11205.

134. Sidhu, S. and Edwards, P., Role of Phenoxy Radicals in PCDD/F Formation. *Int. J. Chem. Kin.* **2002,** 34, 531-41.

135. Babushok, V. I. and Tsang, W., Gas-phase mechanism for dioxin formation. *Chemosphere* **2003,** 51, 1023-9.

136. Weber, R. and Hagenmaier, H., Mechanism of the Formation of Polychlorinated Dibenzo-p-dioxins and Dibenzofurans from Chlorophenols in Gas Phase Reactions. *Chemosphere* **1999,** 38, (3), 529-49.

137. Mulholland, J. A., Akki, U. Yang, Y., Ryu, J., Temperature dependence of DCDD/F isomer distributions from chlorophenol precursors. *Chemosphere* **2001,** 42, 719-27.

138. Yang, Y., Mulholland, J.A., Akki, U., Formation of furans by gas-phase reactions of chlorophenols. *27th Symposium (International) on Combustion Proceedings* **1998,** Vol. 2, 1761-68.

139. Fadden, M. J., Barckholtz, C., and Hadad, C.M., Computational Study of the Unimolecular Decomposition Pathways of Phenylperoxy Radical. *J. Phys. Chem. A* **2000,** 104, 3004-11.

140. Bader, R. F. W., *Atoms in Molecules: A Quantum Theory*. Oxford University Press: 1990.

141. Loudon, G. M., Organic Chemistry, Second Edition. *The Benjamin/Cummings Publishing Co., Inc., Menlo Park, CA* **1988**.

142. Brigati, G., Lucarini, M., Mugnaini, V., and Pedulli, G.F., Determination of Substituent Effect on the OH Bond Dissociation Enthalpies of Phenolic Antioxidants by the EPR Radical Equilibration Technique. *J. Org. Chem.* **2002,** 67, 4828-32.

143. Manion, J. A., and Louw, R., J., Relative gas phase Desub Rates of Cl-Benzene derivatives by H atoms near 1000K. *J. Chem. Soc. Perkin Trans. 2* **1990**, 551-7.

144. Olariu, R. I., Klotz, B., Barnes, I., Becker, K.H., Mocanu, R., FT-IR study of the ring-retaining products from the reaction of OH radicals with phenol, o-, m-, and p-cresol. *Atmospheric Environment* **2002,** 36, 3685-97.

145. Yazawa, A., Nakazawa, S. and Menad, N., Thermodynamic Evaluations on the Formation of Dioxins and Furans in Combustion Gas. *Chemosphere* **1999,** 39, (14), 2419-32.

146. Lomnicki, S. and Dellinger, B., A Detailed Mechanism of the Surface-Mediated Formation of PCDD/F from the Oxidation of 2-Chlorophenol on a CuO/Silica Surface. *J Phys Chem A,* **2003,** 107, (22), 4387-4395.

147. Dellinger, B., Pryor, W.A.; Cueto, R., The Role of Combustion-Generated Radicals in the Toxicity of PM2.5. *Proceedings of the Combustion Institute* **2000,** 28 (Pt 2), 2675.

APPENDIX: PERMISSION LETTER

05/31/2007 14:48 FAX 2027766112 ☒001/002

American Chemical Society

Publications Division
Copyright Office

1155 Sixteenth Street, NW
Washington, DC 20036
Phone: (1) 202-872-4368 or -4367
Fax: (1) 202-776 8112 E-mail: copyright@acs.org

VIA FAX: 225-578-3463 DATE: May 31, 2007

TO: Cheri A. McPerrin, Department of Chemistry, Louisiana State University
1413 Jim Taylor Dr., Apt. #119, Baton Rouge, LA 70820

FROM: C. Aileen Courtney, Copyright Associate C. Aileen Courtney

Thank you for your request for permission to include your paper(s) or portions of text from your paper(s) in your thesis. Permission is now automatically granted; please pay special attention to the implications paragraph below. The Copyright Subcommittee of the Joint Board/Council Committees on Publications approved the following:

Copyright permission for published and submitted material from theses and dissertations
ACS extends blanket permission to students to include in their theses and dissertations their own articles, or portions thereof, that have been published in ACS journals or submitted to ACS journals for publication, provided that the ACS copyright credit line is noted on the appropriate page(s).

Publishing implications of electronic publication of theses and dissertation material
Students and their mentors should be aware that posting of theses and dissertation material on the Web prior to submission of material from that thesis or dissertation to an ACS journal may affect publication in that journal. Whether Web posting is considered prior publication may be evaluated on a case-by-case basis by the journal's editor. If an ACS journal editor considers Web posting to be "prior publication", the paper will not be accepted for publication in that journal. If you intend to submit your unpublished paper to ACS for publication, check with the appropriate editor prior to posting your manuscript electronically.

If your paper has not yet been published by ACS, we have no objection to your including the text or portions of the text in your thesis/dissertation in print and microfilm formats; please note, however, that electronic distribution or Web posting of the unpublished paper as part of your thesis in electronic formats might jeopardize publication of your paper by ACS. Please print the following credit line on the first page of your article: "Reproduced (or 'Reproduced in part') with permission from [JOURNAL NAME], in press (or 'submitted for publication'). Unpublished work copyright [CURRENT YEAR] American Chemical Society." Include appropriate information.

If your paper has already been published by ACS and you want to include the text or portions of the text in your thesis/dissertation in print or microfilm formats, please print the ACS copyright credit line on the first page of your article: "Reproduced (or 'Reproduced in part') with permission from [FULL REFERENCE CITATION.] Copyright [YEAR] American Chemical Society." Include appropriate information.

Submission to a Dissertation Distributor: If you plan to submit your thesis to UMI or to another dissertation distributor, you should not include the unpublished ACS paper in your thesis if the thesis will be disseminated electronically, until ACS has published your paper. After publication of the paper by ACS, you may release the entire thesis (not the individual ACS article by itself) for electronic dissemination through the distributor; ACS's copyright credit line should be printed on the first page of the ACS paper.

Use on an Intranet: The inclusion of your ACS unpublished or published manuscript is permitted in your thesis in print and microfilm formats. If ACS has published your paper you may include the manuscript in your thesis on an intranet that is not publicly available. Your ACS article cannot be posted electronically on a publicly available medium (i.e. one that is not password protected), such as but not limited to, electronic archives, Internet, library server, etc. The only material from your paper that can be posted on a public electronic medium is the article abstract, figures, and tables, and you may link to the article's DOI or post the article's author-directed URL link provided by ACS. This paragraph does not pertain to the dissertation distributor paragraph above. 06/07/06

VITA

Cheri Ann McFerrin was born on an army base in Heidelberg, Germany,on July 13, 1957. In December of 1988 she obtained a Bachelor of Science in chemistry from Louisiana State University in Baton Rouge, Louisiana. After working in an industrial position in Louisiana for 5 years she moved to Pasadena, California, to pursue employment in the biotechnology sector. After several years there she returned to Baton Rouge in 1999. After contracted analytical work at Dow Chemical, she began pursuing a doctoral degree in chemistry at Louisiana State University in 2001. She will receive her doctoral degree in physical chemistry in August of 2007.